Ana Catarina Martins Pintado

Bachelor of Science in Chemical and Biochemical Engineering

Production of Microparticles of Wax using PGSS – Particle from Gas Saturated Solution Process

Dissertation submitted in partial fulfilment
of the requirements for the degree of
Master of Science in
Chemical and Biochemical Engineering

Adviser: Dr. Daniela Trambitas,
Manager Special Projects,
Feyecon D&I in Netherlands

Co-adviser: Dr. Ana Isabel Nobre Martins
Aguiar de Oliveira Ricardo, Full Professor,
NOVA University of Lisbon

Examination Comitte

Chairperson:	Professor Mário Fernando José Eusébio
Raporteur:	Professor Teresa Casimiro
Member:	Professor Ana Isabel Nobre Martins Aguiar de Oliveira Ricardo

FACULDADE DE CIÊNCIAS E TECNOLOGIA
UNIVERSIDADE NOVA DE LISBOA

November, 2020

Production of Microparticles of Wax using PGSS – Particle from Gas Saturated Solution Process

‘’*Aim for success, not perfection. Never give up your right to be wrong, because then you will lose the ability to learn new things and move forward with your life. Remember that fear always lurks behind perfectionism*.’’ – Dr David M. Burns

Acknowledgements

I would like to thank everyone who helped directly or indirectly and contributed to this project.

Firstly, I want to express my gratitude to Geert Worlee and Daniela Trambitas for having allowed me to develop this project at Feyecon Development & Implementation B.V. and for all the guidance provided and constant support. I would like to thank all my colleagues at Feyecon for their support, help, sympathy and shared knowledge and companionship.

I would like to mostly thanks Pauline van Leusden and Brigitta Bohus for all the support, availability and guidance they have given me over this six months of internship at the company. I thank you both for all the guidance provided, concern and constant support, as well as all the knowledge you both have transmitted and shared.

I would like to thank Dániel Dévényi for his help with the P&ID and the PGSS machine, and I would like to thank Tjerk de Vries for the PGSS mathematical model used in this thesis.

I would like to thank all the teachers of FCT-UNL was part of my academic progress and that I helped in the realization of this thesis. I special would like to thanks my adviser of FCT-UNL, Dr Ana Aguiar Ricardo for all the support, sharing of knowledge, orientation and availability with me. I would also like to thanks the professor Mário Eusébio, for all the support and orientation given to me.

Gostaria de agradecer a todos aqueles que fizeram da faculdade o melhor possível (Afonço Graça, Valeriya Mykhaltsova, Bruno Ferraz, Guiomar Ripado, Ingrid Luiza, João Saraiva, Rafaela Neves e Bernardo Rodrigues). Foram as pessoas que melhoraram a minha vida académica, sem eles não teria sido o mesmo. Por todas as noites passadas no 7 a estudar, por todas festas e jantares por todo apoio e amizade incondiocional que me deram nestes últimos 5 anos.

Por último gostaria de agradecer à minha familía por todo apoio e amor que me deram. Gostaria de agradecer especialmente aos meus pais, ao meu irmão e à minha avó que me ajudaram sempre em todos momentos especialmente nos piores e que nunca deixaram de me apoiar independentemente das minhas decisões.

Abstract

The production of microparticles for encapsulation purpose is widely used in the cosmetic and pharmaceutical industry, having the downside of using pollutant and expensive organic solvents. The PGSS (Particle from gas saturated solution) process is a micronization technique based on supercritical fluids that eliminate the need for organic solvents.

This project focus on the study of the influence of the process parameters of PGSS using Jojoba wax to encapsulate a red natural pigment. Also, we generated particles of mixture fat powder for new cosmetic products. Cocoa Butter, Sunflower oil, Macadamia wax, Beeswax and Lecithin were used to create suitable coatings for encapsulating enzyme for cosmetic application.

The experiments were carried out varying the temperature (76-93ºC), the pressure (75-150 bar), the quantity of the mixture (Jojoba wax + red pigment) in a vessel (50-300g), pigment loading (1-20%) and nozzle diameter (0,093-0,71mm). Lastly, we perform a test without stirring the solution. The results by Optical Microscopy measurements indicate the Pigment/Jojoba wax microparticles have a size range of 7 to 109 µm and by SEM, we observed two morphologies (Hollow spherical particles and sponge-like particles). The bulk density values obtained varied between 95 to 236 kg/$m^{3,}$ and the encapsulation efficiency was up to 74%. The powder flowability was mostly 1.4 on Hausner's ratio, indicating that the powder is cohesive and compressible, and the flow is poor. The yield of the process was high, up to 97%.

A mathematical model based on the theory of the entrainment of the surrounding gas, that explains the influence of the amount of gas trapped on distance from the nozzle and velocity of the spray on spray temperature was also implemented and discussed.

Keywords: Microparticles; Microencapsulation; Supercritical fluids; CO_2; PGSS; waxes; fats; oils;

Resumo

A produção de micropartículas para encapsulamento é amplamente utilizada na indústria cosmética e farmacêutica, porém apresenta como desvantagem a nececessidade de uso de solventes orgânicos poluentes e caros.O processo PGSS (Partícula da solução saturada de gás) é uma técnica de micronização baseada em fluidos supercríticos que elimina a necessidade de usar solventes orgânicos.

Este projeto centra-se no estudo da influência dos parâmetros de processo do PGSS usando cera Jojoba para encapsular um pigmento natural vermelho. Além disso, gerámos partículas de mistura gordura em pó, manteiga de cacau, óleo de girassol, cera de macadamia, cera de abelha e lecitina para encontrar um revestimento adequado para encapsular uma enzima para uma empresa de cosméticos.

As experiências foram realizadas variando a temperatura (76-93ºC), a pressão (75-150 bar), a quantidade (50-300g), quantidade de pigmento (1-20%) e diâmetro do nozzle (0,093-0,71mm). Por último, realizamos um teste sem mexer a solução. Os resultados das medições óticas de microscopia indicam que as micropartículas de pigmento e cera de jojoba têm uma gama de tamanhos de 7 a 109 µm e, por SEM, observámos duas morfologias (partícula esféricas ocas e partículas com o formato de esponja). A densidade do bulk variava entre 95 a 236 kg/m^{3,} e a eficiência de encapsulamento foi até 74%. O escoamento do pó foi maioriariamente 1,4 na razão de Hausner, indicando que o pó é coeso e compressível e o fluxo é fraco. O rendimento do processo foi até 97%.

Foi também implementado e discutido um modelo matemático baseado na teoria do apriosionamento do gás circudante, o qual explica a influência da quantidade de gás preso conforme a distância ao nozzle e a influência da velocidade do spray em relação á temperatura do spray.

Palavras chaves: Micropartículas; Microencapsulamento; Fluídos supercríticos; CO_2; PGSS; ceras; gorduras; óleos;

Table of Contents

List of Figures

List of Tables

Acronyms

ASES	Aerosol Solvent Extraction
ABS	Absorbances
BD	Bulk density (kg/m^3)
CAN-BD	Carbon dioxide Assisted Nebulization with a Bubble Dryer®
C3F8	Octafluoropropane
CoQ10	Coenzyme (ubiquinone)
DELOS	Depressurisation of an Expanded Liquid Organic Solution
DoE	Design of Experiments
EE (%)	Encapsulation efficiency
GMS	Monosodium glutamate
GAS	Gaseous Ant-solvent
GPR	Gas product ratio
PCA	Precipitation by compressed fluid anti-solvent
PLGA	poly(lactic-co-glycolic acid)
PLA	Polylactic acid
PEG	Polyethene glycol
PGSS	Particle from gas saturated solutions
PGSS, drying	Particle from gas saturated solutions drying
RESS	Rapid expansion from saturated solutions
RESSAS	Rapid Expansion of supercritical solution into an aqueous solution

RESS-N	Rapid Expansion of supercritical with a non-solvent
RESOLV	Rapid Expansion of Supercritical into a liquid solvent
RESS-SC	Rapid Expansion of supercritical solution with solid co-solvent
SAA	Supercritical Fluid-Assisted Atomization
SAS	Supercritical anti-solvent process
SCFs	Supercritical Fluids
$scCO_2$	Supercritical carbon dioxide
SEDS	Solution Enhanced Dispersion by Supercritical Fluids
SEM	Scanning electron microscopy
TiO2	Titanium dioxide

Symbology

A	Quantity (DoE)
B	Temperature (DoE)
C	Pressure (DoE)
Cp, gas	Specific heat capacity of the gas, kJ/kg.K
Cp, fat	Specific heat capacity of the gas, kJ/kg.K
CI (%)	Compressibility index
C without heating	Pigment concentration without heating (mg/ml)
$C_{heating}$	Pigment concentration with heating (mg/ml)
d	Nozzle diameter (m)
d, cone	Cone diameter (m)
d, spray vessel	Diameter of the spray vessel (m)
df	Degrees of freedom
fr, gas	Weight fraction gas dissolved in the molten fat
K	Entrainment factor
MS	Mean squared value
MPS	Mean particle size

p_c	Critical Pressure (bar)
Qi	Initial mass flow of spray (kg/s)
Qt	Total mass flow of spray (kg/s)
Re	Reynolds Number
SS	Sum of squares
T_c	Critical Temperature (°C)
T_p	Triple Point (°C)
$T_{, spray}$	Average temperature of the spray (°C)
T_i	Temperature of mixture CO_2-fat in the nozzle (°C)
$v_{,spray}$	Average velocity of the spray (m/s)
$v_{,i}$	Initial velocity of the spray (m/s)
$v_{,f}$	Final velocity of the spray (m/s)
$v_{,gas}$	Average velocity of the cooling gas (m/s)
V_0	Untapped apparent volume
V_F	Tapped apparent volume
W_1	Quantity of mass initially introduced in vessel
W_2	Weight of collected particles
x	Axial distance from the nozzle (m)
ρ_{bulk}	Bulk density (kg/m^3)
ρ_{tapped}	Tapped density (kg/m^3)
ρ_i	Initial density of the gas (kg/m^3)
ρ_s	Density of surrounding gas (kg/m^3)
ρ_t	Density of the gas in the function of axial distance from the nozzle (kg/m^3)
μ	Viscosity of the surrounding gas (Pa.s)
$\Delta H_{cr, fat}$	Heat of fat crystallisation (kJ/kg)

$\Delta H_{exp, gas}$	Enthalpy change of gas under pressure to ambient pressure (kJ/kg)
ΔP	Pressure Difference (before and after spray)

1

1 Introduction

The demand for producing micro and nanoparticles via precipitation is growing. Micronization is a field of research that has been quite active in the last years and widely applied in the pharmaceutical, cosmetic and food industry.[1][2]

Microparticles are generally produced from plastic sources and once discharged in the waters (rivers or oceans) have a huge negative impact on fisheries and marine plants. The tendency of microparticle production worldwide is expected to have an important growth in the following coming years with great impact on food and pharmaceutical applications.[3]

The global Micronized Wax market is getting more attention from the main players (e.g. BASF, Clariant, Sasol, Honeywell, etc.) which is translated into a growth expectation for approx. 24,5 million USD in a forecast period 2020 – 2025, from 516,5 to over 541million USD. This will aim to replace most of the synthetic plastic micronized particles.[4]

Working on the development of green processing of such micronized particles will give a direct benefit to main market players giving them the possibility to rapid scale-up implementation and production. This generates new engineering solutions for processing scale up with a direct application in the production of innovative green technologies. [5]

Micronization is the process to reduce the particle size to obtained micro or nanoparticles. This process provides variations in particle structures, surface areas, and functional properties and uses hydrodynamic and mechanical techniques to destroy internal linkages causing the breakdown of the materials. [6]–[8]

One of the main reasons for this process growth is the possibility of obtaining fine particles with biocompatible or biodegradable carrier materials. These microparticles can also be used in

micro-encapsulation via co-precipitation or coating. Encapsulation is a process to store and preserve any material such as active ingredients within a shell, surrounded by a coating or material wall, producing a capsule. [9]

The production of microparticles by micronization allows the precise control over the particle'a properties, size and morphology. These features provide the information necessary for developing or selecting suitable capsules for microencapsulation. Therefore, in the literature, a lot of formulation and stabilization procedures are mentioned, for the manufacturing of solid dosage forms and well as for, the solubilization and release of active components of interest. These microcapsules are important for the sector because ensure improved storage stability and activity. [1][4][7][8]

There is a wide range of materials which can be used in microparticle production, depending on the industry and application. In this thesis, we are focusing on using natural materials such as waxes, fats and oils from the food industry. These ingredients are excellent options for stabilizers because they easily digested, are not soluble in water and inexpensive. Micronized wax, for example, is used for coating, as sealant or for influencing the pastes rheology.[9][10]

To produce microparticles with these materials, a technique based on supercritical fluids called PGSS (Particles from Gas Saturated Solution) was used. The supercritical fluid micronization techniques are environmentally friendly, an attractive alternative to conventional tecnhiques, due to the absence of organic solvents, eliminating large volume waste and additionally, requiring less energy and costs, promoting at the same time a sustainable process. Nowadays the most used supercritical fluid is carbon dioxide because in non-toxic, non-flammable, cheap, and considered a "green solvent". Also, the supercritical conditions of the CO_2 are rather easily attained, with mild pressure and temperature compared to other fluids. [14]

The PGSS process, also known as supercritical melt micronization, was patented by Weidner.[15][16] In this process, a melted material is mixed with $scCO_2$ and expanded through a nozzle to produce a fine powder. This process operates at mild conditions and does not use any solvents, harmful to the environment, thus is environmentally compliant.

PGSS is one of the most attractive methods of micronisation using supercritical fluids. It is a process that does not rely on the solvent strength of CO_2 and does not need organic solvents. One of the essential advantages of PGSS is the reduced consumption of CO_2 (lower than 5 kg CO_2/ kg solute) compared with other processes. Furthermore, the processing cost is very low due to its simplicity and operation at the low pressures. Naturally, the PGSS can run at low. Besides, it is a process easily scalable and very viscous samples can be processed. [17]–[19]

Another advantage of this process is the possibility to micronize materials which are not soluble in CO_2, thus being able of processing a wide range of materials. This process is recommended for materials sensitive to heat or oxidation, thus being able to process thermolabile compounds. For example, it has already been used for emulsions and suspensions of active

ingredients (APIs) in polymers or carrier substances leading to composite particles. Also, the process uses changes in material properties to its advantage. Properties such as swelling, change in surface tension and viscosity, plasticization, softening and melting depression of the materials. The best materials to be processed are polymers and fats that have moderate melting temperatures and where CO_2 presents a large solubility.[20]–[23]

The main limitation of these process is the need to melt the materials of interest, which can be problematic for materials more sensitive to heat. Another disadvantage is the difficulty to control the morphology and the particle size of the particles produced. Nevertheless, the PGSS process shows excellent potential in the production of capsules of several materials such as fats, lipids or polymers. Also, this technique has already been used to encapsulate some APIs with these materials. The success of the PGSS process with these materials is because of the solubility of $scCO_2$. In these materials, supercritical CO_2 has high solubility at moderate pressures. [18][24]

Despite having some difficulties, this process has already demonstrated that it is an efficient process for microencapsulation even for thermally sensitive polymers composites carrying bioactive materials. Also, this process is highly suitable for powder coating applications. [20][21]

In this thesis, we expected to produce spherical particles, hollow or solid, with a reasonably narrow size distribution with fat or wax since the size, shape and structure are the most important properties for applications in industry, such as food and cosmetic.

1.1 Context and Motivation

This dissertation is a requirement for the completion of my Master degree in Chemical and Biochemical Engineering program at Nova School of Science and Technology in Lisbon.

The internship was performed at the company Feyecon Development & Implementation B.V in the Netherlands, for six months (01-03-2020 to 31-08-2020) with the topic: Microparticles production of wax by the PGSS process.

The Feyecon company uses innovative processes based on supercritical fluid properties of CO_2, being a global leader in CO_2 technology. Feyecon offers tailor-made process design and equipment at bench, pilot and production scales. This company is focused on research and development using CO_2 technology, working in many industries such as cosmetic and pharmaceutical.

My project appears on the development and optimization of CO_2 processing methods for the encapsulation and stabilization of active ingredients for a cosmetic product, a water continuous cleansing cream. Therefore, the objective is to produce a loose and fine powder.

In this thesis, we further investigated the $scCO_2$-assisted PGSS process for various commercial applications, especially in developing new products based on wax microcapsules. This

process is seen as a sustainable replacement of current processes which are done using larger solutions batches (larger volumes) where the wax is first melted and then gradual cooling is applied. The wax is further crystallised forming either the required structuring agents for cosmetic emulsion (cream and/or foundation bases) or directly to encapsulate sensitive active natural ingredients (like pigment, antioxidants, essential oils, etc.). The $scCO_2$-assisted PGSS can produce instant powders with minimum exposure of the sensitive ingredients to external agents during processing (as CO_2 is inert), simultaneously saving energy (in cooling and heating) and limiting the complicated handling of larger solutions volumes. The present study focuses mainly on product development, specifically on different variables of the process and how those ones influence the powder structure. Essentially the tests were conducted at various conditions of the process parameters such as temperature, pressure, mixture ratios, nozzle types, loading of the active ingredients with or without assisted stirring. The previous test ran at Feyecon, proved that the process conditions are determining for the morphology, size and density of the produced particles. For example, Feyecon proved in previous studies, that using other types of materials (than wax), the PGSS process, can yield different spherical particles which can be completely solid material, hollowed or with sponge-like interior structures, and with a relative narrow size distribution. Based on these results, in this study, we will conduct similar experiments using a wax type of material, and we shall test this process for making microencapsulates, using similar materials for the exterior coatings. For the coatings tests, enzymes and pigments will be used as active ingredients, both sensitive materials which have a short life-times when contacted with water, air, or exposing to light and high temperatures. By coating these ingredients within a wax matrix, it is possible to increase their life-times and also promote a wider application in various cosmetic products.

One of the developed products will be based on enzyme encapsulation. This stabilised enzyme will be further used in the development of a water cleansing cream. For this application, we focus on varying process conditions to yield loose and small size powder particles which are more stable and less sensitive to ambient conditions. Another product will be based on a natural coating pigment (anthocyanin type). The pigment shade is sensitive to pH variation as well as to air, light and temperature. By coating, it is possible to confer the pigment with better stability than of the original red shade, which is a mandatory requirement for cosmetic products such as lipstick, foundations, eyelashes, etc. The influence of other materials in the PGSS process applied for particle coating will be assessed.

Overall our study will try to underline the dependency of the PGSS process conditions and the choice of the material, especially the relation with its ductility performance necessary in the coating.

The results will be confirmed via a mathematical model (developed internally at Feyecon) which will evidence the dependency between the nozzle used in the atomisation (varying the type of nozzle, flows) and the obtained particle structures.

1.2 The aim of this study and research questions

This study aims to further investigate the $scCO_2$-assisted PGSS process and produce a loose and fine powder with natural materials at different conditions. Also, it was in the interest of the company to study different types of natural coating materials (fats, waxes and oils). This dissertation will point out the influence of PGSS parameters in the wax encapsulation.

In order to be able to achieve these goals, the following research questions were formulated:

- Is the PGSS process cost-effective?
- What are the variables that most influence the particle's morphology?
- What are the variables that most influence particle size?
- What is the flow character of the produced powder?
- What are the conditions that most influence the encapsulation efficiency?
- Which mixture of coating materials is best for encapsulating an enzyme using PGSS?
- What is the most suitable particle size for encapsulation?
- What is the spray temperature at which particles begin to crystallize? And what is the temperature at which we have 100% crystallized particles?
- Does the velocity of the spray decrease as the spray cools down?
- With which nozzle there is a higher higher amount of gas entrained in drum?

1.3 Outline of the Thesis

Chapter 2 covers a literature review of some important publications (articles, books and dissertations) related to microencapsulation where a coating material was used, the industrial applications of microparticles, an overview of current micronization techniques, supercritical fluids (CO_2) and their applications; the development and the concept of the PGSS process, as well a short explanation of the mathematical model used.

Chapter 3 covers a concise overview of the materials and methodologies used in this thesis.

Chapter 4 focusses on presenting and discussing the results of this thesis. The results are analysed against PGSS process parameters used for microparticles production. Also, the obtained results will be evaluated and compared with other similar products obtained before at Feyecon, and a mathematical model will be used for the final confirmation.

Chapter 5 encompasses all conclusions made from this project and the contributions of this study for possible futures works or reports.

2

2 Theoretical Background

2.1 Microencapsulation and Microparticles

Microencapsulation is a rapidly expanding technology that has been developed in the last years. It is widely used in the food, pharmaceutical and cosmetic industries in order to maintain the stability, efficiency, and bioactivity of various active compounds**.** This technology is used to entrap micron-sized particles of solids, droplets of liquids and/or gasses in an inner shell material. The purpose of microencapsulation is to isolate and protect the sensitive active ingredients from the adverse environment while enabling their controlled release at the desired time, rate, dose, and site of action. This technology prevents external reaction or degradation linked to interactions with environmental factors.

As result of this process microparticles, microcapsules, microspheres and microemulsions can be obtained, which differentiate in terms of morphology and internal structure. These microparticles vary in size, composition and function. When the particle size is ranged between 1-1000 µm they are called as microparticles, microcapsules or microspheres. Particles larger than 1000 µm are known as macroparticles. Particles below 1 µm are termed as nanoparticles, nanocapsules and nanospheres.

The usual structure of microparticles consists of two components, core material (inner component) and shell or coat material (outer component). The core material represents an active ingredient or the substance needed to be protected/released. While the coating material covers and protects the core material. **(Fig. 2.1)**

The main goal of the coating materials is to protect a generally unstable substance from outside influences. In food and cosmetics, for example, external factors such as water, oxygen, bacteria, enzymes, light, heat, are considered as external factors of risk which affects directly the stability of the active ingredients. [27][28]

There are many different types of coatings materials or matrixes, or mixtures of coating materials, and their selection for microencapsulation depends on their inertness towards core material, availability, chemical compatibility, and stability. In addition the physical-chemical properties, including cohesiveness, permeability, sorption, solubility, clarity, and stability for target-selected delivery must be assessed. [9][29]–[31]

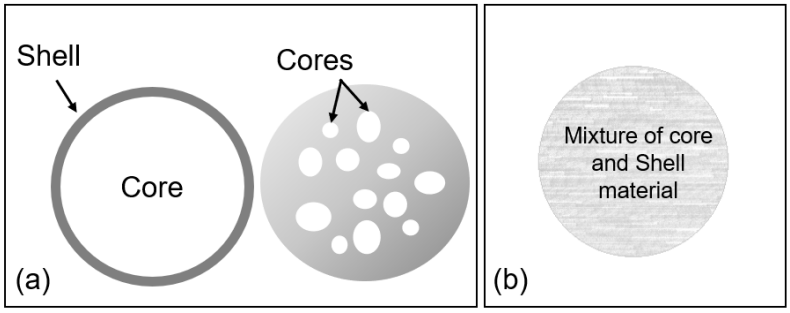

Figure 2.1. Structure and type of microparticles:(a) single-core and multi-core microparticle; (b) microsphere; Adopted from [32]

2.1.1 Wax and fat as Coating Material

The selection of any coating material depends on the field of application, and the desired characteristics of the final product. In our case, a cosmetic company has an interest in stabilising an enzyme in a water continuous cleansing cream. Therefore, we used the PGSS process to find a better type of coating to protect the enzyme. This coating material cannot have a high melting temperature (because high temperatures can alter enzyme activity or break enzyme down) and needs to protect the substance of water damage (because it is for a water cleansing cream). Also, it was in the interest of the company that the coating material was natural.

Therefore, we decided to use as coatings hydrophobic materials which have medium/high melting points (solid at ambient conditions). So, this type of coatings are insoluble in water, and at ambient conditions their physical state is solid. We decided to use as a coating a mixture of waxes, fats and oils for this project. The basis of our choice was the fact that these materials present the properties characteristics mentioned before. Also, these materials are natural, non-toxic, cheap, renewable and powdered wax is especially useful in specialized coatings. Additionally, fats and waxes have already been used in the PGSS process, since they present to be a significant molecular weight and thus can melted at moderate temperatures. [19][27][33]

Waxes, fats and oils are mixtures of lipids and are constituted by hydrophobic organic substances containing medium and long-chains of carbons atoms. Normally, they present long-chain

esters hydrocarbons, long-chain carboxylic acids, free fatty acids sterols etc. These compounds have different physical, chemical and physiological properties. [28][29]

Microencapsulation processes based on supercritical fluids have already proved to successfully yield coated particles made out of various fats, oils, waxes and their mixtures as coating materials which did not alter the functional properties of the loadings, (e.g. volatile oils, flavours and nutraceuticals). Also, they have ensured targetted controlled release profiles. Such processes have high yields of around 90% producing particles of 1-200 μm size. The shape of the particles are generally spherical or irregular (broken particles) depending on the ratio CO_2/hydrophobic coating. [33]

Powdered wax is especially useful in specialized coatings and present many advantages. **(Fig. 2.2).** Micronized wax presents high resistance to surface scratching, as well as high chemical and abrasion resistance. Also, it presents reduced gloss at the surface due to its structure that can migrate to the surface coating. Waxes coatings present a non-stick character that decreases the tendency for preventing unwanted transfer or adhesion. They are hydrophobic materials, and therefore they can block moisture migration. In addition, waxes present a smooth feel and texture can be rough or fine depending on the size and shape of the particles. Lastly, they support the release of air bubbles. [35]–[37]

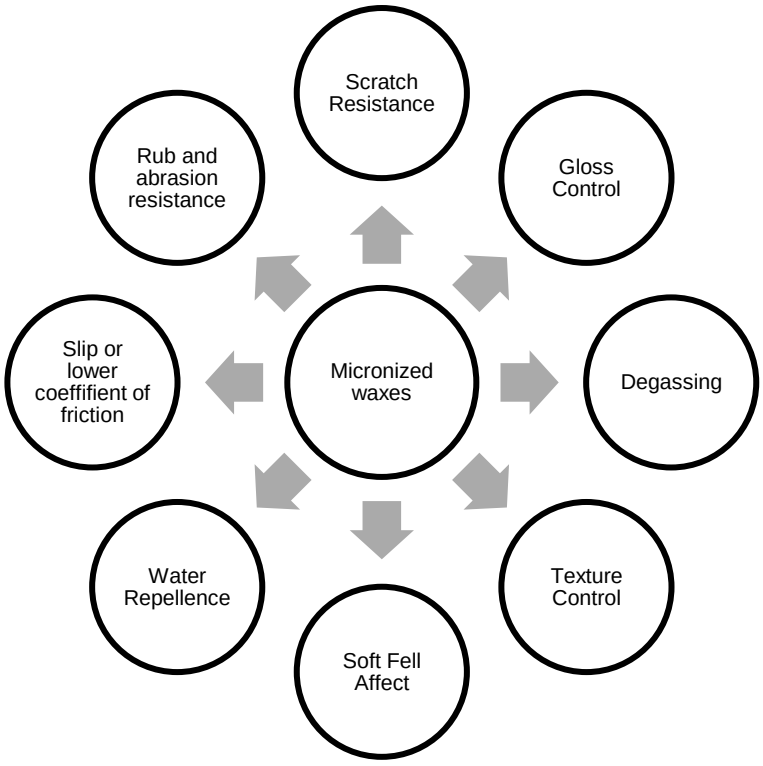

Figure 2.2 Advantages of Micronized wax

2.2 Industrial applications of Microparticles

The pharmaceutical, food and cosmetical industries are the first beneficiaries of this technology. There are various well-established procedures to produce micronized particles using $scCO_2$ (chapter 2.4).

Later, from these basic processes, new variants supporting new applications have been developed. These applications targeted composite particle formations, coating of solid or liquid dosages, obtaining of liposomes, etc. Micronised drugs are desirable for drug targetting and controlled release systems. The creation of capsules promoted an increase in bioavailability providing reliable and stabilised drugs medicines. The application of the obtained products is quite wide from topical applications (in creams, unguents, etc.) to aerosols (inhalators) or solid formulations with specific targeted diseases. The success was so great that there are already microparticles for cancer treatments.[29][38][39]

Similarly, in the cosmetic industry, there is a wide variety of products (of beauty creams, lotions, shampoos and toothpaste) that require different types of texture. Micronisation technology allows obtaining the necessary quality in products. In addition to micronization, encapsulation is key to the formulation of cosmetic products. Thanks to this technology, lipophilic active compounds can be incorporated into aqueous dispersions without the need for a solvent and hydrophilic ingredients can be delivered in hydrophobic systems, to improve skin permeation. Also, it is possible to encapsulate essential oils for solid perfume (the capsule preserves the fragrance) and active ingredients like enzymes for a beauty cream. The combination of both techniques permits the protection and preservation of active ingredients and enhances their penetration in the skin. An excellent cosmetic application using microparticles is exfoliating cream to scrub in the skin with solid particles removing the dead cells and the impurities. This product is made from micronized polymer powders produce with some additives and compounds, with excellent properties excellent for exfoliation. In addition, there is a great interest in the microencapsulation of vitamins, slimming agents, skin-moisturising agents, or compounds for energising, perfuming, refreshing, relaxing and UV protection, and also to improve the firmness and elasticity of the skin. Thus, we can conclude that micronization can produce biologically beneficial and safety products for the cosmetic field.[9][40]–[42]

Several food components, especially nutrients like antioxidants and vitamins, are unstable at certain conditions of temperature and humidity, losing their natural flavour and colour, limiting their availability in food processing. Encapsulation can help prevent food degradation by exposing antimicrobial compounds, inactivating microbes and inhibiting enzymes, thus promoting food stability and preservation. Therefore, creating processes and formulations is crucial for stabilizing and solubilizing food. Micronization guarantees the efficient use of active agents, decreasing fermentation time and improving dissolution rate, thus indulging the quality and viability of products at low cost.[8][10][43]

2.3 Microparticles production: Techniques

There are many chemical and physical techniques to produce micro and nanoparticles. Among the methodologies used in the formation of microparticles (the conventional techniques), there is one that has been recently studied and that has shown promising results. Microencapsulation using supercritical fluids (SCF) is a technology that has received setup attention from the scientific community in the past few years, and it is called a "green technology" [11][20]

While classic processes can produce particles with reduced size of high viscous materials, methods using SCFs offer a wide range of applications for micronization and encapsulation. Besides, classical approaches have shown to have several disadvantages and limitations such as thermal and chemical solute degradation, high residual solvent concentration and structural changes of the particles. **(Table 2.1)** Furthermore, typically these techniques present problems in controlling and distribution on the particle size.

Despite this, the biggest concern of using these processes was environmental due to excessive use of solvents which are toxic and dangerous to the environment, to the people involved in the manufacturing industry or the final user. [1][7][8][11][44]

Table 2.1. Disadvantages of Conventional techniques for microparticles production [44]

Process	Disadvantages
Milling, Grinding, Pulverisation	Broad size distribution, High Temperatures, Loss of crystallinity, Large particles
Lyophilization-sieving	Broad size distribution
Spray Drying	Broad size distribution, High Temperatures, Thermal degradation
Precipitation	Broad size distribution, Residual solvent, Agglomeration, Excessive use of solvents
Coacervation	Residual solvents, Excessive use of solvents
Interfacial polymerisation	Residual solvents and additives
Impregnation	Residual solvents, High temperatures

Since the appearance of the compressed fluids in the early 1990s, such as supercritical fluids (SCFs), in industrial processes, they have been progressively replacing the conventional techniques used until then, due to their far less potentially damaging environmental impact. The supercritical fluid technology shows to be a better alternative by being economically friendly and sustainable. It

was developed to minimize environmental impact, by reducing energy consumption, reducing toxic residues and producing better quality and safer materials in manufacturing.

Another advantage of this technology is the reduced complexity of the processes. The processes that use this technology have a reduction of steps improving control and understanding.

Furthermore, the SFCs demonstrated their capacities to replace toxic industrial solvents. So we can conclude SFCs are viable, beneficial for the environment, cost-effective and provide a possibility of getting new products. Therefore, numerous supercritical fluids processes for a micro-particles generation have been developed, and some industries have started to use these processes. [14][45][46]

The technology has already been used in various industries and applications like in food preparation, pharmaceutical products, functional material, micro/nanosystem, and biofuel. [14][45][46]**.**

The processes that use SCF technology produce controlled-size particles with a narrow particle size distribution, crystal structure, and surface properties through the control of parameters and processing equipment. They use some distinct properties of gases at supercritical conditions, such as adaptable solvating power and selectivity that can be obtained by varying pressure and temperature. Additionally, they do not leave any residues in the final materials. [47]–[49]

Among the available supercritical fluids, supercritical carbon dioxide is ($scCO_2$) is the most used in the industry. In addition, besides non-toxic, the critical conditions are easily achieved, making it the best alternative for replacing organic solvents. Furthermore, CO_2 at ambient conditions is a gas, simplifying the solvent residues problem. Also, the use of carbon dioxide in the industry promote high purity products and allows the micronization of thermolabile compounds. [50]

2.4 Supercritical fluids properties

A fluid is supercritical (SCF) when its pressure and temperatures values are above the critical point determined by T_c (critical temperature) and p_c (critical pressure). The critical point represents the end of the vaporization curve in the p.T. phase diagram and the highest temperature and pressure at which the substance can exist as a vapour and liquid in equilibrium. **(Fig. 2.3)** Above the critical temperature, it is impossible to liquefy a gas by increasing the pressure. The intermolecular hydrogens bonds and polarity as well as the molecular weight of the substances cause an increase of both critical values (T_c and p_c).

Once at the supercritical contions, the surface tension is nearly zero; there is no more separation of liquid and gas phases. A supercritical fluid exists in a unique phase, having its macroscopic appearance with a homogeneous and translucent system.

In the supercritical region, the substance has physicochemical properties (density, viscosity and diffusivity) intermediate between those of the liquid and gas. **(Table 2.2)** The SCFs exhibit mass transfer like gas properties, by having lower viscosity like a gas, which ensures them a high diffusivity (compared to the liquids). Nevertheless, at the same time, they present densities like a liquid, which provides a good solvation power. In addition, these characteristics are straightforward to manipulate near the critical point, by a slight change in pressure and temperature. Additionally, near the critical point, the compressibility and the heat capacity are much higher than in the other conditions. So, in conclusion, the SFCs present low surface tension, low viscosity, high diffusivity and density-dependent solvating power. [18][19][24][43][45][51]–[54]

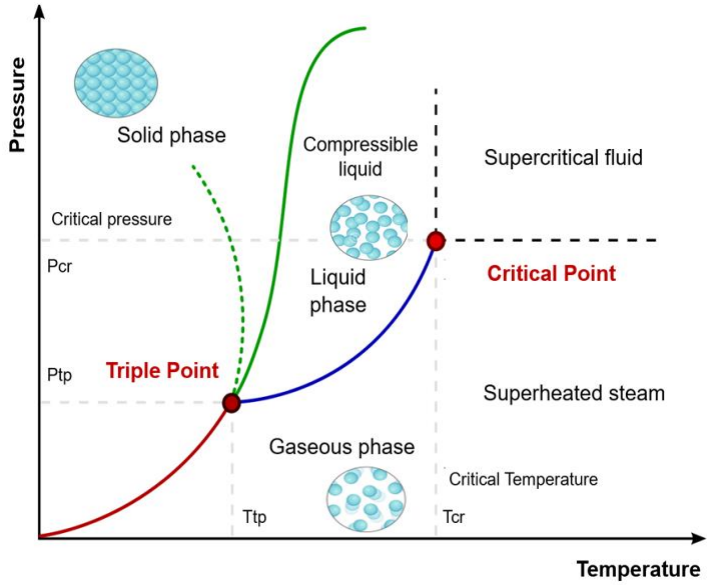

Figure 2.3 Phase diagram of supercritical fluid. Adopted from [55]

Table 2.2. The physicochemical properties of gases, supercritical fluids and liquids [53]

	Gas	SCF	Liquid
Density ρ (kg/m^3)	**1**	**5x10^2**	**10^3**
Viscosity μ (Pa.s)	**10^{-5}**	**10^{-4} – 10^{-5}**	**10^{-3}**
Diffusivity D (cm^2/s)	**10^{-1}**	**10^{-3} – 10^{-4}**	**10^{-6}**

Supercritical fluids have also unique recognized thermophysical properties. For example, the density of the gas increases significantly with the pressure, increasing its ability to dissolve compounds without increasing its viscosity. [53]

2.4.1 Carbon dioxide as supercritical fluid

The most used SCF is carbon dioxide (CO_2), and it is the most suited solvent for SFE in comparison with other compounds. CO_2 is considered inert, non-flammable, non-toxic; it exists in large quantities, has low cost, and high purity. Supercritical carbon dioxide acts like a lipophilic solvent. Additionally, it has a low critical point, having a critical temperature and pressure of 31ºC and 73.8 bar, which is suitable to process with heat-sensitive materials. **(Table 2.3).** Besides that, its moderate critical temperature allows working near to ambient temperature with slight above the critical pressure. However, CO_2 presents limitations on the solubility of most compounds with high molecular weight and non-polar behaviour and therefore has little affinity for polar compounds. Even so, carbon dioxide can act as a solvent, as anti-solvent or solute depending on the application and phase equilibria.

SCO_2 is advantageous due to its selectivity and solvation power which are easy to adjust by controlling temperature and pressure. Furthermore, its low critical conditions, allow processes at mild conditions, reducing the process cost and energy, the equipment is more simple and cheap, and avoid thermal or chemical degradation of the final product. [18][45][51][56]

Also, carbon dioxide is known as the main greenhouse gas produced and released by oil and gas, coal and hydrocarbon plants. [57]

Due to its numerous advantages and properties, CO_2 is the most used supercritical fluid in the nanomaterial field, thus being able to eliminate the solvents and lead to effective downstream processes.

Table 2.3. Critical points of some compounds [24]

Compounds	Critical Temperature (T_c) (ºC)	Critical Pressure (p_c) (bar)
H_2O	374	220
SF_6	46	38
N_2O	37	41
CO_2	31	74
CHF_3	26	47
Xe	17	59
C_2H_4	9	51

2.4.2 Comparison of supercritical fluids processes

Initially, $scCO_2$ was applied on a larger scale for decaffeination of coffee beans. Later the properties of $scCO_2$ were more valorized by putting them into technical solutions for new industrial applications like wood impregnation, drying, impregnation & dyeing and more recently in particle formation & micronization. These processes had great influences in the scientific micronisation community. Different review articles have supported the use of this technology in various processes. [51][58][59]. **(Table 2.5)**

The signficant difference between the above mentioned processes is the role of CO_2 in the process and its solvent strength and phase equilibira. Based on the solvent strength, we can separate the supercritical fluid methods in two mains groups: [60]

- The first group**:** Processes that are driven by the solvent power of CO_2:
    - CO_2 act as a solvent such as rapid expansion from saturated solutions (RESS)
    - CO_2 act anti-solvent, such as in the supercritical anti-solvent process (SAS).

Briefly, in the RESS process a solute is dissolved in supercritical fluid in a vessel forming a solution, and then the solution is rapidly depressurised over a heated nozzle at higher speed into a low-pressure chamber (atmospheric pressure). The rapid depressurisation provokes a dramatic and instantaneous decrease of the solvent power that causes faster nucleation of the substrate in tiny particles. As presented earlier, the RESS process has different approaches:

- RESSAS (Rapid Expansion of supercritical solution into aqueous solution);
- RESOLV (Rapid Expansion of Supercritical into a liquid solvent);
- RESS-N (Rapid Expansion of supercritical with a non-solvent);
- RESS-SC (Rapid Expansion of supercritical solution with solid co-solvent);

The differences between RESSAS, RESOLV and RESS, are in the spray. In RESS the solution is sprayed into atmospheric pressure, in RESSAS the solution is sprayed into the water-solvent mixture and in RESOLV into a liquid solvent. In the RESS-N a non-solvent is added to SCF and in RESS-SC solid co-solvent is added to SCF.[18][21][43][51]

SAS is a semicontinuous process that is applied mainly as a recrystallization technique for processing solids that are insoluble in the SCF. This method exploits the ability of SCFs to dissolve in organic liquids and to lower the "solvent power" of the liquids for the compounds in solution, inducing the solids to precipitate. Therefore, the first step is to dissolve the solid into an organic solvent. The resulting solution is put in contact with the dense gas which acts as antisolvent. The dense gas (such as $scCO_2$) dissolves partly into the organic solvent promoting solubility reduction and precipitation of the solid compound. The solvent with $scCO_2$ formes one phase which is consequently, separated into the CO_2 gas and solvent precipitates. The SAS process has different

methodologies based on the operation mode (that differs from SAS) and mixing models between solution and supercritical fluid: [20][25][26][61][62]

- Gaseous Ant-solvent (Gas) operates at batch mode;
- Solution Enhanced Dispersion by Supercritical Fluids (SEDS) operates at continuous mode (solution and $scCO_2$ are sprayed simultaneously through the coaxial nozzle);
- Aerosol Solvent Extraction (ASES);
- Precipitation by compressed fluid anti-solvent (PCA) operate at semicontinuous mode;

➢ The second group**:** Processes that are not driven by the solvent power of CO_2:

- CO_2 act as solute such as PGSS
- CO_2 act as co-solute such as CAN-BD, SAA, PGSS-drying and DELOS

The second group embrace all the methods that are not dependent on the CO_2 solvent strength. As an alternative, use as their advantage a large volume expansion and the great cooling effect generated by the depressurization of CO_2 as in Particles from Gas Saturated Solutions (PGSS). Other processes were subsequently developed: **(Table 2.4)**

Table 2.4 Differences between PGSS-based techniques [60]

Process	Liquid solvents	Saturation	Precipitation	Drying
CAN-BD (Carbon dioxide Assisted Nebulization with a Bubble Dryer®)	Water and alcohol	CO_2 solubilisation occurs in a low volume tee	Spray tower	With N_2
SAA (Supercritical Fluid-Assisted Atomization)		Packed tower	Spray tower	With N_2
PGSS-DRYING		Static mixer	Spray tower	With CO_2
DELOS (Depressurisation of an Expanded Liquid Organic Solution)	Organic solvents	Autoclave	High-pressure vessel equipped with a filter	With CO_2
PGSS (Particle from gas saturated solution)	-	High-pressure reactor with mixing or in a static mixer	Spray tower	-

In the CAN-BD, SAA and PGSS-drying processes the SCF acts as co-solute and use liquid solvents like water and alcohol. In CAN-BD and SAA, the solution is depressurised through a suitable device into the precipitator at atmospheric pressure to produce aerosols of micro-bubbles and micro-droplets that are dried by a flux of heated N_2. In DELOS process and SAA processes, the SCF acts as co-solvent and organic solvents are used. Additionally, in the DELOS and PGSS-drying processes, the microparticles are dried with CO_2 or N_2. [53][63]–[65]

In the PGSS process, the supercritical fluid acts as a solute. No organic solvents are used in oppsition to the anti-solvent or DELOS processes. In addition, there is no need to operate at high pressures like RESS process. Also, there is no need to use liquid solvents or any compound (N_2 or CO_2) to dried the substances such as co-solute processes. This process is used for micronizing solids that are not miscible in the $scCO_2$, but they can swell by the $scCO_2$ addition. It is a process suitable for materials that cannot be dissolved into $scCO_2$, but instead, $scCO_2$ can dissolve into these molten materials. Since this project is a study of the PGSS process, it will be explained in detail in the next chapters. [21][51][66]

Table 2.5 Classification of supercritical fluid processes according with CO_2 function [43][60][67]

CO_2 function	**Application**	**Process**	**characteristics**
Solvent	Compounds soluble in $scCO_2$	RESS	Supercritical solution spray into atmospheric pressure
		RESSAS	Supercritical solution spray into a water-solvent mixture
		RESOLV	Supercritical solution spray into a liquid
		RESS-N	Supercritical solution spray into a non-solvent
		RESS-SC	Solid co-solvent added to $scCO_2$
anti-solvent	Compounds with almost zero solubility in $scCO_2$, soluble in a solvent that has a good affinity with $scCO_2$	GAS	Batch operation; Organic solvents;
		SAS	Semi-continuous separation; Organic solvents;
		SEDS	Semi-continuous operation, $scCO_2$ and solvent mixed in tube injector; Organic solvents;
		ASES	semi-continuous operation; Organic solvents;
		PCA	Semi-continuous operation, CO_2 at subcritical conditions; Organic solvents;
solute	Compounds in which $scCO_2$ is soluble	PGSS	Depressurisation of melted substances, SCF removal; operates in continuous and batch mode
co-solute (aerosolization add)	Compounds with almost zero solubility in $scCO_2$, soluble in a solvent in which $scCO_2$ is soluble	CAN-BD	Low volume mixture for $scCO_2$ solution; Drying with N_2
		DELOS	Compressed CO_2 used to homogeneous cooling of the solution with solid particle precipitation; organic solvents; Drying with CO_2
		SAA	Enhance solubilization mixing $scCO_2$ solution; Drying with N_2
		PGSS-drying	Depressurization of Aqueous solution; operates in continuous mode; Drying with CO_2

2.5 Particles from Gas Saturated Solution (PGSS)

2.5.1 History and Applications

The first publication about PGSS processes was found earlier in 1982 (Graser and Wickenhauser) and later in 1995, Weidner and co-workers developed it further.[68]

A patent overview reveals that in fact PGSS had been used in 1979 when Graser and co-workers used the process without name it as PGSS, for making fine-milled organic pigments by crystallisation using supercritical fluids under high pressures and temperatures. [69]

Later the PGSS found new applications, for example in drying pollution-free adhesives by Kishimoto and co-workes in 1991. The adhesive prepolymer by manufacturing under high pressures is compressing with CO_2 followed by pulverisation on a surface to obtain dry particles. Also, this process does not use a significant amount of dispersion medium. [58][70]

Later, Union Carbide developed a technology for a powder coating, it called UNICARB. Union Carbide patented this process where a solid is suspended in a liquid carrier and mixed with a supercritical solvent. The mixture is then pulverised onto a substrate to form a coating. Countless patents described this process with a concept of using supercritical CO_2 to reduce the viscosity of the materials for paint application. [58][71]–[73] Also, another similar process was developed and patented by Nordson. [74] These two approaches involve the use of $scCO_2$ as anatomisation agent and as a solvent. Besides that, with this technology, it was possible to produce smooth and high-quality coatings without defects or bubbles. Also, there was a reduction in the release of volatile organic compounds. After that, Morton, Nippon Paint and Otefal Spa patented this technology to produce powder coating on a large scale.[58]

In 1994, the PGSS process concept was described by Mandell and patented by Ferro Corporation.[54] This process, named VAMP™ incorporated a mechanical mixing step before pulverisation. However, this process only claimed for paint coating materials applications. The mixing between supercritical fluids and the raw materials (resins, hardens, fillers and additives) causes polymers and resins to swell. Due to this, in this process, better results are obtained which was an improvement due to the additives in dispersion. This technology has many advantages that increase the quality of the product such as better colour control, hiding and gloss control. Besides, this technology used low temperatures, low shear forces and molecular weight control. [54][58]

A year later, in 1995, Weidner developed another patent which had a much broader claim than the Ferro's patent because it covered more materials. This technology quite resembles the previous one, altought it did not have a mechanical mixing step. Weidner created this patent and developed a batch process to prepare particles and powders and called Particles from gas saturated solutions process (PGSS). A supercritical fluid is dissolved into a melted substance or suspended in material

to produce a gas-saturated solution. This mixture is then expanded through a nozzle, and solid particles are formed due to the sharp temperature decrease induced by fluid expansion. [54][16]

Also, in the same year, Sievers patented a process related to PGSS, calling it the aerosolisation process, that permits the use of any material that is water-soluble. The active substance is dissolved into aqueous solutions and mixed under high pressure with scCO2 producing an emulsion. The supercritical emulsion flows through a restrictor, and it is rapidly decompressed to form an aerosol spray. This patent also describes a static mixer.[75]

In 1997, Karasawa patented a method of pulverising solid particles using supercritical fluids. The solid particles were suspended in a SFC, and the solution expanded through a jet to form particles. The significant advantage of this method is that agglomeration of the particles is avoided.[76]

After that, we can find several examples in the literature of the different materials used in the PGSS process. Reviews found in literature like the one from Weidner were important for the development of the knowledge of the process. [77] He discusses the thermo fluid dynamics aspects and their advantages. Also, the study of Knez considered this when he studied the micronisation of polymers. [77][78] The first material successfully produced as finely dispersed powder was Polyetheneglycols by Weidner. [79]

Furthermore, the process itself was studied and optimised by different reseachers. Kappler used polymer powders production to study the different morphologies at different conditions of the process (pre-expansion temperature, pressure and the CO_2 concentration) to evaluate how those variables change the properties of the final product.[61][80]

Petra Sencar-Bozic studied the particle size distribution under the influence of pre-expansion conditions of the PGSS, to improve the poorly water-soluble nifedipine. Also, Kerck used nifedipine, felodipine and the hypolipidemic agent fenofibrate in the PGSS. He studied the micronisation of insoluble calcium channel blockers of the materials (nifedipine and felodipine) with the purpose of increasing the dissolution rate and the biovability of these drugs.

Later, Rodrigues studied the effect of pressure on the particle size and morphology. He used the process for the particle formation of hydrogenated palm oil for new controlled-release of theophylline. [81]–[83]

Additionally, some researchers (Elvassore, Jun-li and Strumendo) investigated mathematically of the process. In these studies, we find a description of jet-spray hydrodynamics, fluid droplet dynamics, supercritical thermodynamics, crystallization kinetics, bubble formation and droplet coalescence. In 2003, Elvassore developed a thermodynamic analysis to interpret the influence of pressure and temperature in the process by studying the lipid system of micronization for pharmaceutical applications. A year later, Jun Li and co-workers developed a mathematical model for particle formation of hydrogenated palm oil by considering the nozzle hydrodynamic for the PGSS

process. The model is based on the atomization and crystallization mechanisms considering both the melt crystallization and the gas-solution crystallization. This model describes the change of the atomisation pressure, the temperature, velocity and density along with the nozzle. In 2007, Strumendo investigated the behaviour of an isolate gas-saturated solution droplet in a gaseous environment and developed a mathematical model that describes the transport phenomena within the droplet and in the surrounding atmosphere.[22][84]–[86]

In the literature, we can find few applications for the PGSS process and some reviews of the process. Jacques Fages and Jennifer Lung also discuss in their studies this technology. [58][87] Over the years, the PGSS process proved to have high potential by successfully processing and encapsulating numerous solids and liquids materials. It has been applied in processing polymers, resins, natural products and active pharmaceutical ingredients. Recently, it proved to be suitable for producing microparticles for food applications. Hydrogenated oils, phospholipids, mono and diglycerides, citric acid, menthol, β-carotene, cocoa butter, shea butter soy lecithin, sunflower lecithin, chocolate, palm fat, cheese and natural waxes are some examples of food products powdered with PGSS**.** [88] (**Appendix A** shows more materials produced with the PGSS process)

FeyeCon also developed for Unilever the light margarine concept based on PGSS of the fat mixture. The process was further patented and implemented on a large scale for margarine production. Basically, margarine is an emulsion formed by max 16% water, and 80% blends refined oils and fats. This kind of spreads is generally stabilized by the crystal fats which are seen as the structuring agents. Classical process bled the oils and fats at high temperatures and then slowly cools down the mixtures as the aqueous phase is added. This is an energy-consuming process which limits the water phase to max 20%. When using PGSS, the blends fats and oil phase is first crystallized (fat powder mixture) and then mixed with the other aqueous ingredients. By this process, one can produce aerated margarine (or light margarine) which contains fewer fats and more aqueous phase. This process can be used in processing different spreads, ice creams, etc. (Patents from feyecon [89]–[91])

Table 2.6 Literature Review of some materials (fats, oils and wax) and pigment (β-carotene) of the PGSS process

Core Material	Coating Material	T (°C)	P (bar)	Morphology and size	Ref
β-carotene	poly-(ε-caprolactone)	50–70	110–150	110–650 μm	[92]
Lecithin	PEG 8000	40–50	150–300	0,37–2,4 μm	[93]
	hydrogenated Castor oil	90–100	70–250	60–90 μm	[94]
water	hydrogenated Castor oil	86–96	59–152	3–22 μm	[95]
Cydia pomonella granulovirus	Palm oil-based fat	65	100	23 μm Spheres	[96]
Cocoa power	-	32	-	3–10 μm	[97]
-	Rapeseed 70 (RP 70)	60–100	70–180	15–20 μm Spheres/ Aggregates	[94][15]
Cocoa Butter	-	20–100	200–320	Agglomeration of smaller particles	[98]
Theophylline	Hydrogenated palm oil	85	120–180	2–3 μm spheres/Needles	[83]
-	Hydrogenated palm oil	60–100	90–220	2–3μm spheres and crystals	[85]
-	Microparticles from anhydrous milk fat (AMP) and a diacylglycerol-based modified milk fat (D-AMF)	33–61	70–200	Spherical hollow and sponge-like particles	[99]
Menthol	Beeswax	60	60–200	2–50μm	[100]

2.5.2 Concept of the PGSS process

In the PGSS technique, a compressible gas ($scCO_2$) is dissolved under high-pressure conditions in a melted or liquid material. In this case, the supercritical fluid behaves like a solute. It is the process to produce microparticles of materials like fats, oils and polymers (substances with high-molecular-weight) that can absorb SCFs at high concentrations. In other words, the solubility of the supercritical fluids in melted materials is much higher than the solubility of these substances in SCFs. [19][53][67]

In the PGSS process, the materials are always melted, and when these materials mix or are saturated with CO_2, a gas saturated solution is generated. The solution is formed as the concentration in the molten solute increases with increasing pressure. These solutions and easier to spray because the SCF dissolved reduce the viscosity and surface tension. Also, the initial materials suffer a significant reduction in their melting temperatures by mixing with $scCO_2$. (e.g., up to 30 wt% in PEG with pressure less than 15MPa) [17][19][25][67][79]

The solubilisation of $scCO_2$ reduces the melting point of the materials (leading to melting point depression), decrease the viscosity and increases the formation of tiny droplets after the expansion. [61]

This melting point depression effect allows to spray materials that under classical conditions are difficult or impossible to pulverise. The intensity of melting point depression depends on the quantity of CO_2 that solubilise into the substance as a result of molecular interactions between dissolved CO_2 and the compound of interest. Determination of solid-liquid transitions in pressurised systems is essential as it gives us the information about the pressure needed to melt the substance of interest and form a liquid phase at a given temperature.[24]

In conclusion, PGSS is the chosen process for substances that are not quite soluble in SFCs, but they can absorb high amounts of it. Furthermore, this process eliminates solubility limitations and there is no need of using large quantities of gas. [17]

A schematic representation of a PGSS setup is shown in **figure 2.4.** The design is composed of solvent cylinder, cooler, high-pressure pump, heater, autoclave and expansion chamber of precipitation.

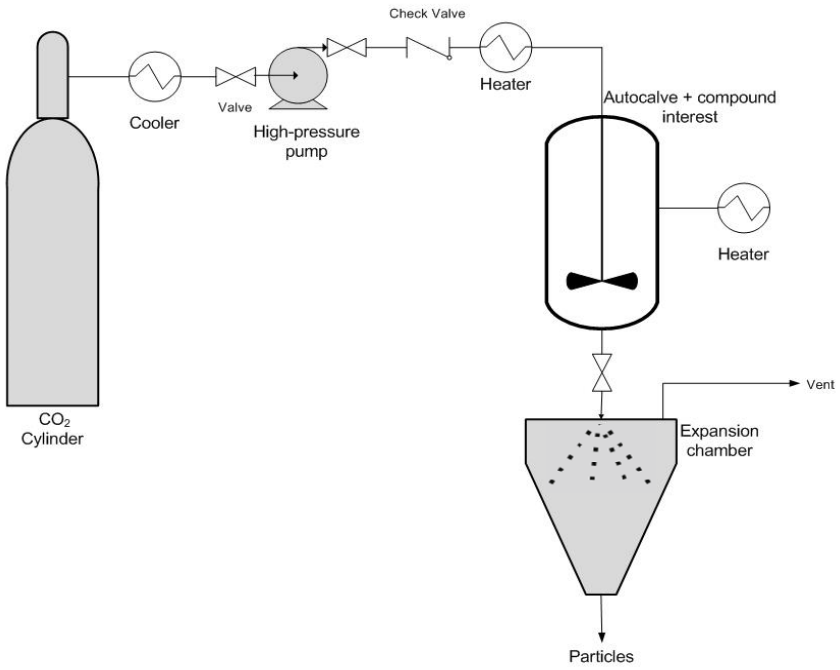

Figure 2.4. Schematic representation of the PGSS process. Adopted from [4]

As mentioned before, PGSS is a process to obtain microparticles by the formation of a saturated supercritical solution. In this method, $scCO_2$ is a solute and fed into the high-pressure vessel. The compound of interest is solid, that is melted and stirred with CO_2 until a certain pressure is reached (pressurisation). The CO_2 is dissolved into the molten material, resulting in a gas saturated solution (typically contain between 5-50 wt% of the compressed gas) combined with a viscosity reduction. After intensive mixing, the saturated melt solution is quickly expanded through a nozzle into a spray tower at a lower pressure (usually ambient).[17]–[19][24][53][54]

This quick expansios leads to the release of CO_2 with a significant effect thanks to the energy consumption, finally leading to the precipitation of the compounds, thus, inducing the formation of solid or liquid particles. [24]

In other words, this expansion caused by the rapid depressurisation is what it turns the melted substance into small droplets or particles. Also, in the meantime, the intense cooling produced by the Joule-Thomson effect (decrease of the temperature during an adiabatic expansion) generate solidification of the droplets. Thereby due to a high supersaturation, the CO_2 evaporates from the droplets. It was thus causing the precipitation and solidification of the particles due to a decrease in temperature. This solidification is rapid because of the direct heat transfer from particles into the CO_2. [17][18][25][53][61]

Therefore, during expansion, the Joule-Thomson effect can induce a fast reduction in temperature, causing particle formation by the solidification of the material.[19]

The PGSS process can be run in batch (high-pressure vessel) or continuous (static mixer) modes as shown in **figure 2.5**

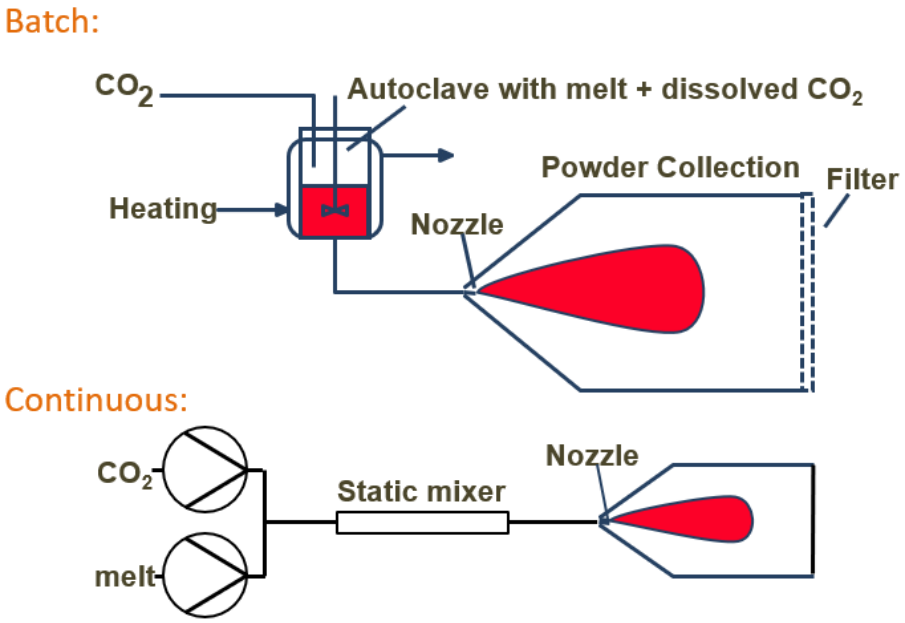

Figure 2.5 Scheme of the PGSS process in batch and continuous mode (with permission of Feyecon Development in the Netherlands)

Typically, in this process spherical particles are obtained with a size range from 10 µm to 100 µm (higher than those obtained via RESS or SAS). The morphological properties of the particles depend on several parameters.[19]

In general, adjusting some parameters such as the amount of SCF used to dissolve into solution, pre-expansion temperature and pressure, the geometry of the nozzle, pressure and temperature of spray tower and even the geometry of the equipment used to perform the process can control the morphology product. **Figure 2.6** shows the influence of the concentration of CO_2 and melting temperature in the morphology of the particles. These parameters are those that will be studied in this thesis, and chapter 2.5.3 will be further discussed.[19][24][53][101]

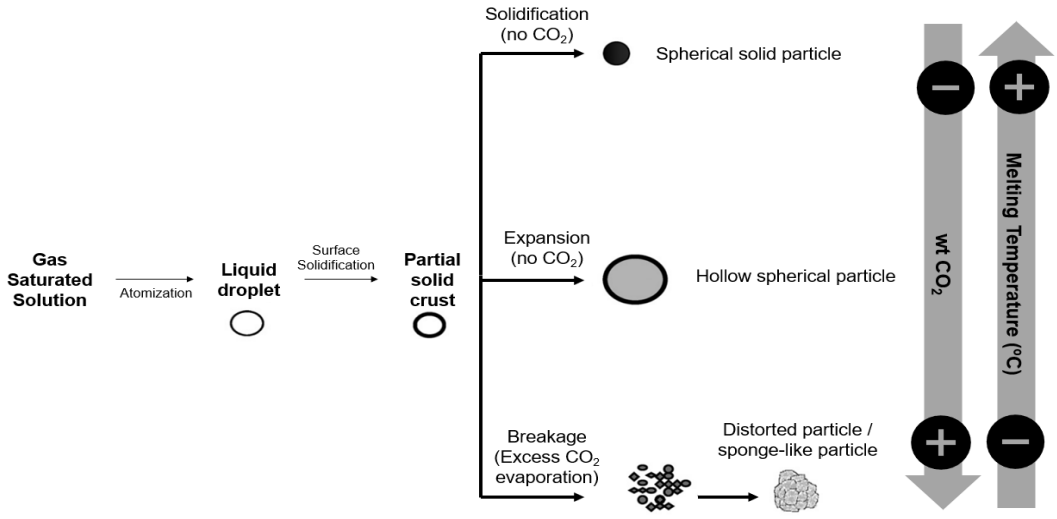

Figure 2.6 Different particles obtained by the PGSS process, at increasing %w CO2 and decreasing the melting temperature. Adopted from [55]

2.5.3 Influence of Parameters in PGSS

As mentioned before, the properties of the powders can be adjusted by some process parameters. The experimental results demonstrated these parameters: pre-expansion temperature and pressure, spray tower temperature, GPR and size of the nozzle are the most critical for the PGSS process. Our goal is to obtain small and spherical particles without gas entrapped inside. [23][24][80][101]–[107]

Pre-expansion temperature:

The pre-expansion temperature influences the properties of the used substances, such as viscosity, density and solubility of CO_2 in the high-pressure vessel. The viscosity and density of sprayed substances will decrease with the increase of the temperature. Because of this, the solubility of CO_2 in the vessel will decrease. This fact will influence the solution formation in the vessel. The pre-expansion temperature together with the spray tower, will affect the solidification time of the particles, and as consequence the morphology and the size of the obtained particles. The decrease of solubility of CO_2 in the static mixer, leads to a decrease in the solution atomization. Promoting particle size reduction and increasing the number of spherical particles. [99]

Pre-expansion pressure:

The pre-expansion pressure has more influence on the solubility of CO_2 in the solution and particularly in the fatty phase and influences the spraying of the mixture. Thereby, increasing pre-expansion pressure will lead to better solubility of CO_2 in the mixture. In consequence, the viscosity and the melting point of the shell material in the vessel will decrease. Promoting increasing of the atomization and therefore finer and smaller particles will be produced. The particles will be more spherical too. As pressure increase, smaller particles and lowers values of bulk density are obtained. However, the more we increase the pressure higher the influence of the amount of CO_2 used. Because of this, the amount of CO_2 will be more significant, and so there will be more gas entrapped inside the core of the particles. [99]

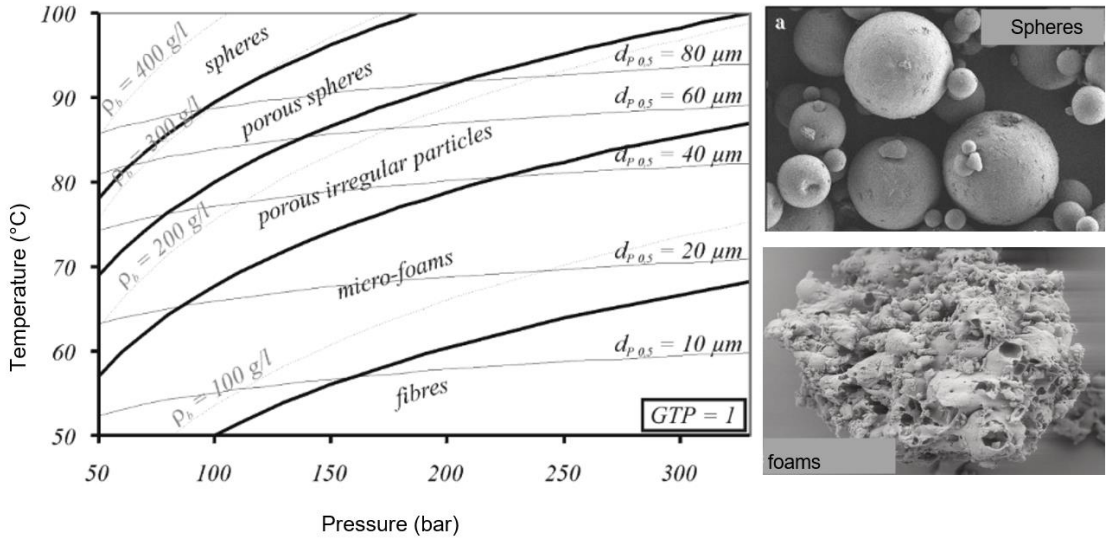

Figure 2.7 The influence of pressure and temperature on morphology, mean size of the particles and bulk densit. Adopted from [61]

Spray-tower temperature (quantity of cooling put inside the drum):

The spray tower temperature influences the solidification time of the droplets produced after spraying. Therefore, decreasing the drum temperature leads to an increase of the solidification speed. However, the CO_2 entrapped in the capsules may not have enough time to diffuse from the coating material, causing holey and burst particles. In addition, the increase of the temperature of the drum, will cause more particles to clump together (more agglomerations). Under these circumstances, the particle size and bulk density of the powder will increase.

Gas to product ratio (GPR):

The gas to product ratio (GPR) is the gas (CO_2) mass flow divided by the sum of the core and the shell materials mass flows.

$$GPR = \frac{\dot{m}_{gas}}{\dot{m}_{core} + \dot{m}_{shell}} \quad \textbf{(Eq.2.1)}$$

The gas to product ratio influences the solidification time of the droplets, and also the properties of the obtained particles such as particle size and bulk density. If we increase the GPR, it implies a decrease in the amount of the mixture in the vessel. Therefore, the speed of solidification and cooling of the droplets in the spray tower will increase, due to the Joule-Thomson effect. Due to this, the number of burst particles will increase, and the particle size and value of bulk density will decrease. [99]

Size of the nozzle: [108]

The nozzle design influences the atomization of the spray because of droplets directly formed at the orifice of the nozzle. The structure of the nozzle is shown in **figure 2.8**. The size of the particles increases with the increasing of the nozzle disc orifice diameter. We obtained bigger particles because, at the exit of the nozzle, the density and pressure of the fluid will decrease significantly.

Also, to pulverize less mass of material from the nozzle in each spray, it is better to use diameters with a smaller bore. That way the solidification is slower, leading to smaller particles. However, the particles will be less spherical because of the shear forces applied to the capsule.

Furthermore, a smaller bore diameter leads to a lower mass of a substance from the nozzle for each spray, leading to smaller particles, slower solidification but also less spherical particles because of the shear forces applied on the capsules.

Lastly, the core of the nozzle influences the dispersion angle during spray. The spray angle influences the repartition of the powder in the drum (sided or bottom) and consequently the size and distribution of the particles.

Figure 2.8 Structure of the nozzle, (with permission of Spray Drying Systems in the Netherlands) [109]

2.6 Mathematical Model

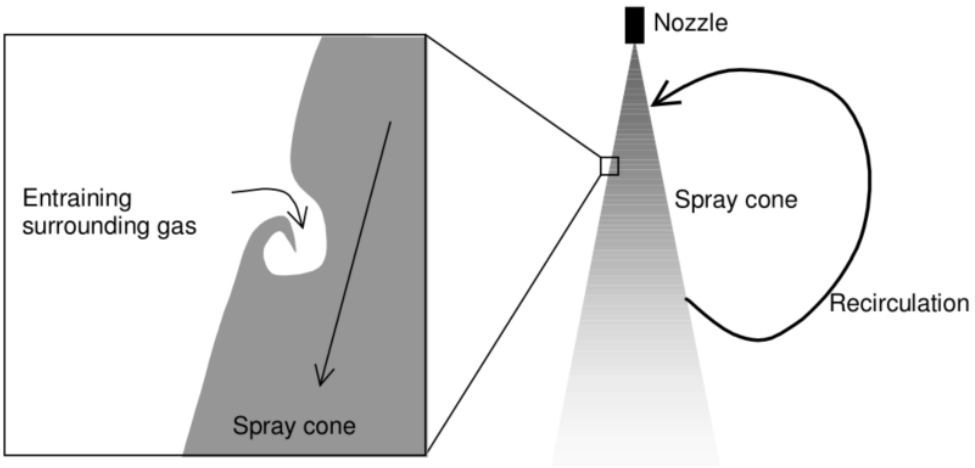

Figure 2.9 Mechanism of gas entrainment (with permission of Feyecon Development in the Netherlands)

As mentioned before, dense gas-assisted spray processes are able to produce either powders or composites. In this thesis, we studied the PGSS process using fats, waxes and oils. The PGSS, uses CO_2 as dense gas for two purposes, one for mixing with the fat and the other for cooling the drum. It ensures that the drum is cold enough so there are no clumped particles since the spray occurs inside the drum. In conclusion, the interaction between CO_2 and the fact, affects the final product, the powder.

The mathematical model used establishes the dependence of two gases (entraining CO_2 gas and CO_2 from the atomization) on the final product, based on the theory of entrainment of the surrounding gas. Also, it considers that the spray from the nozzle has a cone shape. **(Fig. 2.9)**

This mechanism is triggered by applying different velocities in both the spray and the surrounding gas (cooling gas), thus forcing the cooling gas to be entrained by the spray. However, the entrainment of gas in sprays only occur when the velocity of the spray is much higher than the surrounding gas. Furthermore, according to the model, the amount of entrapped gas increases linearly with the distance from the nozzle. Also, depending on the amount of cold gas entrained, more cold the spray will be, and slower the spray velocity will be.

In some cases, the surrounding gas is so cold promoting its cooling capacity that it produces dry ice. In this model, for the calculations performed, we assume that the surrounding gas in the spray chamber is all at gaseous state.[110]

Before using the equations of the model, we calculated the initial mass flow of CO_2, Q_i (kg/s) trough the equations provided by the Spraying Systems company. The equation **(Eq. 2.2)** depends solely on the type of nozzle chosen and the pressure selected to spray.[108]

$$Capacity\ of\ liquid\ being\ sprayed = Capacity\ of\ water \times \frac{1}{\sqrt{Specific\ gravity}} \quad \textbf{(Eq.2.2)}$$

After calculating the initial mass flow of CO_2 (Q_i), we used the following equation **(Eq. 2.3)** to calculated the total mass flow of spray, Q_t (kg/s):

$$Q_t = Q_i \times K \times \frac{x}{d} \times (\frac{\rho_s}{\rho_i})^{0,5} \quad \textbf{(Eq.2.3)}$$

Note: This equation is valid when the flow is "full developed," i.e. at x/d>15.

Also, the equation **(Eq. 2.3)** is only valid when Re > 5000. So it is necessary to confirm Reynolds number with the following equation **(Eq. 2.4)**:

$$Re = \frac{\rho_t \times v_{spray} \times d_{cone}}{\mu} \quad \textbf{(Eq.2.4)}$$

Due to the preservation of momentum, the average velocity of the spray is calculated by the following equation **(Eq. 2.5)**:

$$v_{spray} = \frac{v_i \times Q_{initial}}{Q_{total}} \quad \textbf{(Eq.2.5)}$$

When cooling gas is supplied co-currently in a confined tube:

$$v_{spray} = v_{gas}$$

Where v_{gas} is the average velocity of the cooling gas (cooling gas volume >> expanded fat-gas mixture). The pressure difference before and after spray when supplying cooling gas co-currently is given by:

$$\Delta P = \frac{Q_i \times v_i}{\pi \times \frac{1}{4} \times dspray\ vessel^2} \quad \textbf{(Eq.2.6)}$$

For the calculation of the diameter of the cone, the following equation **(Eq. 2.7)** was used:

$$d_{nozzle}^2 \times v_i \times \rho_i = d_{cone}^2 \times v_f \times \rho_t \quad \textbf{(Eq.2.7)}$$

The average temperature in the spray is calculated by the following equation **(Eq. 2.8)**:

$$T_{spray} = (C_{p,gas}.T_{gas}.(Q_t/Q_i - 1) + \Delta H_{cr,fat}.(1 - fr_{gas}) + \Delta H_{exp,gas}.fr_{gas} + C_{p,fat}.T_i.(1 - fr_{gas}) + C_{p,gas}.T_i.fr_{gas})/(C_{p,gas}.(Q_t/Q_i - 1) + (C_{p,fat}.(1 - fr_{gas}) + C_{p,gas}.fr_{gas}) \quad \textbf{(Eq.2.8)}$$

This mathematical model considers, that the α-crystallisation is dependant on the temperature of the spray. Therefore, $\Delta H_{cr,\,fat}$ is a function of T_{spray}:

$\Delta H_{cr,fat} = 0$ for $T_{spray} > 35$ °C

$\Delta H_{cr,fat} = C_1.(35 - T_{spray})$ for $-5 > T_{spray} > 35$ °C

$\Delta H_{cr,fat} = 77{,}4$ KJ/kg fat for $T_{spray} < -5$ °C

With $C_1 = 77{,}4/40 = 1{,}93$ kJ/kg.K

3

3 Materials and Methods

3.1 Materials

The CO_2, 99.998% of purity, was provided by Air liquid (Netherlands). The red pigment was a mixture of anthocyanins produced and supplied by Feyecon Development & Implementation B.V. The Lecithin, 20% of purity, was provided by Lycotec (U.K.). The materials used for coating material were used as received without any further purification. All materials in **table 3.1** are fats and for that reason, are not soluble in water and only soluble in oils or organic solvents.

All materials chosen are 100% natural and from plant origin, except beeswax which is produced by bees (animal wax).

Jojoba wax is extracted from the seed of the jojoba tree. This wax is produced via a chemical-free hydrogenation process using the unsaponifiable matter of jojoba oil. [111]

Beeswax is the material that bees use to build their hives. It is produced by bees that secrete it as a liquid through their wax glands. Beekeepers extract beeswax by a different process; it is subjected to hot water or steam to melt the wax, then leaks are made to increase its purity. It is a very stable material and highly appreciated by its properties.[111]

Macadamia wax is produced via a chemical-free hydrogenation process using the unsaponifiable matter of macadamia oil. The nuts of macadamia produce macadamia oil.[112]

Sunflower oil is obtained from the sunflower seed. Sunflower seeds are processed by cold extraction to get the oils. Sunflower oil extraction involves cleaning the seeds, grinding, pressing, and extracting the crude oil and then refining. This oil contains a high concentration of vitamin E and low levels of saturated fat. [111]

Revel A (micronised fat powder) is a fractionated, non-hydrogenated, refined palm oil of non-lauric origin. It may be suitable as a structuring fat, a stabilising fat in peanut butter and as a crystallising aid in lauric fat based compound coatings.

Cocoa Butter is a natural fat found in cocoa beans and is removed during the manufacturing process of chocolat, being separated from the cocoa mass by pressing. [111]

Lecithin is an emulsifier, and it is a mixture of phospholipids in oil. It is produced by soybean oil. [113]

Table 3.1 Physical properties of materials [83]

Name	Supplier	Appearance	Colour	Density 25°C (g/mL)	Melting Temperature (°C)
Jojoba wax	Naturally Balmy (U.K.)	Solid (Flakes)	White	0.863–0.873	67–73
Beeswax	Dewerkbij (Netherlands)	Solid (Flakes)	Yellow	0.950–0.965	62–64
Macadamia wax	Worlée (Netherlands)	Solid (Flakes)	White	0.921–0.929	65
Sunflower oil	Lidl (Netherlands)	Liquid	Yellow	0.915–0.919	-
Fat powder	Bunge Loders Croklaan (Netherlands)	Solid (Flakes)	White	-	50–65
Cocoa Butter/Powder	Lycotec/ Callebaut (Netherlands)	Solid	White/Brown	0.973–0.980	31–33

3.2 Macro Test

As mentioned before, one of the purposes of this thesis is to produce a loose and fine powder that does not melt immediately at ambient temperature, for a project. Before we run the test in PGSS, we made some macro tests. The purpose of these tests was to choose which mixture of waxes, fats and oils would be run in the PGSS process. The tests were performed as follow: melting two compounds at a certain temperature (Tm) and put the mixture in a petri dish. After that, we waited until the mixture solidified and in the next day the texture of the mixture was anlyzed by touch. **(Fig. 3.1) (Table 3.2)**

Table 3.2 Macro test made for a cosmetic project

Test	Compound 1	Compound 2	Emulsifier
1	50% Beeswax	50% Sunflower oil	-
2	75% Fat powder	25% Cocoa Butter	-
3	50% Jojoba wax	50% Sunflower oil	-
4	90% Macadamia wax	10% Sunflower oil	-
5	75% Macadamia wax	25% Sunflower oil	-
6	50% Macadamia wax	50% Sunflower oil	-
7	75% Macadamia wax	25% Cocoa Butter	-
8	50% Macadamia wax	50% Cocoa Butter	-
9	50% Beeswax	50% Cocoa Butter	-
10	75% Jojoba wax	25% Sunflower oil	-
11	75% Fat powder	25% Sunflower oil	-
12	50% Jojoba wax	50% Fat powder	-
13	75% Jojoba wax	25% Fat powder	-
14	50% Macadamia wax	50% Fat powder	-
15	75% Beeswax	25% Fat powder	-
16	25% Macadamia wax	75% Cocoa Butter	-
17	75% Fat powder	25% Cocoa Butter	0.5% Lecithin
18	75% Jojoba wax	25% Cocoa Butter	0.5% Lecithin
19	50% Jojoba wax	50% Cocoa Butter	0.5% Lecithin
20	25% Jojoba wax	75% Cocoa Butter	0.5% Lecithin
21	50% Cocoa Butter	50% Sunflower oil	0.5% Lecithin

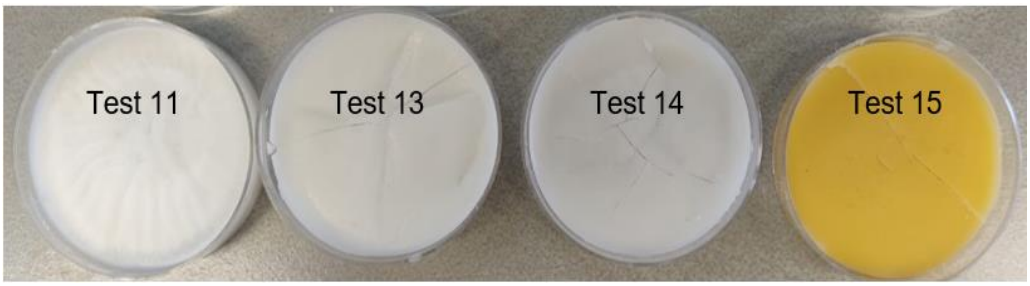

Figure 3.1 Examples of some macro tests

3.3 PGSS process apparatus

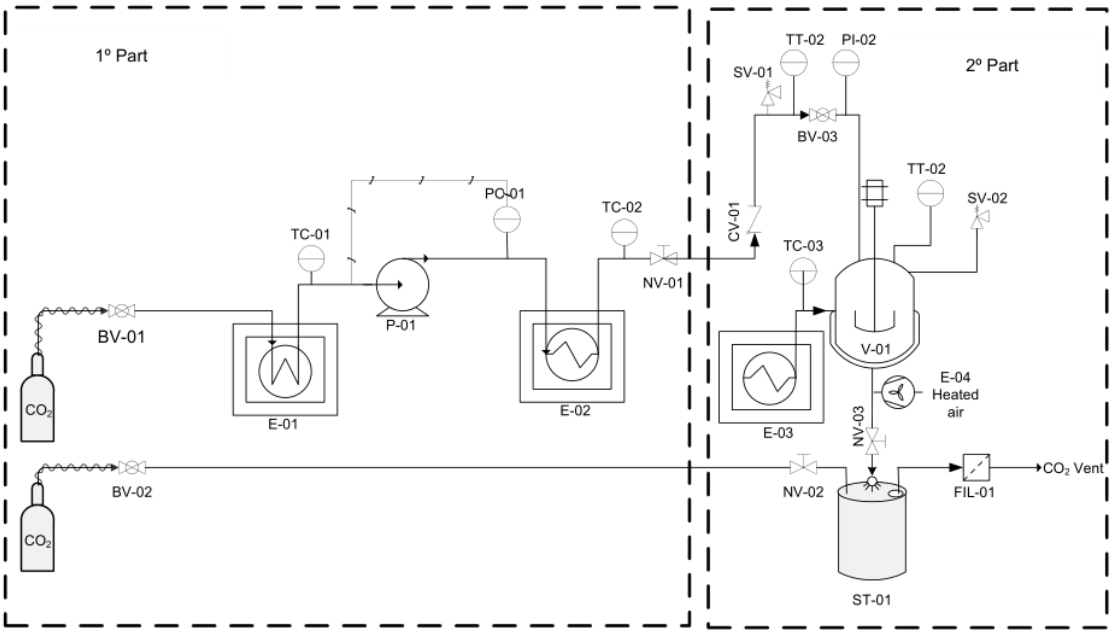

Figure 3.2 Schematic diagram of the **P**article from the **G**as **S**aturated **S**olution process (PGSS) apparatus.

The apparatus used for the experiments was built by Feyecon Development & Implementation B.V. **(Fig. 3.2).** In **appendix B** is the PFD of the PGSS and figure/illustration of all the equipment used. The system can be separated in two parts: the first part consists in CO_2 pressurization and heating, and the second part consists in the formation of the gas saturated solution and its expansion through the nozzle into atmospheric pressure.

In the first part, the process is constituted with two bottles of CO_2, a cooler unit (E-01), a pump (P-01) and heater bath (E-02). One bottle of CO_2 has a function of cooling the drum (the drum needs to be very highly cooled or else the particles will be warmed and will form aggregations), and the other is for the CO_2 entering the system. The second bottle is on a scale and has a sensor to control (weight in Kg) how much CO_2 is spent during the process.

The cooling unit has a function of condensing the CO_2 before entering the liquid pump.

First, the CO_2 enters in the system to be cooled down in the heat exchanger (E-01) before being pumped (P-01) to the heater bath (E-02). After heating and pressurizing the CO_2, it enters into the vessel. The pressure of the pump is controlled with a sensor. The cooler (E-01) and heater bath (E-02) have a system with sensor for controlling the temperature.The first part is finished at this stage.

The second part is formation of the particles. The CO_2 is mixed with the molten fat inside the vessel (V-01), forming the gas saturated solution which is then expanded through a nozzle into the cooled drum. The equipment is constituted by a high-pressure precipitation vessel of stainless steel, with a volume of 1L with a mechanical stirrer. The vessel is connected to a heating bath (heater E-03). The setup temperature of this heater controls the temperature of the vessel, and pressure is controlled with a sensor on a vessel. This unit has one more heater (E-04) that has the function to heat the pipeline connecting the vessel and nozzle. This whole unit needs to be very hot so that the mixture does not solidify in the process. The system was designed for a maximum pressure of 300 bar. In a typical essay, the mixture (CO_2 and molten fat) was stirred for 50 seconds and then depressurised through a nozzle (0,5 mm) and sprayed into a cooled drum (ST-01).

3.3.1 Experimental Procedure

Figure 3.3. PGSS apparatus (Valve A (BV-03) – Injected CO_2 in the system)

All trials/experiments are conducted following a similar procedure. **(Fig. 3.3 and 3.4)**

First, we need to set the temperature of the heaters E-02 and E-03 (both heaters must be at the same temperature) and pressure of the pump (P-01). The setup temperature is always 10°C above the melting point of the fat chosen. After melting the fat in a microwave, we put the melted fat into the heated pressure vessel that is then closed. We turn on the third heater (E-04) and open both bottles of CO_2. Following we open the first valve (A) and the pressurised fluid is injected into the vessel. We start to stir for 50 seconds (turn on the mixer). The CO_2 and liquid fat are mixed. After the desired pressure is reached, we open the second valve (B) allowing the

mixture to expand through the nozzle. Finally, the particles are sprayed into the drum and collected. After we collect the powder, and its weight is measured with a scale.

We measure the weight of the powder twice. Once after the process and other is the next day because it will have CO_2 entrapped in the microparticles or even ice.

Figure 3.4 PGSS apparatus (Valve B (NV-03) – sprayed microparticles)

3.4 Microparticles Characterisation

3.4.1 Bulk Density

The bulk density is an important property of the powders for transport and storage purpose. It is desirable to have a high bulk density because of the packaging, storage and transportation cost. Many properties influence the bulk density, such as the size and shape of the particles. Also, the manufacturing procedure and conditions influence the bulk density. In general, non-spherical particles have a low bulk density, and spherical particles have higher bulk density. [114]

The bulk density of the powder is measure according to the standard method. A specific volume of the powder is poured in a cylinder (45 ml), and the weight of the known volume is measured. The bulk density is defined as the mass of the particles (m_{powder}) of the material divided by the fixed volume (v_{powder}) that they occupy. **(Eq. 3.1)** [115]

$$\rho_{bulk} = \frac{m_{powder}}{v_{powder}} \quad \textbf{(Eq.3.1)}$$

3.4.2 Tapped Density

Tapped density was measured by transferring approximately 7,5g of microparticles into a 45ml measuring cylinder. The cylinder is then mechanically tapped, and the volume occupied by the microparticles was measured. Tapped density is estimated by using the following formula. [115] **(Eq. 3.2)**

$$Tapped\ Density = \frac{Weight\ of\ the\ microparticles}{Bulk\ volume\ of\ microparticles} \quad \textbf{(Eq.3.2)}$$

Tapped density values are higher for more regularly shaped particles (i.e., spheres), as compared to irregularly shaped particles such as needles.

3.4.3 Compressibility index and Hausner ratio

The compressibility index (CI) is a measure of the propensity of a powder to consolidate. This index is important for interparticle interactions of the particles.

The percentage of compressibility of microparticles was determined by using the following formula **(Eq. 3.3)**, where V_0 = untapped apparent volume; V_f = tapped apparent volume; ρ_{tapped} = tapped density; ρ_{bulk}=bulk density.

$$CI\ (\%) = \frac{(V_0 - V_f)}{V_0} \times 100 = \frac{(\rho_{tapped} - \rho_{bulk})}{\rho_{tapped}} \times 100 \quad \textbf{(Eq.3.3)}$$

Hausner's ratio is an important flow property. It is the ratio between tapped density and bulk density. It is calculated by using the formula of **(Eq. 3.4).** [115]

The Hausner ratio measures the ability of the powder particles to rearrange, and it is an indicator of the compressibility. It also measures the powders cohesiveness. Since generally, the structure of a cohesive powder collapses significantly on tapping whilst a free-flowing material has a low tendency for further consolidation. Therefore, a drop in Hausner Ratio indicates a decrease in the powder cohesiveness.

$$Hausner's\ Ratio = \frac{V_0}{V_f} = \frac{\rho_{tapped}}{\rho_{bulk}} \quad \textbf{(Eq.3.4)}$$

Table 3.3 The scale of Flowability for Compressibility Index and Hausner Ratio [90]

Flow character	Compressibility index	Hausner ratio
Excellent	≤10	1.00–1.11
Good	10–15	1.12–1.18
Fair	16–20	1.19–1.25
Passable	21–25	1.26–1.34
Poor	26–31	1.35–1.45
Very poor	32–37	1.46–1.59
Very, very poor	>38	>1.60

The higher values of the Hausner ratio and compressibility index indicate the powder is more cohesive and more compressible and less compact.

3.4.4 The yield of collected particles

The yield of the collected particles obtained in the PGSS process was determined by the ratio of the mass of particles obtained after micronisation (W2) and the quantity of mass initially introduced in the vessel (W1). [92][116] **(Eq. 3.5)**

$$yield\ (\%) = \frac{W2}{W1} \times 100 \quad \textbf{(Eq.3.5)}$$

3.4.5 Microscopy

Optical microscopic analysis was carried out to estimate the particle size. The microscope used was manufactured by Olympus and was equipped with RisingView imaging software. The particle size measurements were performed at four different magnifications, 4X, 10X, 20X and 40X for all samples.

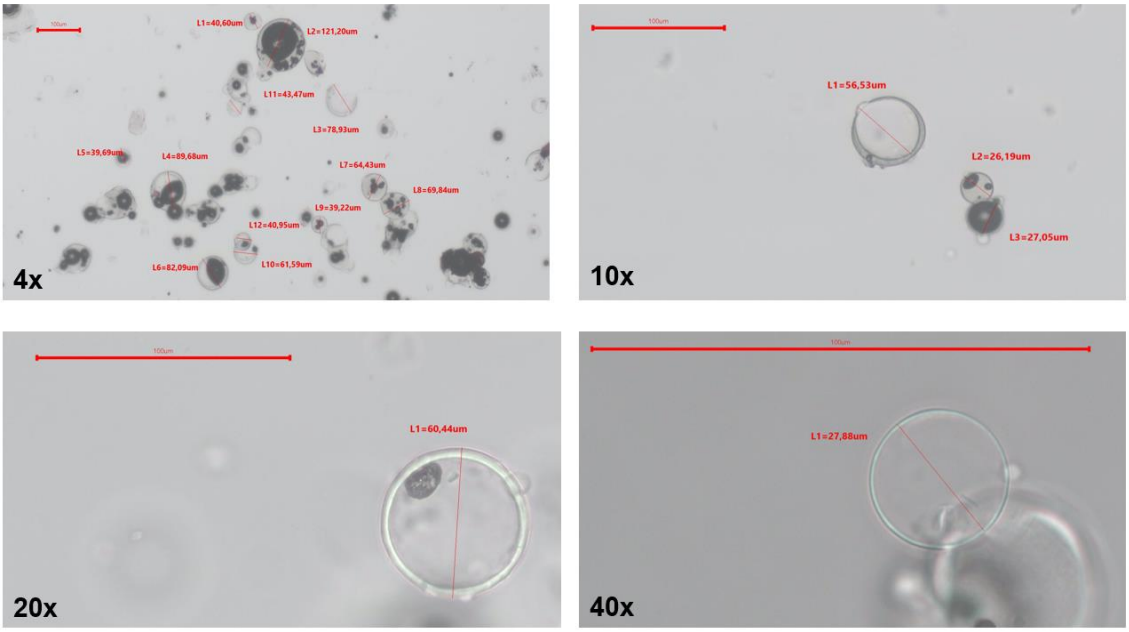

Figure 3.5 Example of particles measured at four different magnifications

3.4.6 SEM

The morphology and the surface structure of the particles were investigated using a Phenom ProX Scanning Electron Microscope (SEM) at Feyecon Development & Implementation B.V. The SEM used was manufactured by Phenom-World and using Phenom Prosuite v.2.9 imaging software. The accelerator voltage for scanning was 15.0 kV.

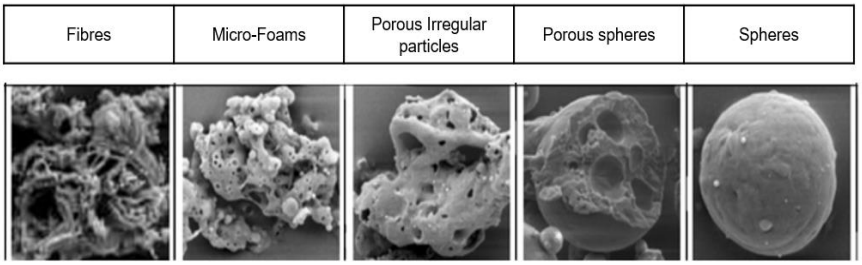

Figure 3.6 Types of particle shape taken by SEM. Adopted from [80]

3.4.7 Spectrophotometry

The pigment concentration was measured by spectrophotometry, and two calibration curves were calculated. **(Appendix B.3)**

To determine the efficiency of the microencapsulation of the particles with the red pigment, absorbances of the different powders produced were measured. To be able to calculate the efficiency of the microencapsulation, two absorbances were measured. One sample is previously heated to 70ºC for 1min, and another sample analysed is without heating.

The spectrophotometer used was a Helios Omega UV-vis equipment from Thermo Scientific.

A scanning spectrum was previously performed, for which the maximum absorption wave compressed was selected, and a calibration straight (Lambert-Beer Law) was performed at the same compressing (520nm) to relate absorbance, with the concentration of the measured solutions.

For the construction of the analytical standard curve, an aqueous solution was prepared with the pigment with a concentration of 1mg/ml. This mother solution was used to prepare the more diluted solutions, in 10mL volumetric balloons and the volume was supplemented with distilled water in order to obtain solutions of different concentrations (0.1 mg/ml, 0.2mg/ml, 0.3mg/ml, 0.4mg/ml, 0.5mg/ml).

The different absorbances were measured for the different concentrations three times, and the two calibration lines were thus obtained, and concentration of the pigment in each powder was calculated.

The encapsulation efficiency is calculated by the following formula **(Eq. 3.6).**

Where c = concentration of the pigment.

$$EE\% = \frac{c\ without\ heating}{c\ heating} \times 100 \qquad \textbf{(Eq.3.6)}$$

3.4.8 Design of experiments (DoE)

Design of experiments (DoE) is a statistical method used in many industries of investigation, such as the Pharmaceutical industry to maximise the efficiency of scientific work and minimise waste and cost. It is recommended to investigate the development of any method. [117] This concept is a smart choice and very useful because, in fewest experiments, it is possible to obtain a lot of information.

The major advantage of DoE is to reduce the number of required experiments and perform the research of the process faster and more effective. [118] Additionally, another advantage is the interactions between factors. An interaction results when the effect of one factor is dependent on the level of another. The effect that occurs when the combined change in two factors produces an effect greater (or lower) than that of the sum of effects expected from either factor alone.[119]

The usual terminology adopted refers factors as the conditions to be varied in order to obtain a determined response, variables are the responses obtained by the employment of different factors, and levels are the values varied in each factor.

The maxima, minima and how trend parameters are changed are given by an empirical function, a model, usually linear or quadratic with interaction terms and a graphical relation is created where are randomisation of the experiments guarantee that any uncontrollable variables contribute to the repeatability variance and replicates in order to have statistical significance.

We used an experimental design to find which factors are the most significant that will influence more the response of an experiment. After that, we will study the significant factors of the process and discover how to optimise the process itself.

In literature, we can find several studies of PGSS using experimental design that indicate which factors affect more the result in the process. Taking that into account, 3 factors were chosen: temperature, pressure and quantity. In the PGSS process, the responses of most interest are particle size, particle size distribution, and yield. [117][120][121]

In the present work, the optimisation of the response residues are the minimisation of the particle size and the bulk density and maximisation of microencapsulation efficiency and process yield.

In the present study, we will use a full factorial design to determine the significant effects of the model. A response surface design was then used for modelling a curved surface to the selected continuous factors. [122]

In **table 3.5** are summarised the experiments of full factorial design for the PGSS process. In **table 3.4** is represented the meaning of each sign in the matrix of **table 3.5**. In this experiment, we performed two repetitions with the purpose to discover the experimental deviation between them. The central points are used to estimate the error when we only get one observation by experience.

Table 3.4 Process parameters range used in the Full Factorial Design

Test	-1	0	1
Temperature (°C)	76	83	93
Pressure (bar)	75	120	150
Quantity (g)	50	100	300

Table 3.5 Full Factorial Design with standard order for the PGSS micronisation

Test	Quantity	Temperature	Pressure
1	+1	-1	-1
2	+1	-1	+1
3	-1	-1	-1
4	-1	-1	+1
5	+1	+1	-1
6	+1	+1	+1
7	-1	+1	-1
8	-1	+1	+1
9	0	0	0
10	0	0	0

The responses obtained by the experimental work are used. A factorial model is then constructed using a list of coefficients multiplied by associated factor levels. This model is in the form of presented in **equation 3.7**.

$$Y = \beta_0 + \beta_1 A + \beta_2 B + \beta_3 C + \beta_{12} AB + \beta_{13} AC + \beta_{23} BC \quad \textbf{(Eq.3.7)}$$

Where β, is the coefficient associated with factor n, and the letters A, B, C represent the factor in the model. Combinations of factors, such as AB, represent an interaction between the individual factors in the term.

STATISTICA then runs the ANOVA test. The results given allow determining the significance of the model.

4

4 Results and Discussion

This chapter presents the results of experiments performed with the PGSS process. One of the purposes of this study is to produce fine and loose powder without agglomerations by varying the conditions and parameters of the PGSS process. Therefore, we performed a study of the characteristic properties of the powder concerning the process used. Sections 4.1 and 4.2 presented the results of the powder and the process obtained under different conditions. The study performed in section 4.1 is a more global one, and we study all possible conditions. Section 4.2 presents the results of the Design of experiments (DoE): full plan factorial 2^3 with the addition of 2 central points of 3 conditions we choose (Quantity, temperature and pressure). We expected that this statistical analysis was able to confirm our results and observations of section 4.1. Section 4.3 presents the manufacturing of different powders with different materials for the cosmetic project. The mathematical model results for the PGSS process are presented in section 4.4. We studied the average temperature and velocity of the spray depending on the nozzle used. Also, we observed the dependency of diameter cone of the spray with % fat crystallized.

4.1 Influence of process conditions of particle formation

This section presents the characteristics properties of the powders under different conditions. The investigated properties are the size and morphology of the particle, the bulk density and flowability of the powder. Also, it presents the results of encapsulation efficiency as well as the yield of the process. In this part of our study, we always use the same materials, Jojoba wax as coating material and red pigment as core material. Also, we used sunflower oil to dissolve the pigment before mixing with Jojoba wax. We start to perform a standard sample for comparison purposes. After that, we perform different test varying pressure, temperature, the quantity of the mixture and the pigment loading **(Table 4.1).** Also, we used four different nozzles

provide by Spraying Systems. **(Table 4.2)** Lastly, we performed a test without stirring. In the other tests performed, we stirred the mixture for 50 seconds. **Appendix B.2** briefly describes the calculations performed for flows of Jojoba wax and carbon dioxide.

Table 4.1 Different conditions of the parameters studied in the process (Note: the range of temperatures chosen are based on the melting temperature range of the jojoba wax 68 – 73 °C)

Parameters				
Pressure (bar)	75	100	120	150
Temperature (°C)	76	83	93	
Quantity (g)	50	100	200	300
Pigment loading (%)	1,00%	5,00%	10,00%	20,00%

The different nozzles selected varied in core type, orifice diameter and spray angle:

Table 4.2 Different nozzles used to study the process

Nozzle type	**Core type**	**Diameter (mm)**	**Spray angle (°)**
63M	SKY 16	0.093	88
80M	SKY 20	0.340	51
76M	SKY 17	0.500	59
70M	SKY 21	0.710	59

As already mentioned, we performed all experiments of the PGSS process in the same way, varying the different types of parameters (varying only one condition and fixing the remaining conditions). In total, we performed 16 tests (**Appendix C** presents the remaining results obtained). For the realisation of the standard sample, we used 76M; SKY 17 for the nozzle and we stirred 50 seconds. The conditions used and the results obtained are in the following table: **(Table 4.3)**

Table 4.3 Conditions of parameters and results of standard sample

Test	Standard	
Parameters	Pressure (bar)	120
	Temperature (°C)	83
	Quantity (g)	100
	Pigment loading (%)	1
	nozzle diameter (mm)	0.5
Results	% wt CO_2	80
	GPR	1.7
	Yield (%)	80%
	Mean size (µm)	42
	Bulk density (kg/m^3)	173
	Tapped density (kg/m^3)	246
	CI (%)	30%
	Hausner's ratio	1.4
	Flow Character	Poor
	EE%	66%

4.1.1 Influence of the pressure

Table 4.4 Particle size, bulk density, % wt CO_2, GPR and yield of collected particles (%) by varying pressure

Test number	Pressure (bar)	Particle size (µm)	Mean size of particles (µm)	Bulk Density (kg/m^3)	% wt CO_2	GPR	Yield %
2	75	55–83	67	191	67	0.8	88
3	100	32–91	56	179	75	1.3	91
1	**120**	32–50	42	173	80	1.7	80
4	150	21–29	25	95	89	3.4	85

From **table 4.4**, it is possible to observe that the particle size distribution ranged between 21 and 91 µm. As it was expected, the size of particles increased with the decrease of pressure. **(Fig. 4.1)** According to the literature, increasing the pressure the size of particles decreases. Also, due to the Joule-Thomson effect, the particles are cooled very quickly, thus producing finer and smaller particles. However, by increasing the pressure, it will increase the wt% CO_2 and therefore, less spherical particles are obtained because we will obtain more trapped gas inside in the particles, as shown in **figure 4.2**. For instance, at 150 bar, we used 0,8 kg of CO_2, and at 75 bar,

we only used 0,2 kg of CO_2; Lastly, it is observed an increase in GPR (because of the increase on the quantity of CO_2 used) leads to a reduction in the particle size. **(Fig. 4.3)**

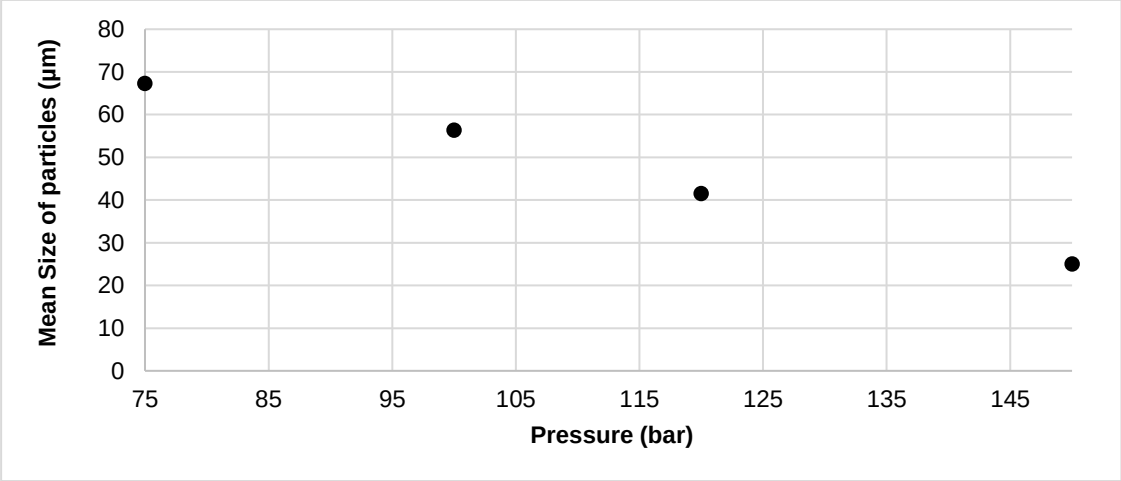

Figure 4.1 Mean size of a particle under the influence of pressure

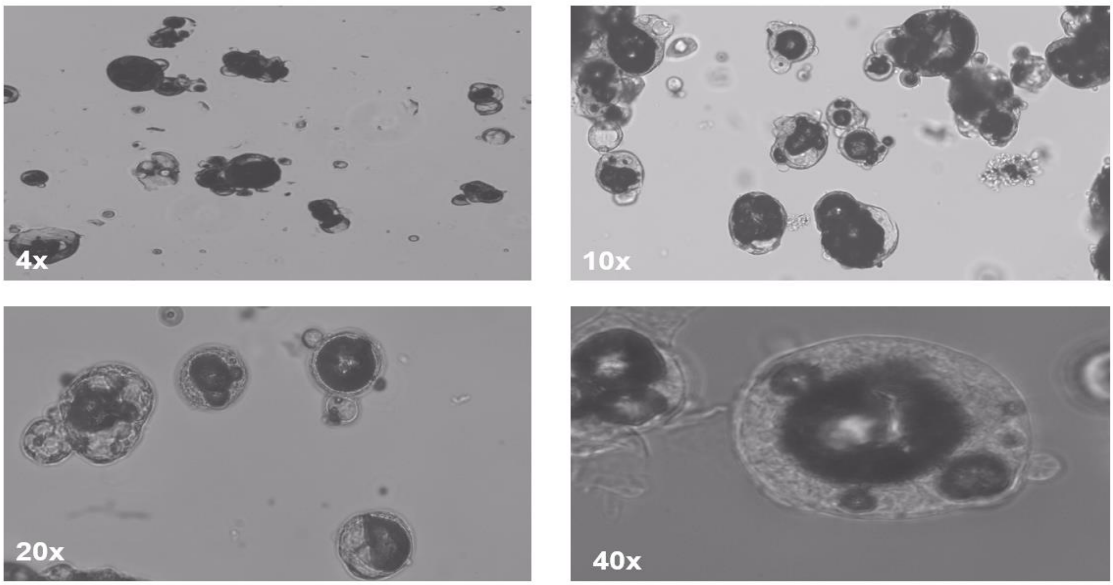

Figure 4.2 Microscopy picture of the particles at 150 bar with differents magnifications (black stuff represents gas trapped inside in the particle)

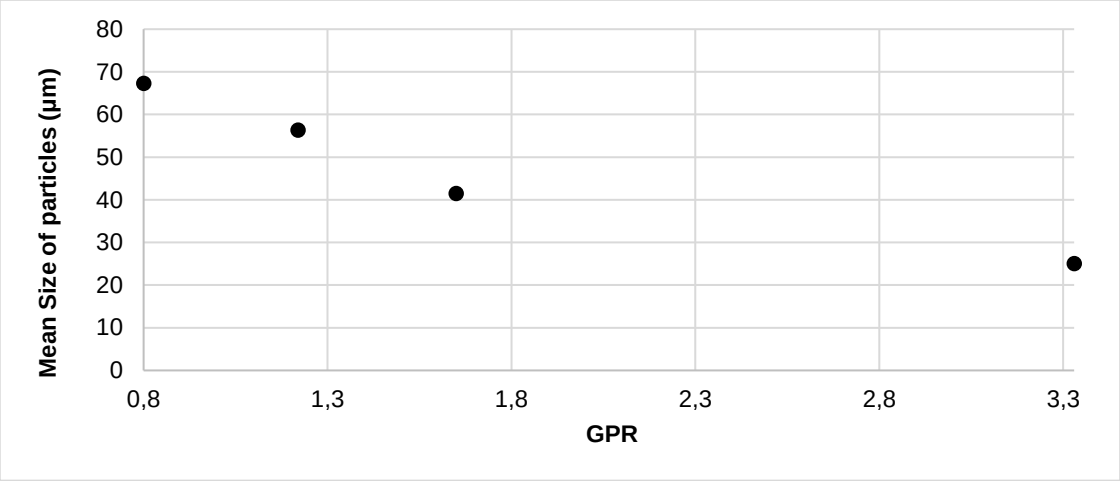

Figure 4.3 Mean particle size under the influence of GPR

In **figure 4.4**, the powder bulk density is plotted versus the pressure. Bulk density demonstrates a comparable dependence on the pressure as the particle size. As it was expected, the bulk density increases with the decrease of pressure. According to literature, an increase in pressure leads to finer/smaller particles with more porous morphologies. Consequently, lower bulk density values are achieved.

In contrast, lower pressures lead to bigger particles, with fewer with spherical porous shape and possibility of more particle agglomerations generating higher values of bulk density. The bulk density at 150 bar had the lowest value (95 kg/m^3) and at 75 bar had the highest value (191 kg/m^3). Test 4 presents the lowest value of bulk density of all the tests from section 4.1.

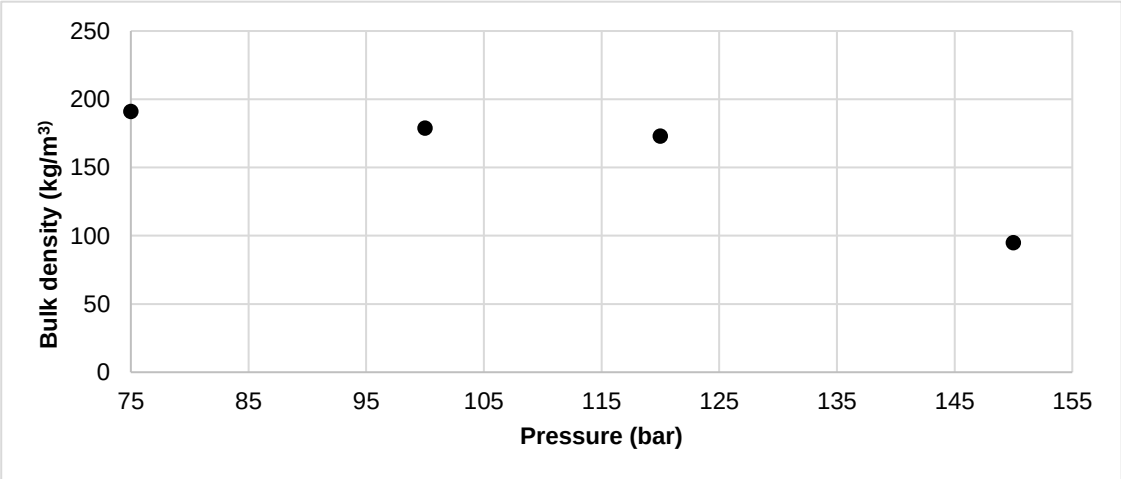

Figure 4.4 Bulk density under the influence of pressure

The flowability of the powder was studied by calculating the compressibility index and Hausner's ratio from the bulk density and tapped density. The flow character is presented in the following table:

Table 4.5 Tapped density (kg/m^3), Compressibility index (%), Hausner's ratio and Flow character by varying pressure

Test number	Pressure (bar)	Tapped density (kg/m^3)	CI %	Hausner's ratio	Flow character
2	75	293	35	1.5	Very poor
3	100	260	31	1.5	Very poor
1	**120**	246	30	1.4	Poor
4	150	117	19	1.2	Fair

The flow character at 150 bar is fair, meaning fine particles. The flow character at 75 bar and 100 bar is very poor, meaning the powder is very cohesive and compressible. The flow at 100 bar is poor meaning is cohesive but less than at 75 and 100 bar. The powders from tests 2, and 3 have higher values of compressibility index, and the Hausner's ratio indicates that they are highly compressible powders. The powder from test 4 is more fluidised compare to the one produced in test 1. Test 4 has the lowest value of tapped density, CI (%) and Hausner's ratio in section 4.1.

Table 4.6 Encapsulation Efficiency (%) and Outside (%) by varying pressure

Exp number	Pressure (bar)	EE%	% Outside
2	75	67	33
3	100	64	36
1	**120**	66	34
4	150	66	35

As we can see from **table 4.6**, the pressure is not a decisive factor for encapsulation efficiency, as these presented similar values at different pressures. Although at 100 bar, as we can see in **figure 4.5**, there is a bit more colour than in the others, leading to lower % of encapsulation efficiency.

Figure 4.5 Powder obtained under the influence of pressure

4.1.2 Influence of Temperature

Table 4.7 Particle size, bulk density, % wt CO_2, GPR and yield of the collected particles(%) by varying temperature

Exp number	Temperature (°C)	Particle size (µm)	Mean size of particles (µm)	Bulk Density (kg/m^3)	% wt CO_2	GPR	Yield %
5	76	14–35	24	132	80	1.7	83
1	**83**	32–50	42	173	80	1.7	80
6	93	57–88	69	186	75	1.3	76

From **table 4.7,** the particle size distribution ranged from 14 to 88 µm. The size of particles increases with the increase in temperature. **(Fig. 4.6).** However, according to the literature, increasing the temperature promotes particle size reduction and increase in the number of spherical particles. The range of % wt CO_2 with the temperature is not significant, presenting similar values.

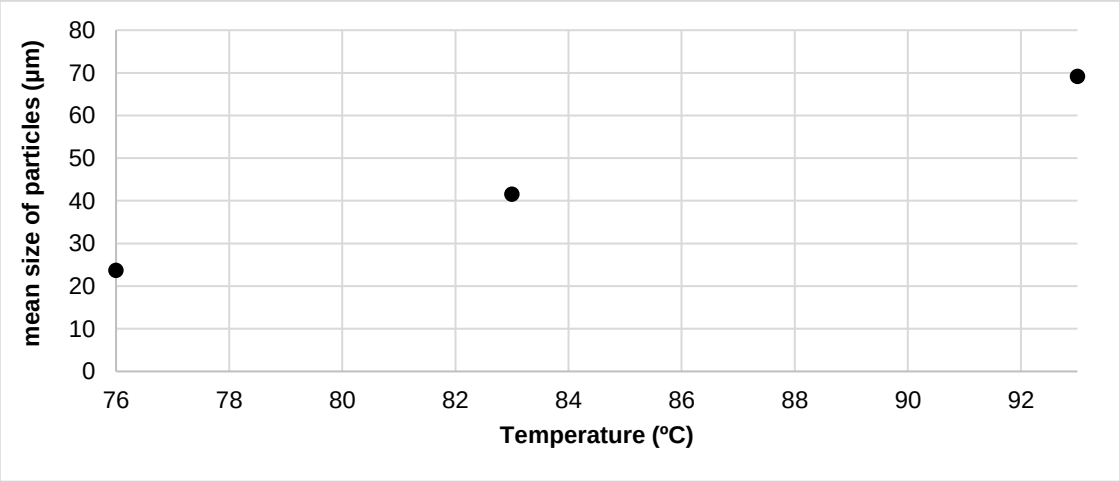

Figure 4.6 Mean size of the particle under the influence of temperature

In **figure 4.7**, the powder bulk density is plotted versus the temperature. Bulk density demonstrates a comparable dependence on temperature as the particle size. As we expected, an increase in temperature promotes an increasing agglomeration and therefore an increase of the particle size, and also of the bulk density. The bulk density at 76°C had the lowest value (132 kg/m^3), and at 83°C had the highest value (186 kg/m^3).

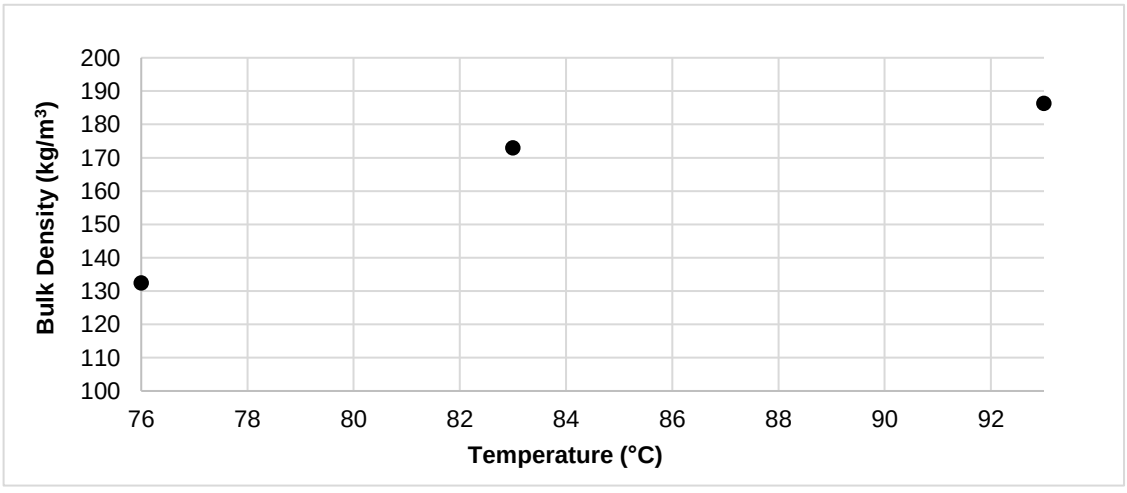

Figure 4.7 Bulk density under the influence of temperature

Table 4.8 Tapped density (kg/m^3), Compressibility index (%), Hausner's ratio and Flow character by varying temperature

Exp number	Temperature (°C)	Tapped density (kg/m^3)	CI %	Hausner's ratio	Flow character
5	76	205	35	1.5	Very poor
1	**83**	246	22	1.4	Poor
6	93	279	33	1.5	Very poor

From **table 4.8** it can be seen the flow character is the same at temperatures 76°C and 93 °C indicating that the powder is very cohesive and more compressible than at 83 °C. The powders of tests 5 and 6 are less fluidised than in test 1.

As we can see from **table 4.9**, the pressure is not a decisive factor for the encapsulation efficiency, as these presented similar values at different pressures. Although at 100 bar, as we can see in **figure 4.8**, there is a bit more colour than in the others samples, it led to a lower % encapsulation efficiency. Test 2 presented the highest value of encapsulation efficiency.

.

Table 4.9 Encapsulation Efficiency (%) and Outside (%) by varying temperature

Exp number	Temperature (°C)	EE%	% Outside
5	76	67	33
1	**83**	66	34
6	93	64	36

Figure 4.8 Powder obtained under the influence of temperature

4.1.3 Influence of quantity of mixture in vessel or GPR

Table 4.10 Particle size, bulk density, % wt CO_2, GPR and yield of collected particles (%) by varying the quantity of mixture in a vessel

Exp number	Quantity (g)	Particle size (μm)	Mean size of particles (μm)	Bulk Density (kg/m^3)	% wt CO_2	GPR	Yield %
7	50	25–60	37	161	93	6.9	70
1	**100**	32–50	42	173	80	1.7	80
8	200	51–89	72	214	60	0.7	90
9	300	71–109	88	236	40	0.4	92

From **table 4.10**, it can observed that the particle size distribution ranged between 25 and 109 μm. Test 9 presents the highest value of the particle size from all the tests performed in section 4.1. As we expected the size of particles increased with increasing quantity. **(Fig. 4.9)** According to literature, increasing the GPR (gas product ratio), which means decreasing the quantity of mixture in a vessel, decreases the mean particle size **(Fig. 4.10)**. Also, a decrease in the quantity of mixture leads to an increase in the amount of CO_2 used (wt % CO_2). Therefore, increasing wt% CO_2 will promote the shape of the particles to be less spherical. So in conclusion, decreasing the quantity of mixture will increase wt% CO_2, and therefore smaller and less spherical particles are obtained. For instance, the highest value % wt CO_2 from all the test is test 7 (the test with the lowest quantity of mixture) and the lowest value % wt CO_2 of all the tests is test 9 (the test with the highest quantity of mixture).

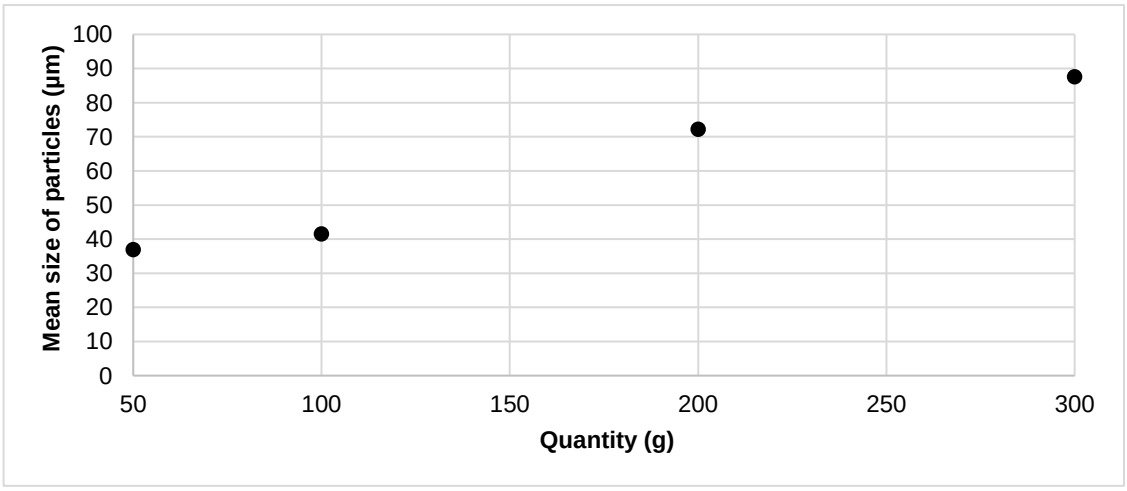

Figure 4.9 Mean size of the particle under the influence of the quantity

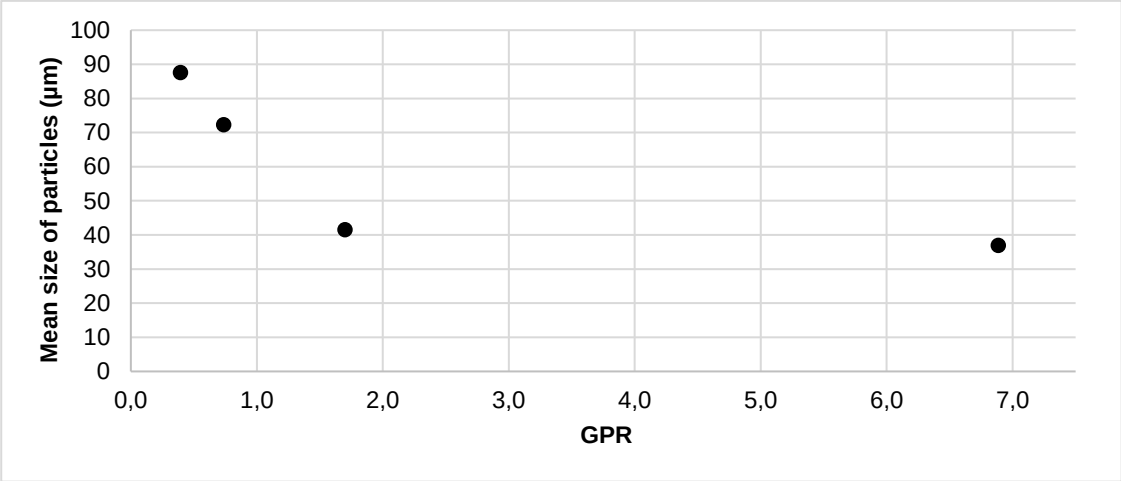

Figure 4.10 Mean size of the particles under the influence of the GPR

In **figure 4.11**, the powder bulk density is plotted versus the temperature. The bulk density increases with the increasing quantity of the mixture. A higher GPR and therefore less quantity of mixture in the vessel lead to an increase in the speed of cooling and solidification of the particles promoting a decrease of the size of the particles and of the values of bulk density. The bulk density with 50g presented the lowest value (161 kg/m^3) and with 300g had the highest value (236 kg/m^3). Test 9 presents has the highest value for bulk density compared to all the tests in section 4.1.

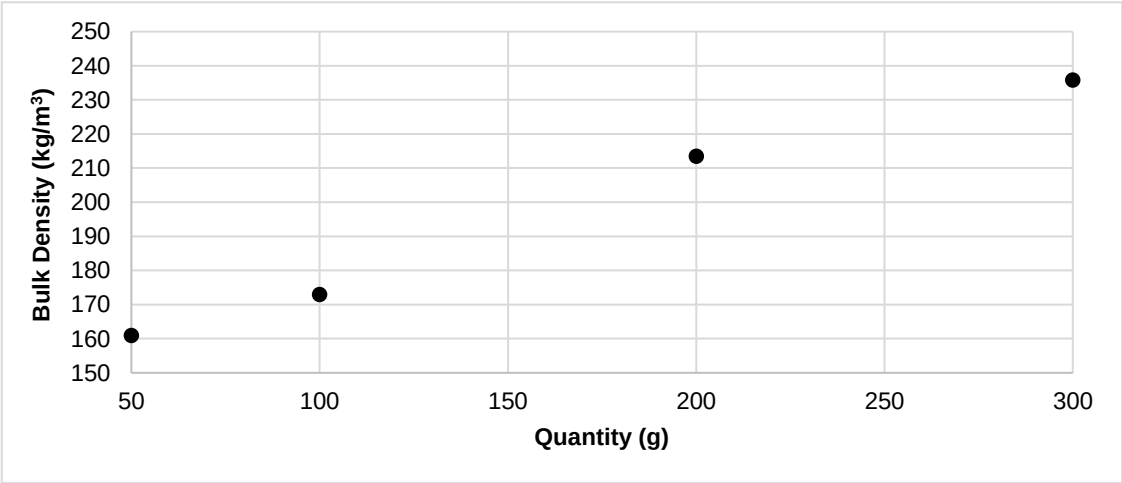

Figure 4.11 Bulk density under the influence of the quantity

The flow character is presented in **table 4.11**. All the tests presented the same flow character that indicates the powder is cohesive. However, the compressibility index shows that the powder of test 1 is less compressible than of the remaining tests.

Table 4.11 Tapped density (kg/m^3), Compressibility index (%), Hausner's ratio and Flow character by the varying quantity

Exp number	Quantity (g)	Tapped density (kg/m^3)	CI %	Hausner's ratio	Flow character
7	50	230	30	1.4	Poor
1	**100**	246	22	1.4	Poor
8	200	296	28	1.4	Poor
9	300	325	28	1.4	Poor

As it was expected, the quantity of the sample influences the efficiency of the encapsulation. In the variation of the quantity, to maintain the 1% pigment loading, we also change the amount of pigment. An increase in the colour of the samples means that there is more quantity of pigment outside than inside. Therefore there is a decrease in the % of the encapsulation efficiency. As we can see from **table 4.12** and **figure 4.12**, the sample that has the lowest encapsulation efficiency and in turn, more colour is the 50g sample. The 200g and 300g samples have similar values and colours but have a lower efficiency than the 100g sample. However, we expected that the encapsulation efficiency would increase with the increase in the quantity of Jojoba wax.

Table 4.12 Encapsulation Efficiency (%) and Outside (%) by varying the quantity

Exp number	Quantity of Jojoba wax (g)	Quantity of pigment (g)	EE%	% Outside
7	49.5	0.5	41	59
1	**99**	1	66	34
8	198	2	58	42
9	297	3	57	43

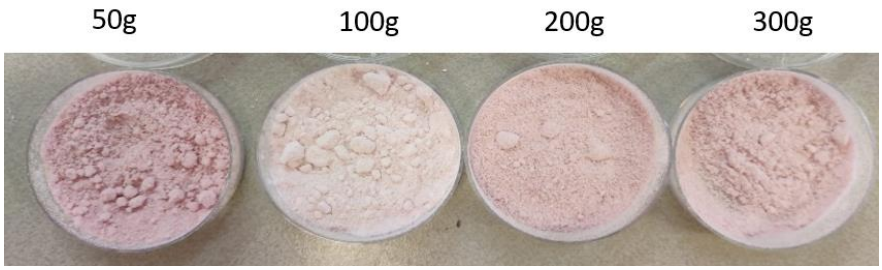

Figure 4.12 Powder obtained under the influence of the quantity

4.1.4 Influence of the Pigment loading in particle

Table 4.13 Particle size, bulk density, % wt CO_2, GPR and yield of collected particles (%) by varying the pigment loading

Exp number	Pigment loading	Particle size (μm)	Mean size of particles (μm)	Bulk Density (kg/m^3)	% wt CO_2	GPR	Yield %
1	**1%**	32 – 50	42	166	80	1.7	80
10	5%	35 – 85	53	174	80	1.7	65
11	10%	23 – 57	42	166	75	1.3	68
12	20%	26 – 63	40	134	83	2.1	81

From **table 4.13**, it is possible to observe that the the particle size distribution range between 23 and 85 μm. In the pigment loading, it was not expected to have significant differences in the size of particles. As we can see, the values are similar, showing that the quantity of pigment used is not significant for the size of the particle. Test 10 presents the lowest yield of collected particles in section 4.1.

The flow character is presented in **table 4.14**. As we observe, the compressibility index and Hausner's ratio increase by increasing the pigment loading. The flow character is very, very poor, and the higher values of Hausner's ratio indicate that the powder is non-flow and more consolidated, and they are highly compressible powders. Also, the considerable variation between the values of bulk density and tapped density indicates that powder is less compact. Test 12 has shows the highest value of CI%, Hausner's ration and tapped density in section 4.1. From **figure 4.14**, we observed the powder is not loose or fine, instead has many agglomerations.

Table 4.14 Tapped density (kg/m^3), Compressibility index (%), Hausner's ratio and Flow character by varying the pigment loading

Exp number	Pigment loading	Tapped density (kg/m^3)	CI %	Hausner's ratio	Flow character
1	**1%**	246	22	1.4	Poor
10	5%	304	45	1.8	Very, very poor
11	10%	403	67	3.0	Very, very poor
12	20%	596	72	3.6	Very, very poor

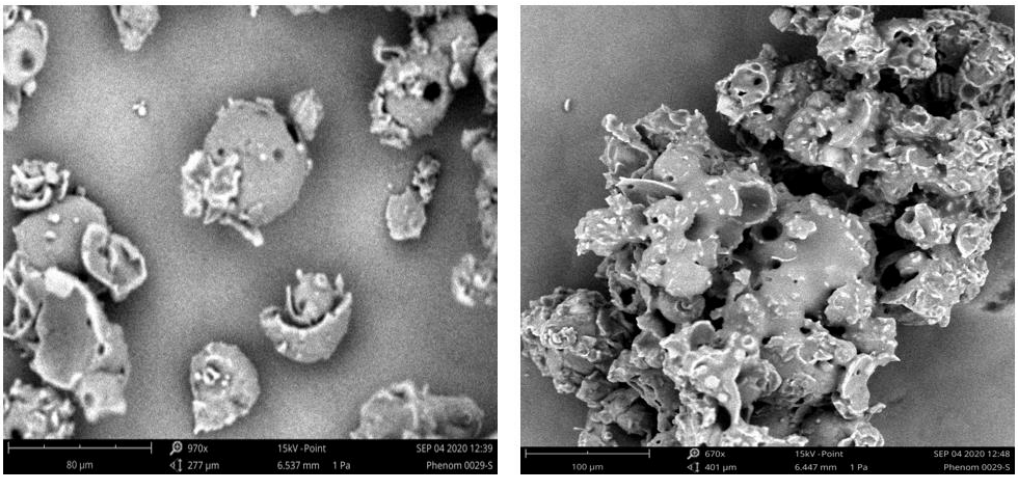

1% pigment, pressure 120 bar 20% pigment, pressure 120 bar

Figure 4.13 SEM pictures of the tests 1 (right) and 12 (left). Scale bar: 80 µm (right) and 100 µm (left)

As we can observe from **figure 4.13**, test 1 (standard sample) presents hollow particles and in test 12, we have sponge-like particles (foam-like particles). The CO_2 can induce the little holes on the surface of the particle before it evaporates from the particles. Test 12 was considered the worst powder produced.

As we can observe by the results obtained in **table 4.15** and **figure 4.14**, the pigment loading is the most significant parameter for the encapsulation efficiency—the encapsulation efficiency decrease with the increase of the % of pigment used. Test 10 to 12 have the lowest values of % encapsulation efficiency in section 4.1. We can observe that these samples have more colour than the other samples produced, which means that there is more pigment outside than inside. Also, it was possible to observe more colour in the microscope than for the other tests **(Fig. 4.15)**

Table 4.15 Encapsulation Efficiency (%) and Outside (%) by varying the pigment loading

Exp number	Pigment loading	Quantity of Jojoba wax (g)	Quantity of pigment (g)	EE%	% Outside
1	**1%**	99	1	66	34
10	5%	95	5	36	64
11	10%	90	10	26	74
12	20%	80	20	18	82

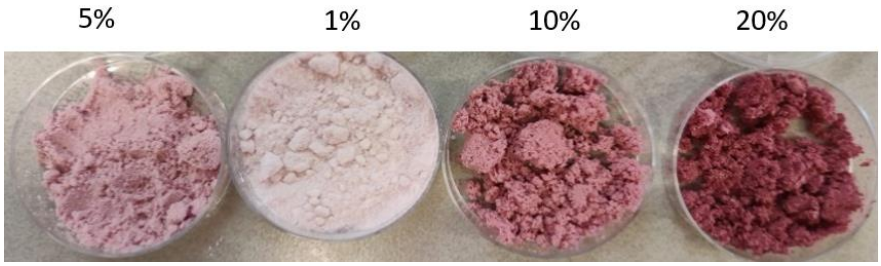

Figure 4.14 Powder obtained by varying the pigment loading

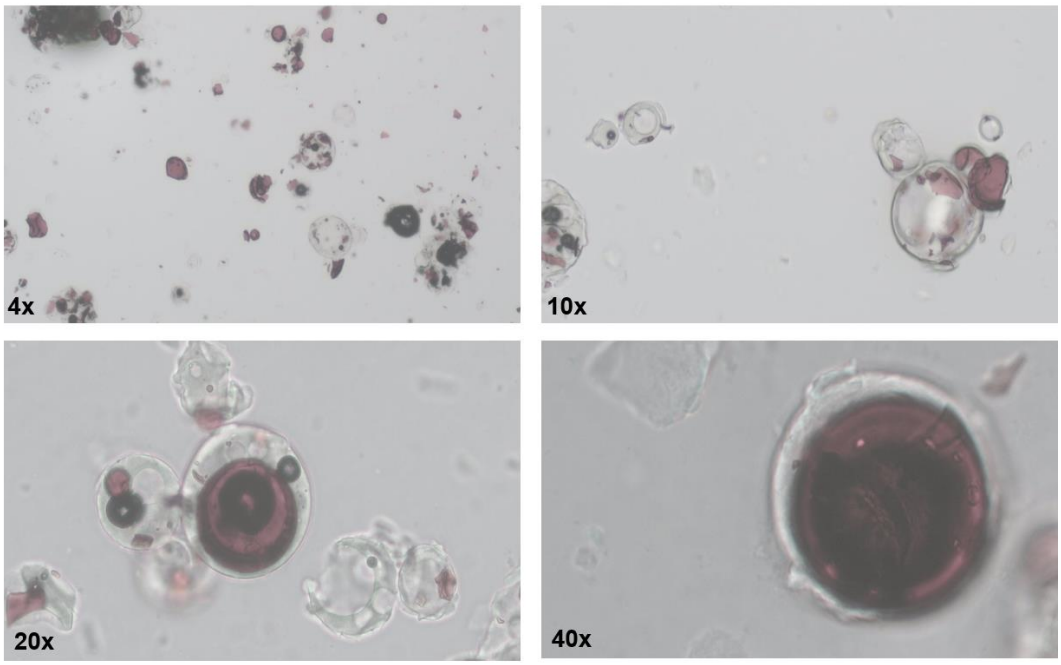

Figure 4.15 Microscopy picture of the particles with 20% pigment loading with different magnifications (red represent pigment trapped inside in the particle).

4.1.5 Influence of the nozzle

Table 4.16 Particle size, bulk density, % wt CO_2, GPR and yield of collected particles (%) by the varying nozzle diameter

Exp number	Nozzle diameter (mm)	Particle size (µm)	Mean size of particles (µm)	Bulk Density (kg/m^3)	% wt CO_2	GPR	Yield %
13	0.093	7 – 34	19	134	80	1.7	97
14	0.340	32 – 48	39	146	75	1.3	96
1	**0.500**	32 – 50	42	173	80	1.7	80
15	0.710	53 – 77	63	180	75	1.3	90

From **table 4.16**, the particle size distribution ranged from 7 to 77 µm. Test 13 presented the lowest value of the particle size. The nozzles with the lower diameters (Test 13 and 14) presented the highest values of the yield of the collected particles in section 4.1. Therefore we can conclude that it is possible to produce more powder with smaller diameter nozzles than with a larger ones.

As we expect, the size of the particles increases with increasing diameter of the nozzle. **(Fig. 4.16)** According to literature, particles are smaller with a smaller diameter of the nozzle. However, the particles will be less spherical. Furthermore, a smaller bore diameter leads to a lower mass of material from the nozzle for each spray, leading to smaller particles, slower solidification but also less spherical particles because of the shear forces applied on the capsules.

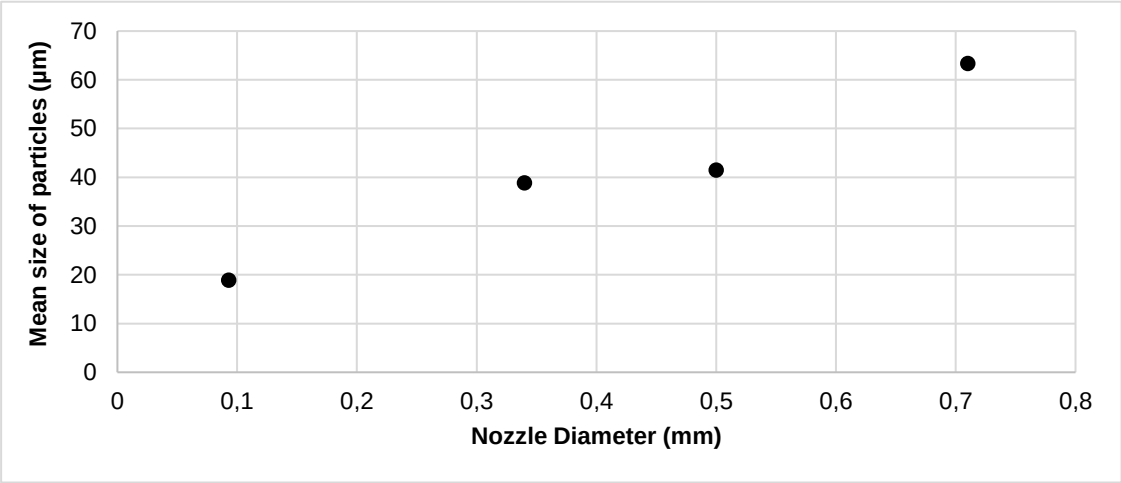

Figure 4.16 Mean size of the particle by varying nozzle diameter

As we can observe from **figure 4.17**, the bulk density demonstrates a comparable dependence on the nozzle diameter as the particle size. As we expected the bulk density increases with the increase of nozzle diameter.

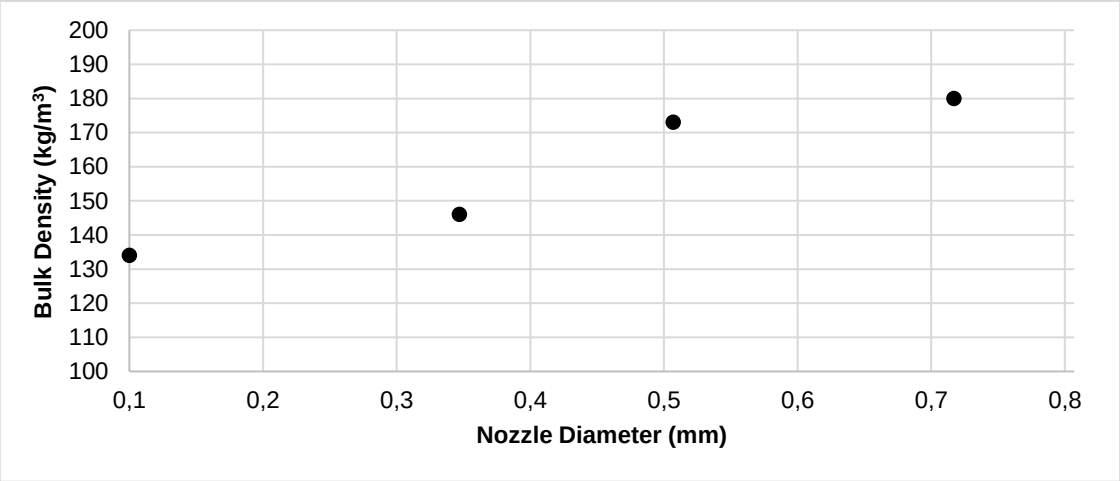

Figure 4.17 Bulk density by the varying nozzle diameter

The flow character is presented in **table 4.17**. The tests 13, 14 and 1 presented the same flow character that indicates that the powder is more cohesive and less compressible than in test 15.

Table 4.17 Tapped density (kg/m3), Compressibility index (%), Hausner's ratio and Flow character by varying the nozzle diameter

Exp number	Nozzle diameter (mm)	Tapped density (kg/m^3)	CI %	Hausner's ratio	Flow character
13	0.093	194	31	1.4	Poor
14	0.340	203	28	1.4	Poor
1	**0.500**	246	30	1.4	Poor
15	0.710	268	33	1.5	Very poor

From **table 4.18,** we can verify that the increase in the nozzle diameter promotes an increase in encapsulation efficiency. Nevertheless, the values presented are similar, showing that the nozzle is not significant for encapsulation efficiency. **(Fig. 4.18)**

Table 4.18 Encapsulation Efficiency (%) and Outside (%) by the varying nozzle diameter

Exp number	Nozzle diameter (mm)	EE %	% Outside
13	0.093	64	36
14	0.340	65	35
1	**0.500**	66	34
15	0.710	66	34

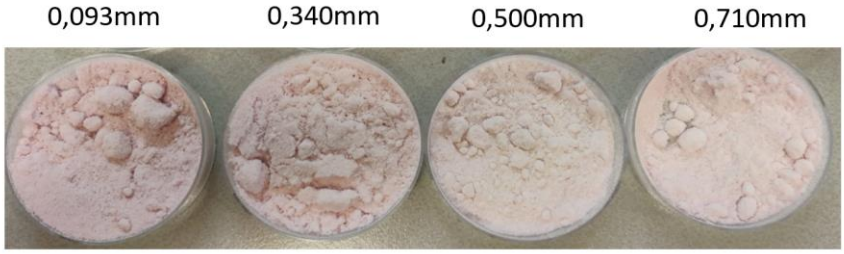

Figure 4.18 Powder obtained with different nozzle

4.1.6 The Influence of stirring

Table 4.19 Particle size, bulk density, % wt CO_2 and yield of collected particles (%) with and without stirring

Exp number	Time of stirring (seconds)	Particle size (µm)	Mean size of particles (µm)	Bulk Density (kg/m^3)	% wt CO_2	GPR	Yield %
1	**50**	32 – 50	42	173	80	1.7	80
16	0	8 – 44	29	162	67	0.8	88

From **table 4.19**, it is possible to observe the particle size distribution ranges from 8 to 50 µm. The particles without stirring are smaller than with stirring. A possible explanation is because the quantity of CO_2 is lower without stirring (presenting the value of 0.2 kg) than with stirring (presenting the value of 0. 6 kg). According to the literature, decreasing the % wt of CO_2 promotes a particle size reduction and increases spherical particles. Because we have smaller particles without stirring, we also have lower values of bulk density. One important aspect of making the

test without stirring is that it was expected having particles with less gas entrapped inside them, as shown in **figure 4.19**.

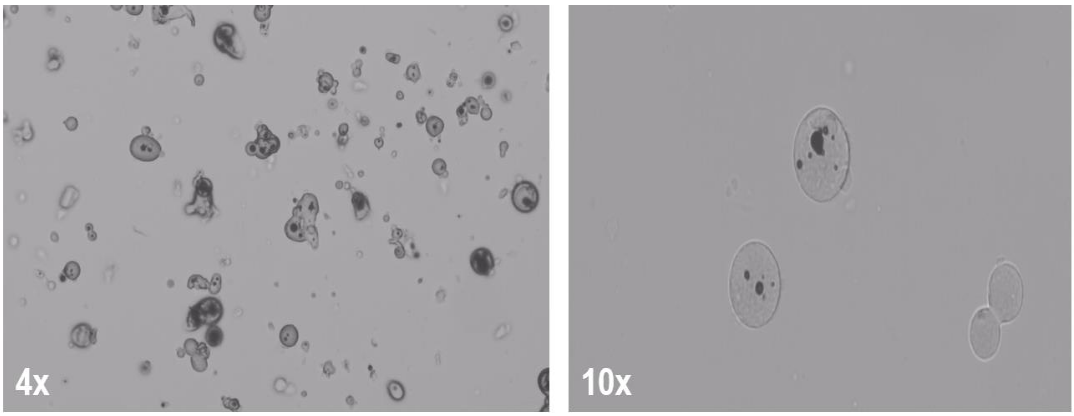

Figure 4.19 Microscopy pictures of the particles without stirring with 4X and 10X of magnification

The flow character is presented in **table 4.20**. Both tests presented the same flow character that indicates the powder is cohesive. However, test 16 sample is more compressible than the sample from test 1.

Table 4.20 Tapped density (kg/m3), Compressibility index (%), Hausner's ratio and Flow character under the influence on the time of stirring

Exp number	Time of stirring (seconds)	Tapped density (kg/m^3)	CI %	Hausner's ratio	Flow character
1	**50**	246	30	1.4	Poor
16	0	230	33	1.4	Poor

From **table 4.21**, it can be observed that the stirring, does not influence the efficiency of the encapsulation. These tests have equal values, as well as their colours. **(Fig. 4.20)**

Table 4.21 Encapsulation Efficiency (%) and Outside (%) under the influence on the time of stirring

Exp number	Time of stirring (seconds)	EE %	% Outside
1	**50**	66	34
16	0	66	34

Figure 4.20 Powders obtained without and with stirring

4.2 Design of Experiments (DoE)

In this study, a full factorial design using STATISTICA software was used for the estimation and optimization of effective parameters. It was used a full factorial plan 2^3 with the addition of 2 central points. The chosen factors were the ones that verified more influence in the process, in which the independent variables are: quantity, temperature and pressure. The range selected for each factor was: 50 to 300 g for quantity, 76 to 93 °C for temperature and 75 and 150 bar for pressure. The main goal of the experiments was to determine which factors are more significant, in other words, which factors will influence our response. In this method, we can also observe the level of the factors according to maximization or minimization of the response. The total matrix design comprise that 10 runs (see **appendix D.1**) which are described in **table 4.22**. Experiments were performed by order of **table 4.22**, which was already randomized by STATISTICA software.

The experimental results obtained for the responses at each run were evaluated using STATISTICA software, and it was possible to observe that the evaluation was valid, since the obtained matrix showed degrees of freedom (df). The ANOVA analysis tables were calculated for each response, and it is considered being that factors with a p-value below 0.05 have a significant effect. Also, it was possible to perform a plot of surface responses using STATISTICA software.

The ANOVA analysis for the encapsulation efficiency and yield of the collected particles shows the effects, which were not be significant for the studied model. (see **Appendix D.4** and **D.5**)

Table 4.22 Matrix for Full Factorial Design at 3 factors (Pressure, Temperature, Quantity) and 4 responses (Yield of collected particles, mean particle size, bulk density and encapsulation efficiency)

Run	Quantity (g)	Temperature (°C)	Pressure (bar)	Yield %	Mean Particle size (µm)	BD (kg/m^3)	EE%
1	50	76	75	74%	50	159	51
2	50	93	75	65%	54	189	74
3	300	76	75	93%	66	219	64
4	100	83	120	83%	47	174	66
5	50	76	150	79%	25	166	55
6	300	93	75	83%	90	376	67
7	300	93	150	92%	71	219	74
8	50	93	150	72%	44	182	61
9	300	76	150	96%	49	207	67
10	100	83	120	83%	46	210	65

4.2.1 Statistical Analysis of Particle size

In order to analyse the effect of each process variable on the mean particle sizes, **(table 4.22)** estimed from the optical microscopic measurements, the size data were modelled using factorial design. Factors studied for this analysis were quantity (A), temperature (B) and pressure (C).

Table 4.23 ANOVA results for mean particle size analysis

	SS	df	MS	$F_{observed}$	p-value
A	0.065373	1	0.065373	451.2421	**0.000228**
B	0.011902	1	0.011902	82.1551	**0.002837**
C	0.007011	1	0.007011	48.3927	**0.006094**
AB	0.000045	1	0.000045	0.3130	0.614874
AC	0.000006	1	0.000006	0.0421	0.850585
BC	0.000750	1	0.000750	5.1770	0.107398
Error	0.000435	3	0.000145		
Total SS	0,085522	9			

Note: SS = Sum of squares, df= degrees of freedom, MS = mean squared value

From the statistics presented in the ANOVA **table 4.23**, it can be concluded that there is a significant effect of A (Quantity), B (Temperature) and C (Pressure) on particle size at 95% confidence level. However, the effect interactions do no prove to be significant for the studied model. The goal is to get smaller particles, and after analysing the isolated effects, we can conclude at 95% confidence level that: the lower the quantity, the lower the temperature and the higher pressure promoted the smallest particle size. These observations confirmed the previous study made in chapter 4.1. (see **appendix D.2**)

Thus the final Equation in Terms of Factors for mean particle size (MPS) analysis is the following equation **(Eq. 4.1)**. The R-square is 0.94139, and adjusted R-square is 0.91209

$$MPS = 54{,}1 + 12{,}98 \times Quantity + 8{,}7 \times Temperature - 8{,}9 \times Pressure + 2{,}9 \times Quantity \times Temperature - 0{,}02 \times Quantity \times Pressure + 1{,}7 \times Temperature \times Pressure \quad \textbf{(Eq. 4.1)}$$

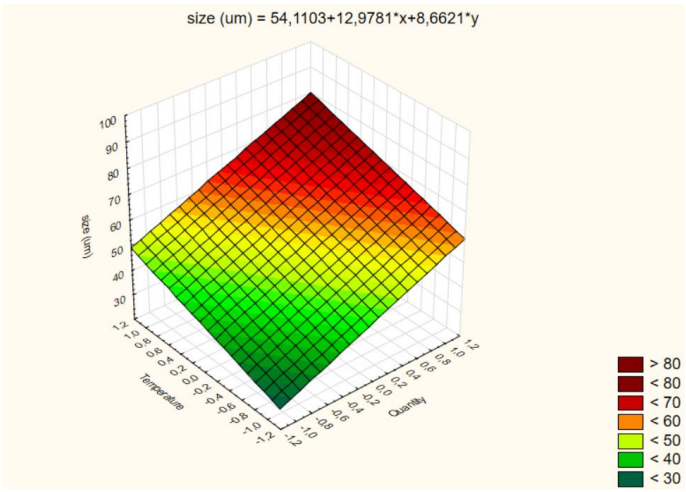

Figure 4.21 3D Surface plot of size against Quantity and Temperature

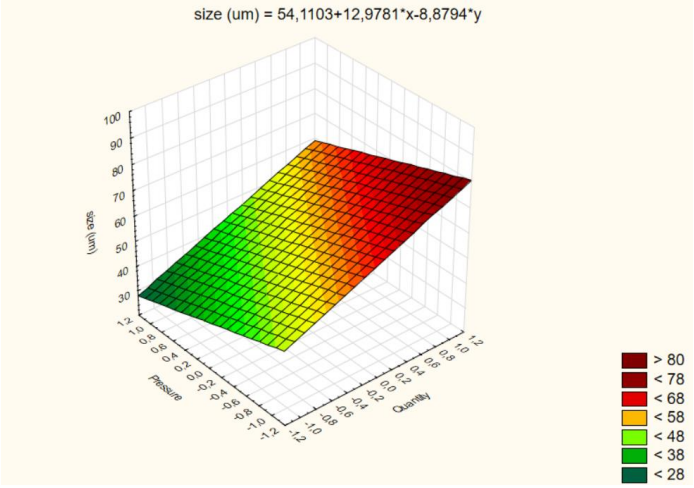

Figure 4.22 3D surface plot of size against Quantity and Pressure

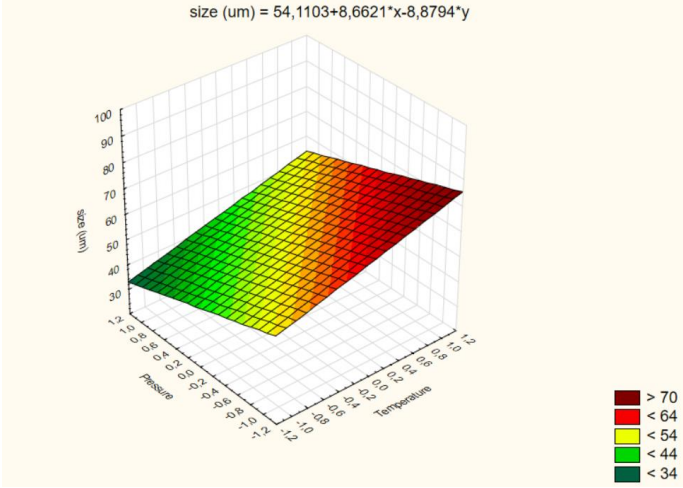

Figure 4.23 3D Surface plot of size against pressure and temperature

4.2.2 Statistical Analysis of Bulk density

In order to analyse the effect of each process variable on bulk density (**Table 4.22**), the bulk density data was modelled using factorial design. Factors studied for this analysis were quantity (A), temperature (B) and pressure (C).

Table 4.24 ANOVA results for bulk density analysis

	SS	df	MS	$F_{observed}$	p-value
A	13201.32	1	13201.32	10.88277	**0.045771**
B	5726.88	1	5726.88	4.72107	0.118145
C	3556.06	1	3556.06	2.93151	0.185387
AB	1912.37	1	1912.37	1.57650	0.298159
AC	3565.43	1	3565.43	2.93924	0.184963
BC	3192.89	1	3192.89	2.63213	0.203176
Error	3639.14	3	1213.05		
Total SS	34794.09	9			

Note: SS = Sum of squares, df= degrees of freedom, MS = mean squared value

From the statistics presented in the ANOVA **table 4.24,** it can be concluded that there is a significant effect of A (Quantity) on bulk density at 95% confidence level. However, the other effects and effect interactions have not proved to be significant for the studied model. After analysing the isolated effects, we can conclude at 95% confidence level that: the lower quantity, the lower the temperature and higher the pressure, lower values of bulk density are promoted. We expected this correlation, from section 4.1, we observed that the value of bulk density is smaller for smaller particles. Therefore, to obtain smaller particles, we increase pressure and decrease quantity and temperature. (see **appendix D.3**)

Thus the final Equation in Terms of Factors for bulk density (BD) analysis is the following equation:

$$BD = 209{,}90 + 40{,}62 \times Quantity + 26{,}76 \times Temperature - 21{,}08 \times Pressure + 15{,}46 \times Quantity \times Temperature - 21{,}11 \times Quantity \times Pressure - 19{,}98 \times Temperature \times Pressure \quad \textbf{(Eq.4.2)}$$

The R-square is 0.89541, and adjusted R-square is 0.68623.

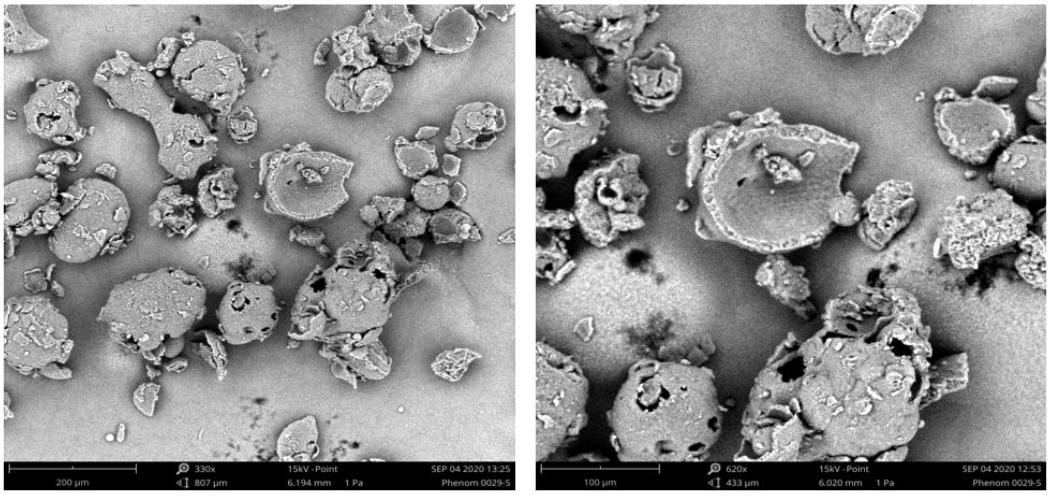

Figure 4.24 SEM pictures of test 6 (300g, 93ºC,75 bar) presented the biggest value of bulk density (376 kg/m^3), with 25 wt% CO_2 Scale bar: 200µm (right) and 100µm (left)

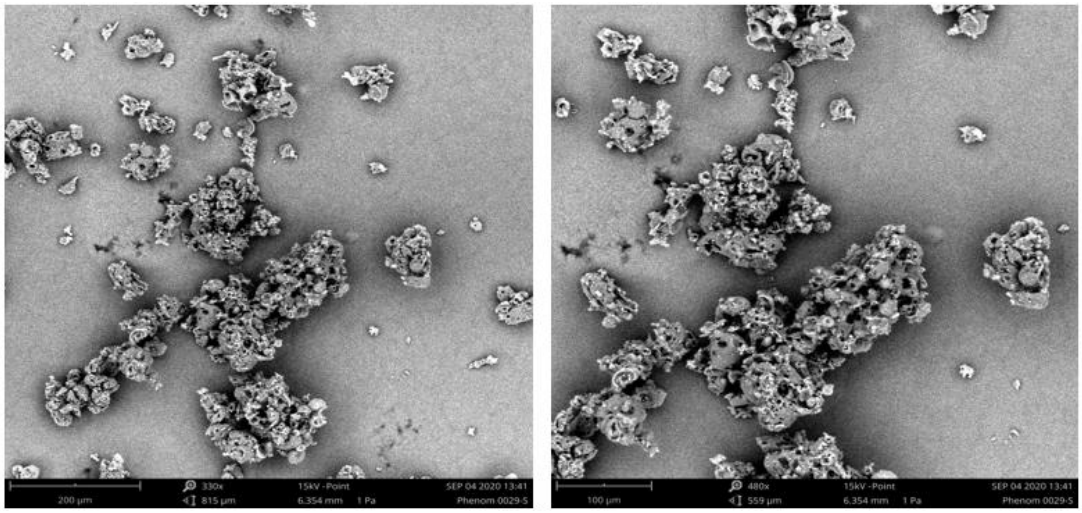

Figure 4.25 SEM pictures of test 5 (50g, 76ºC,150 bar) with 92% wt CO2. Scale bar: 200µm (right) and 100µm (left)

We observe the particles' morphology in function of the amount of CO_2 dissolved and the bulk density: As we can observe from **figure 4.24,** the higher the quantities and temperatures, and lower pressures, and thus lower values of wt% CO_2, promote spherical/hollow-like particles. In contrast, higher pressures, lower quantities and temperatures and therefore higher values of wt% CO_2 lead to more sponge-like particles. **(Fig. 4.25)**

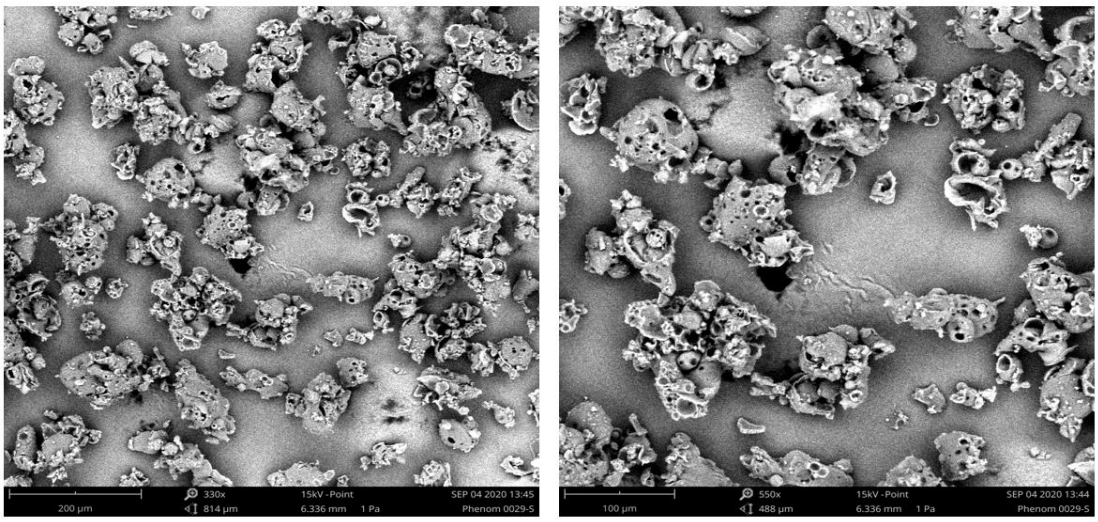

Figure 4.26 SEM pictures of test 1 (50g, 76°C, 75 bar) presented the lowest value of bulk density (159 kg/m3). Scale bar: 200µm (right) and 100 µm (left)

As we can observe from **figure 4.26**, we obtained more agglomerated distorted particles with lower values of bulk density, while we obtain more spherical porous particles with higher values of bulk density. Also, at the same pressure, we obtained more spherical particles with higher quantities and higher temperatures.

Additionally, the CO_2 can lead to the little holes on the particle's surface before it evaporates from the particles. According to literature, more spherical particles are generated at higher temperature and quantity, while agglomerates or burst particles occur at lowers temperatures and quantity.

4.3 Results for the cosmetic product development

The second goal of this study, was to produce a loose and fine powder without agglomeration with a mixture of natural materials for encapsulating an enzyme for a cosmetic application. Also, the powder is not desired to melt rapidly on the skin at environment temperature. Therefore 17 tests of mixtures were performed (see **appendix E**) using different types of waxes, fats and oils. The tests run with PGSS are in the following table:

Table 4.25 Tests performed with PGSS process for the cosmetic project

Test	Compound 1	Compound 2	Emulsifier	Description of the powder
1	87% Fat powder	13% Cocoa Butter	-	Good
2	50% Macadamia wax	50% Fat powder	-	Good
3	75% Macadamia wax	25% Sunflower oil	-	Good
4	75% Jojoba wax	25% Cocoa Butter	-	Good
5	90% Jojoba wax	10% Sunflower oil	-	Good
6	50% Jojoba wax	50% Fat powder	-	Good
7	50% Macadamia wax	50% Cocoa Butter	-	Intermediate
8	75% Macadamia wax	25% Cocoa Butter	-	Intermediate
9	50% Jojoba wax	50% Cocoa butter	-	Intermediate
10	79% Jojoba wax	21% Sunflower oil	-	Intermediate/Bad
11	87% Fat powder	13% Cocoa Butter	2.5% Lecithin	Intermediate/Bad
12	75% Jojoba wax	25% Cocoa Butter	2.5% Lecithin	Intermediate/Bad
13	75% Jojoba wax	25% Sunflower oil	-	Bad
14	50% Beeswax	50% Sunflower oil	-	Bad
15	75% Fat powder	25% Cocoa Butter	-	Bad
16	50% Beeswax	50% Cocoa Butter	-	Bad
17	25% Jojoba wax	75% Cocoa Butter	-	Bad

The tests were ordered by quality and classified as good, intermediate and bad. This classification means:

- **Good:** the powder is loose, constituted with tiny particles, without agglomerates, do not melt too fast in the skin and is not sticky. The powder is free-flowing.
- **Intermediate:** the powder has some agglomerates, stick a little and melted intermediate in the skin. The powder is cohesive.
- **Bad:** the powder is not loose, have many agglomerates, melted too fast in the skin, and the powder is sticky. Also, the powder is considered not flowing.

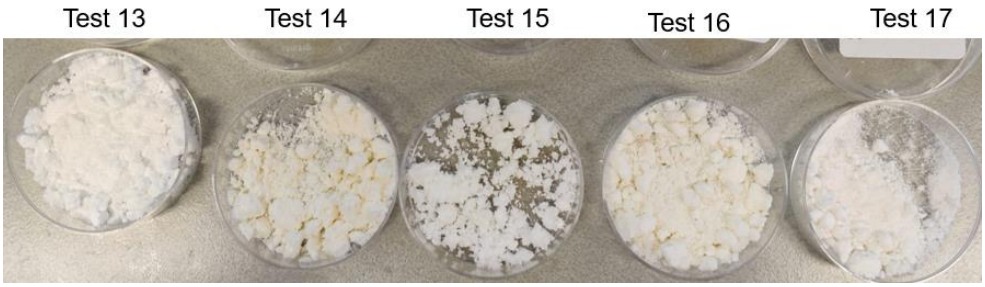

Figure 4.27 The worst powders produced

Figure 4.28 Selected powders for a cosmetic project (containing enzyme)

From **table 4.25** and **figures 4.27** and **4.28**, we can indicate which materials are better for producing a fine and loose powder with PGSS. For instance, in relation to waxes, macadamia wax and jojoba wax are a better choice than the beeswax. The increase of % of cocoa butter and sunflower oil has a negative influence on powder stability; also, the use of lecithin was useless in terms of powder stability. Although one of the best powders produce was with fat powder, we can consider from the other tests performed, is intermediate material for the PGSS.

4.4 Mathematical Model Results

The mathematical model was applied to 4 different nozzles, and all the calculations were performed with the same considerations **(Table 4.26).** The temperature of the surrounding gas (temperature of the drum) is - 10°C and temperature of fat (temperature of the vessel) is 83°C.

Table 4.26 Properties considerations for the mathematical model

Properties	Value	Reference
Density of CO_2 (at 0ºC and 1 bar)	1.95 kg/m^3	[123]
The density of mixture fat and CO_2	873 kg/m^3	[83]
Cp of gas (at 0ºC and 1 bar)	0.85 kJ/kg.K	[123]
Cp of fat (at 83 ºC)	1.96 kJ/kg.K	[124] **(Appendix F.1)**
ΔH exp, CO_2 (120 bar 83 ºC to 1 bar 83 ºC)	-102.34 kJ/kg	[123] **(Appendix F.1)**
K (entrainment factor)	0.5	[110]
fr_{gas}	17%	[94][110] **(Appendix F.1)**

As mentioned in chapter 2.6, we calculated the flow of CO_2 from the equations and values of the water capacity of the Spraying Systems catalogue. However, the catalogue does not have values of water capacity at 120 bar. Therefore, we perform a linearization of the values in order to discover the flow of CO_2 at 120 bar. This calculation is also a consideration/assumption since the CO_2 expands in the nozzle, the actual flow will be lower. **(Table 4.27).** In **appendix, F.2** the calculations for the CO_2 flow are presented**.** [108][125]

Table 4.27 Flow of CO_2 by varying the nozzle type

Nozzle type	Core type	Diameter (mm)	Water Capacity (L/h)	The flow of CO_2 (kg/h)
63M	SKY 16	0,093	60,4	18,86
80M	SKY 20	0,340	19,6	6,13
76M	SKY 17	0,500	38,9	12,13
70M	SKY 21	0,710	86,6	27,00

The temperature (T_{spray}), velocity (v), entrainment ratio (Qt/Qi), elapsed time (Time) and cone diameter (d_{cone}) of the spray are calculated as a function of the distance from the nozzle (x) in the axial direction **(Fig. 4.29)** The surrounding gas (temperature of the drum) is at the same temperature around the spray cone.

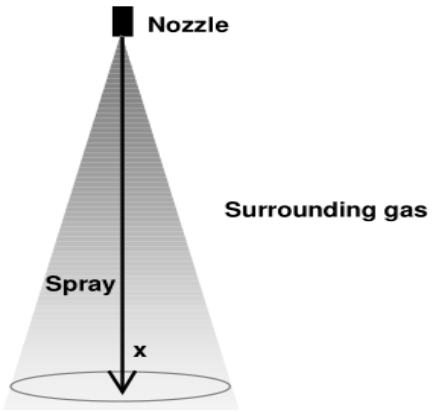

Figure 4.29 Spray profile in function of x

4.4.1 Nozzle 63M

Table 4.28 shows that the produced wax powder is sufficiently cooled down. It also indicates that immense recirculation takes place since the entrainment ratio at the end of the spray tower is 91.8, which means that about 1730 kg gas/h can be entrained. The fat only starts to crystallise at 27.9°C, and after reaching -7.3 °C, the quantity of fat crystalised is 100%. From **figure 4.30**, we can observe that the mass flow of spray is increasing linearly with the distance from the nozzle. As mentioned in chapter 2.6, as the cold gas is entrained, the spray cools down, and the velocity of the spray decreases.

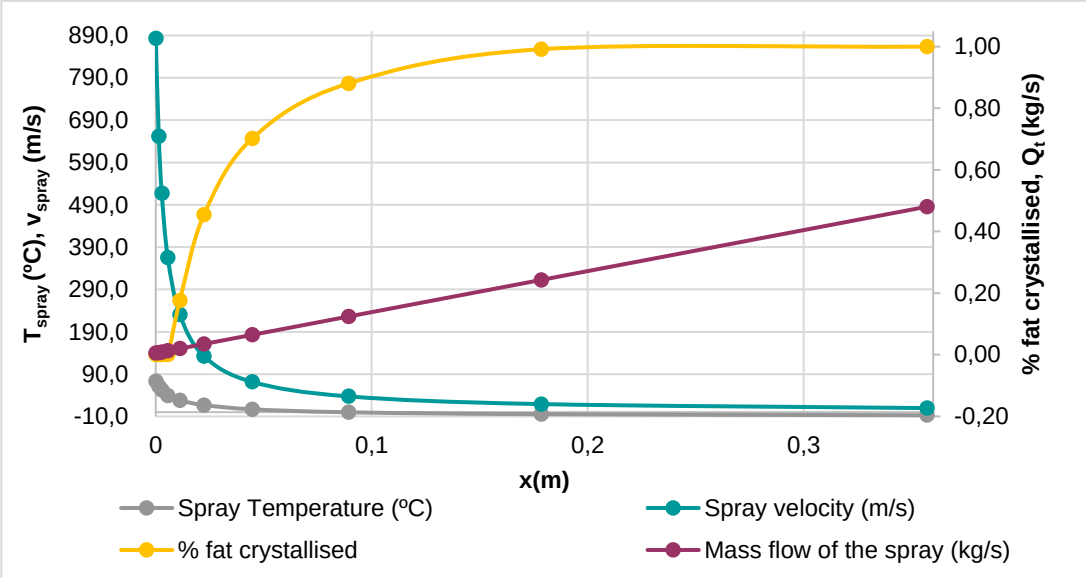

Figure 4.30 Spray profile for nozzle 63M – Axial distance from the nozzle (x); Spray temperature (T_{spray}); Spray velocity (v_{spray}); Mass flow of the spray (Q_t)

Table 4.28 Results of axial distance from the nozzle (x), the total mass flow of spray (Q_t), entrainment ratio (Q_t/Q_i), the velocity of the spray (v_{spray}), a diameter of the cone (d_{cone}), the average temperature of the spray (T_{spray}), % fat crystallised, pressure drop (ΔP) and Reynolds number (Re) for nozzle 63M

x (m)	Q_t (kg/s)	Q_t/Q_i	v_{spray} (m/s)	d_{cone} (m)	T_{spray} (°C)	% Fat crystallised	ΔP	Re
0.000	0,005	1.0	883.3	0.000	73.2	0%	3.7E-03	5646579
0.001	0.007	1.4	652.1	0.001	61.1	0%	2.7E-03	446879
0.003	0.009	1.7	516.8	0.002	52.1	0%	2.1E-03	316487
0.006	0.013	2.4	365.3	0.002	39.5	0%	1.5E-03	223966
0.011	0.020	3.8	230.2	0.003	27.9	18%	9.6E-04	158430
0.022	0.035	6.7	132.4	0.005	16.8	45%	5.5E-04	112049
0.045	0.065	12.3	71.5	0.007	6.9	70%	3.0E-04	79239
0.089	0.124	23.7	37.3	0.009	-0.3	88%	1.6E-04	56033
0.179	0.243	46.4	19.0	0.013	-4.8	99%	7.9E-05	39622
0.357	0.481	91.8	9.6	0.019	-7.3	100%	4.0E-05	28017

4.4.2 Nozzle 80M

Table 4.29, shows that the produced wax powder is sufficiently cooled down. Unfortunately, the model is only valid up until 70% of crystallised fat (after this value, the Reynolds number is lower than 5000). Despite this, there is still immense recirculation of the entrainment

gas. The entrainment ratio at the end of the spray tower is 12.3, which means that about 76 kg gas/h can be entrained. From **figure 4.31**, we can observe that the mass flow of spray is increasing linearly with the distance from the nozzle. Also, we can observe the velocity of the spray decreases as the spray is cooled down.

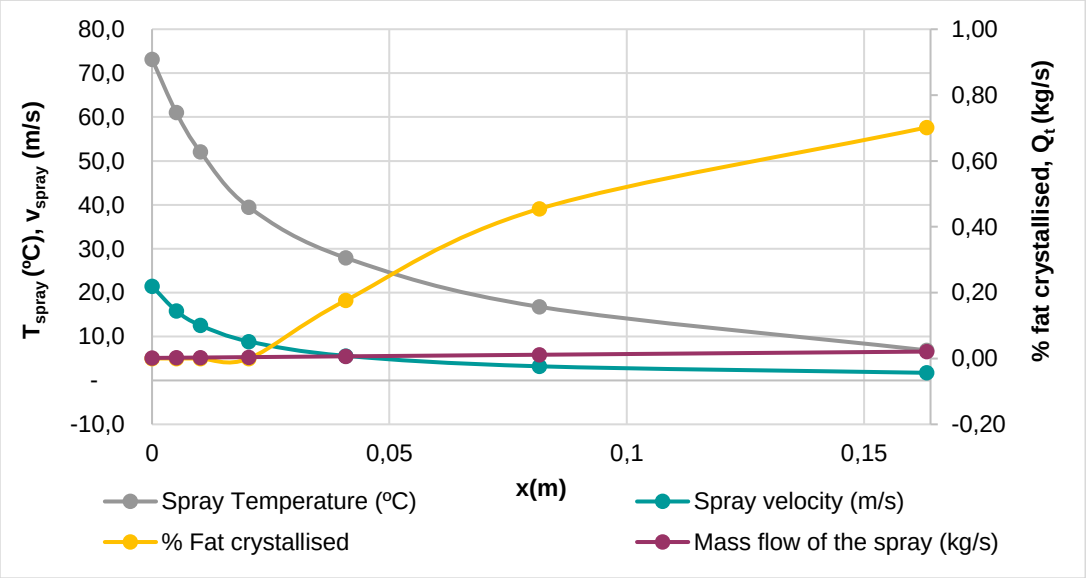

Figure 4.31 Spray profile for nozzle 80M – Axial distance from the nozzle (x); Spray temperature (T_{spray}); Spray velocity (v_{spray}); Mass flow of the spray (Q_t)

Table 4.29 Results of axial distance from the nozzle (x), the total mass flow of spray (Q_t), entrainment ratio (Q_t/Q_i), the velocity of the spray (v_{spray}), a diameter of the cone (d_{cone}), the average temperature of the spray (T_{spray}), % fat crystallised, pressure drop (ΔP) and Reynolds number (Re) for nozzle 80M

x (m)	Q_t (kg/s)	Q_t/Q_i	v_{spray}(m/s)	d_{cone} (m)	T_{spray} (°C)	% Fat crystallised	ΔP	Re
0.000	0.002	1.0	21.5	0.000	73.2	0%	2.9E-05	501923
0.005	0.002	1.4	15.9	0.004	61.1	0%	2.1E-05	39723
0.010	0.003	1.7	12.6	0.006	52.1	0%	1.7E-05	28132
0.020	0.004	2.4	8.9	0.009	39.5	0%	1.2E-05	19908
0.041	0.007	3.8	5.6	0.012	27.9	18%	7.6E-06	14083
0.082	0.011	6.7	3.2	0.017	16.8	45%	4.4E-06	9960
0.163	0.021	12.3	1.7	0.024	6.9	70%	2.4E-06	7044

4.4.3 Nozzle 76M

Table 4.30, shows that the produced wax powder is sufficiently cooled down. Unfortunately, the model is only valid up until 88% of crystallised fat (after this value, the Reynolds number is lower than 5000). Despite this, there is still immense recirculation of the entrainment gas. The entrainment ratio at the end of the spray tower is 23.7, which means that about 287 kg gas/h can be entrained. From **figure 4.32**, we can observe that the mass flow of spray is increasing linearly with the distance from the nozzle. Also, it is observed that the velocity of the spray decrease as the spray is cooled down.

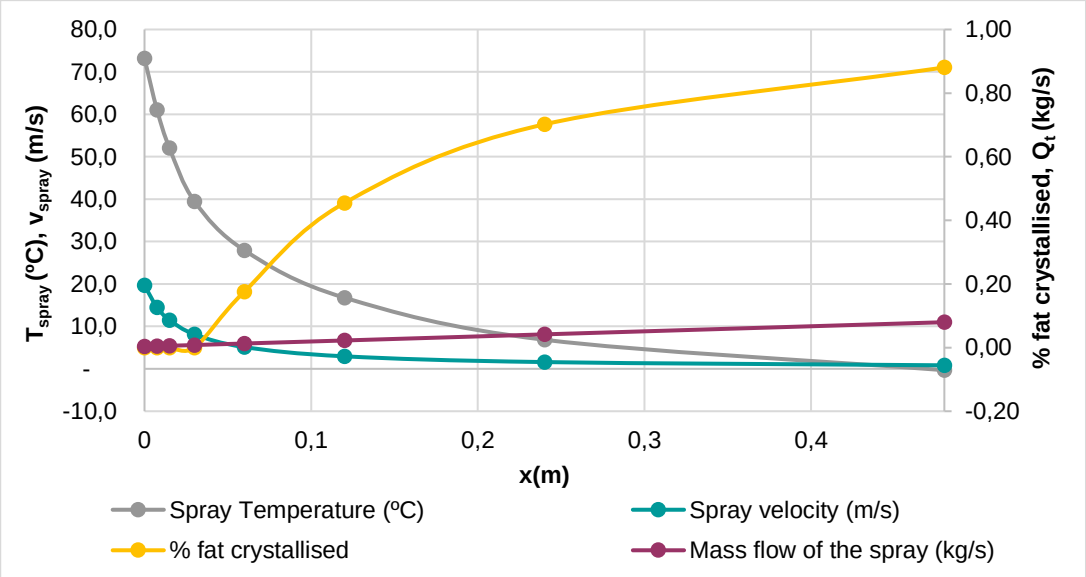

Figure 4.32 Spray profile for nozzle 76M – Axial distance from the nozzle (x); Spray temperature (T_{spray}); Spray velocity (v_{spray}); Mass flow of the spray (Q_t)

Table 4.30 Results of axial distance from the nozzle (x), the total mass flow of spray (Q_t), entrainment ratio (Q_t/Q_i), the velocity of the spray (v_{spray}), a diameter of the cone (d_{cone}), the average temperature of the spray (T_{spray}), % fat crystallised, pressure drop (ΔP) and Reynolds number (Re) for nozzle 76M

x (m)	Q_t (kg/s)	Q_t/Q_i	v_{spray} (m/s)	d_{cone} (m)	T_{spray} (°C)	% Fat crystallised	ΔP	Re
0.000	0.003	1.0	19.7	0.001	73.2	0%	5.3E-05	675880
0.008	0.005	1.4	14.5	0.006	61.1	0%	3.9E-05	53490
0.015	0.006	1.7	11.5	0.009	52.1	0%	3.1E-05	37883
0.030	0.008	2.4	8.1	0.013	39.5	0%	2.2E-05	26808
0.060	0.013	3.8	5.1	0.018	27.9	18%	1.4E-05	18964
0.120	0.022	6.7	2.9	0.025	16.8	45%	7.9E-06	13412
0.240	0.042	12.3	1.6	0.036	6.9	70%	4.3E-06	9485
0.480	0.080	23.7	0.8	0.050	-0.3	88%	2.2E-06	6707

4.4.4 Nozzle 70M

Table 4.31 shows that the produced wax powder is sufficiently cooled down. It also indicates that immense recirculation takes places as the entrainment ratio at the end of the spray tower is 91.8, which means that about 2478 kg gas/h can be entrained. The fat only starts to crystallise at 27.9°C, and after reaching -7.3 °C, the quantity of fat crystalised is 100%. From **figure 4.33**, we can observe that the mass flow of spray is increasing linearly with the distance from the nozzle. Also, it is observed that the velocity of the spray decreases as the spray is cooled down.

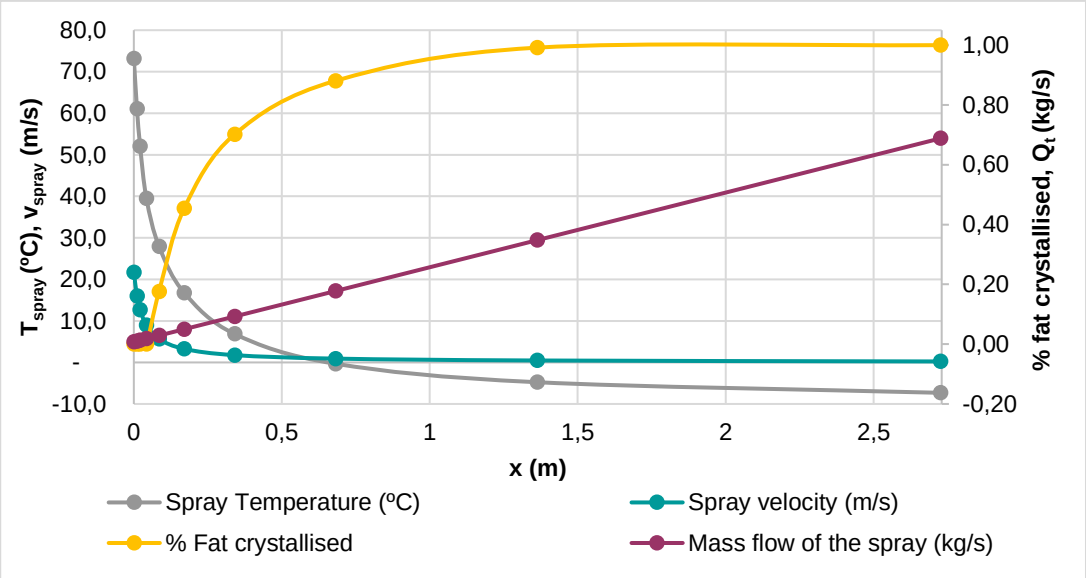

Figure 4.33 Spray profile for nozzle 70M – Axial distance from the nozzle (x); Spray temperature (T_{spray}); Spray velocity (v_{spray}); Mass flow of the spray (Q_t)

Table 4.31 Results of axial distance from the nozzle (x) total mass flow of spray (Q_t), entrainment ratio (Q_t/Q_i), the velocity of the spray (v_{spray}), a diameter of the cone (d_{cone}), the average temperature of the spray (T_{spray}), % fat crystallised, pressure drop (ΔP) and Reynolds number (Re) for nozzle 70M

x (m)	Q_t (kg/s)	Q_t/Q_i	v_{spray} (m/s)	d_{cone} (m)	T_{spray} (°C)	% Fat crystallised	ΔP	Re
0.000	0.008	1.0	21.7	0.001	73.2	0%	1.3E-04	1059164
0.011	0.010	1.4	16.0	0.009	61.1	0%	9.6E-05	83824
0.021	0.013	1.7	12.7	0.013	52.1	0%	7.6E-05	59365
0.043	0.018	2.4	9.0	0.018	39.5	0%	5.4E-05	42011
0.085	0.029	3.8	5.7	0.025	27.9	18%	3.4E-05	29718
0.170	0.050	6.7	3.3	0.036	16.8	45%	1.9E-05	21018
0.341	0.093	12.3	1.8	0.051	6.9	70%	1.0E-05	14863
0.682	0.178	23.7	0.9	0.072	-0.3	88%	5.5E-06	10510
1.363	0.348	46.4	0.5	0.101	-4.8	99%	2.8E-06	7432
2.726	0.688	91.8	0.2	0.143	-7.3	100%	1.4E-06	5255

5

5 Conclusion

Microparticles of jojoba wax encapsulating red pigment were produced using the PGSS process in batch mode. The PGSS procedure was successfully developed and optimized for the particle formation of jojoba wax. The sources used to develop this process are the scientific studies published on similar micronization of the PGSS process. Generation of wax particles from this process demonstrated that PGSS micronization technique is a reasonable alternative to conventional techniques for waxes microparticle production. The particles collected during experimentation were analysed using various analytical techniques, and an investigation on the influence of processing conditions on particle properties and characteristics was performed.

Additionally, a DoE study was performed in order to confirm which parameters have more influence on the particle properties investigated. In DoE, we only study the effect of quantity, temperature and pressure. In total, we performed 26 tests with Jojoba wax.

The wax was capable of dissolving substantial amounts of CO_2, up to 93% at 120 bar. The PGSS experiments were carried out varying the melting temperature (76-93ºC), the expansion pressure (75-150 bar), the quantity of the mixture (Jojoba wax + pigment) in a vessel (50-300g), the pigment loading (1-20%) and varying nozzle diameter (0.093-0.71mm). Lastly, we performed a test without stirring the solution. The properties of the powders were determined by adjusting the process conditions.

The PGSS demonstrated to be an effective technique for producing jojoba wax microparticles, having a good performance. The process yield ranged between of 65% to 97% with an average of 83%, meaning that the process is cost-effective. It is possible to conclude that a higher quantity of powder is produced using nozzles with smaller diameters (0,093 and 0,34mm) and lower quantity with higher pigment loading (5% and 10%). The DoE study shows that the quantity, the pressure, and the temperature do not affect the yield of the collected particles.

The results obtained from Optical Microscopy measurements indicate that the size of jojoba wax particles has a range between 7 and 109 µm. The most critical condition influencing the size of the particle and therefore the bulk density was found to be the quantity of mixture or GPR, followed by the melt temperature, nozzle diameter and pressure. Also, stirring the solution or not shows an influence on the particle size. If we don't stir the solution, we obtain smaller particles because we used less quantity of CO_2. The pigment loading seems to be the least critical condition indicating no influence on the particle size. However, this parameter shows a strong influence on particle morphology. Also, the DoE study confirms these results, the lower quantity, the lower temperature and higher temperatures we obtained smaller particles, and therefore, lowers values of bulk density.

By varying the quantity, we produced particles with a size range between 25 and 109 µm, and bulk densities from 161 to 236 kg/m^3, meaning that an increase of GPR (gas to product ratio) or a decrease on the quantity promotes an increase of wt% CO_2 (40% to 93%) leading to a decrease in the mean particle size. The highest bulk density was observed with 300g and with smaller GPR value 0,39. Also, a decrease in the melting temperature promotes a decrease in the particle size (88 to 14µm), and therefore a decrease in bulk density (186 to 132 kg/m^3). The nozzle diameter shows the same trend. A decrease of the nozzle diameter produced particles with a smaller size (77 to 7 µm) and consequently lower values of bulk density (180 to 134 kg/m^3). Lastly, an increase in pressure promotes an increase of wt% of CO_2 (67% to 89%) leading to a decrease in the particle size. By varying the pressure particles were produced with a size range between 21 and 91 µm—the range of bulk density was 95 to 191 kg/m^3.

The morphology of the obtained particles varied from hollow spheres to sponge-like particles and can be adjusted by the process conditions as well. At higher temperature and quantity, more spherical particles are obtained, while agglomerated particles occur at lower temperatures and quantity of the mixture (or higher values of GPR). Also, it was observed that an increase in the quantity of pigment leads to more sponge-like particles. The pressure does not appear to have a considerable influence on morphology.

Two different particle morphologies were observed (spherical hollow and sponge-like particles) depending on the pigment loading at 120 bar and 83ºC. At higher quantities of pigment (20%), we obtained sponge-like particles (foam-like particles), while spherical hollow particles occur at lower quantities of pigment (1%). Also, it was observed that the increase in the amount of pigment made the powder worse, producing only agglomerates of particles instead of a loose and fine powder.

Furthermore, in the DoE study, three morphology types were obseved: spherical hollow, sponge-like particles and agglomerates of spherical hollow particles at 75 and 150 bar in function of wt% CO_2 and bulk density.

At 76ºC and 150 bar with 50g (with 92 wt% CO_2), we observed sponge like-particles with a mean size of 25 µm. While at 93ºC and 75 bar with 300g (with 25 wt% CO_2), we observed spherical hollow particles with a mean size of 90 µm and with bulk density value of 376 kg/m^3, that indicates that higher quantities and temperatures, with lower pressures and therefore lower value of wt% CO_2 promote the formation of more spherical porous particles. While at a higher pressure and lowers temperatures and quantities, and therefore higher values of wt% CO_2, more distorted particles are generated. Moreover, we can conclude that the % of wt CO_2 has a strong effect on particle morphology.

The agglomerated particles were produced at 76ºC and 75 bar with 50g. The mean size of these particles was 50 µm, and the value of bulk density was 159kg/m^3, meaning that at the same pressure more distorted agglomerate particles are obtained with lower quantities and lower the temperature and therefore with lower values of bulk density.

The flow character was also investigated by calculating the Hausner's ratio and the Compressibility index (%). The statistics mode obtained was 1.4 for the Hausner's ratio meaning that the flow is poor, and thus the powder is cohesive and compressible. The most critical variable for the flow character was the % of pigment used, followed by the pressure. When we increased the % of pigment used, higher values of flowability were obtained. The range of Hausner's ratio values was between 1.8 and 3.6, meaning that the powder is non-flow and is highly compressible and less compact. Also, at higher pressure (150 bar), the flowability was fair (Hausner's ratio 1.2), meaning that the powder is fine and more fluidised than others. The temperature, the quantity of mixture used, the different nozzles and whether the mixture is stirred or not, are not significant parameters for the flow character.

Lastly, the obtained encapsulation efficiency was around 66%. The most critical value affecting the encapsulation efficiency was the % of pigment used, followed by the quantity of wax used. The remain parameters do not show an evident influence. However, the DoE study shows that the quantity, the pressure, and temperature do not influence the encapsulation.

Although the highest values of encapsulation efficiency were observed in the DoE study at 93ºC, at 75 bar and 300g with a mean particle size of 54 µm, we obtained 74% of encapsulation efficiency. The same value of encapsulation effiency was also observed at 150 bar with 300g and the mean particle size of 71 µm. As at 93ºC, 75 bar and 300g, the encapsulation efficiency has a slight a decrease (67%), we can conclude that the pressure does not have an apparent influence on the encapsulation efficiency. Also, we obtained higher values of EE% with higher temperatures and higher quantities.

Within the % of pigment used, we obtained a range of encapsulation efficiency between 18 and 36%, meaning that an increase in the amount of pigment used leads to a decrease in encapsulation efficiency. For lower quantities (50g), the encapsulation efficiency is 41%, and for higher quantities (200g to 300g) is around 57%.

The secondary goal of this thesis was to find a suitable coating material for a cosmetic application, with the objective of stabilising an enzyme in a water continuous cleansing cream. Additionally to the jojoba experiments, we performed more 17 tests with different fats, oils and waxes to produce a loose and fine powder. The materials used were hydrogenated palm oil (Fat powder), Cocoa Butter, Sunflower oil, Macadamia wax, Beeswax, Jojoba wax and Lecithin (emulsifier).

It was possible to conclude that the powders are loose and fine with higher amounts of wax while at higher amounts of fats and oils the powders show more agglomeration. Also, the use of Beeswax and lecithin had a negative effect on the powder structure. The mixtures of materials that produce the best powders were as follows:

- 87% Fat powder + 13% Cocoa Butter
- 50% Macadamia wax + 50% Fat powder
- 75% Macadamia wax + 25% Sunflower oil
- 75% Jojoba wax + 25% Cocoa Butter
- 90% Jojoba wax + 10% Sunflower oil

Finally, we studied the theory of entrainment of the surrounding gas (cooling gas) with a mathematical model for the PGSS process that considers a cone-shapped spray from the nozzle. The model was applied to four different nozzles (Nozzle 63M, 80M,76M and 70M). According to the theory, the surrounding gas is entrained by the spray due to their different velocities. We can conclude, that the mathematical model was well applied, we observed that the amount of gas entrained increases linearly with the distance from the nozzle and the velocity of the spray decreases with the cooling of spray. For the four different nozzles the fat started to crystallize at 28ºC. However, we only obtained 100% fat crystallized with two nozzles (63M and 70M) at -7.3ºC. The model was not valid until we get 100% fat crystallized for the remaining nozzles. The 63M and 70M nozzles lead to higher values of the amount of gas entrained (1730 and 2478 kg gas/hr), while lower amounts of gas entrained are obtained for the 80M and 76M nozzles (76 and 287 kg gas/hr).

Future Recommendations:

Due to the high cost of Scanning Electron Microscopy (SEM) machine analyses, it was only possible to observe five samples of powders (and we performed 26 tests to study the conditions of PGSS in microparticles). In the future, it would be important to observe more samples by SEM to perform more in-depth analysis of the morphology.

We observed a small number of particles with Optical Microscopy for the size analysis. In future works, it would be preferable to use another analytic method to investigate more particles like laser diffraction spectrometry.[126]

The encapsulation efficiency was determined by the construction of calibration curves of absorbances at different concentrations of pigment. In future works, it would be preferable to use a more precise analytic method such HPLC (High-performance liquid chromatography*)* and ICP-MS (Inductively Coupled Plasma Mass Spectrometry) [127][128]

The powders flowability was studied by calculating the Hausner's ratio and Compressibility index (%).In future works, the critical angle of repose (flowability parameter) can also be investigated.[129]

The DoE study was performed only with three parameters by using full plan factorial. In future works, a study with more variables and more tests will be able to give a more in-depth study of the conditions and their impact in the properties of the materials produced.

6

References

[1] A. Montes, M. D., C. Pereyra, and E. J. M. de la Oss, “Particles Formation Using Supercritical Fluids,” *Mass Transf. - Adv. Asp. Dr. Hironori Nakajima (ED.),* vol. 1, p. 824, 2011, doi: 10.5772/21271.

[2] T. K. Fahim *et al.*, “Particle formation and micronization using non-conventional techniques-review,” *Chem. Eng. Process. Process Intensif.*, vol. 86, pp. 47–52, 2014, doi: 10.1016/j.cep.2014.10.009.

[3] E. Of, M. I. N. The, and A. G. Assessment, “Sources, Fate and Effects of microplastics in the marine enviroment: A Global Assessment,” *(Kershaw, P. J., ed.) (IMO/FAO/UNESCO-IOC/UNIDO/WMO/IAEA/UN/UNEP/UNDP Jt. Gr. Expert. Sci. Asp. Mar. Environ. Prot.*, vol. 90, p. 96, 2015.

[4] M. Quest, “Global Micronized wax market 2020 by manufacturers regions type and application to 2025,” *Report 30755*, 2020. [Online]. Available: https://www.marketquest.biz/. [Accessed: 10-Nov-2020].

[5] D. Patel, S. Kellici, and B. Saha, “Green process engineering as the key to future processes,” *Processes*, vol. 2, no. 1, pp. 311–332, 2014, doi: 10.3390/pr2010311.

[6] W. L. Priamo, I. Dalmolin, D. L. Boschetto, N. Mezzomo, S. R. S. Ferreira, and J. V. Oliveira, “Micronization processes by supercritical fluid tecnologies: a short review on process design (2008-2012),” *Acta Sci. - Technol.*, vol. 35, no. 4, pp. 695–709, 2013, doi: 10.4025/actascitechnol.v35i4.18819.

[7] A. A. B. Ruíz, “Conventional and Advanced Food Processing Technologies,” *Suvendu Bhattarcharya*, vol. 3, no. 2, pp. 54–67, 2015, doi: 10.1002/9781118406281.

[8] A. Dhiman and P. K. Prabhakar, “Micronization in food processing: A comprehensive review of mechanistic approach, physicochemical, functional properties and self-stability of micronized food materials,” *J. Food Eng.*, p. 110248, 2020, doi: 10.1016/j.jfoodeng.2020.110248.

[9] F. Salaün, “Microencapsulation technology for smart textile coatings,” *Act. Coatings Smart Text.*, vol. 9, pp. 179–220, 2016, doi: 10.1016/B978-0-08-100263-6.00009-5.

[10] E. Keven Silva and M. Angela A. Meireles, “Encapsulation of Food Compounds Using Supercritical Technologies: Applications of Supercritical Carbon Dioxide as an Antisolvent,” *Food Public Heal.*, vol. 4, no. 5, pp. 247–258, 2014, doi: 10.5923/j.fph.20140405.06.

[11] E. Reverchon and G. Della Porta, “Supercritical fluids-assisted micronization techniques. Low-impact routes for particle production,” *Pure Appl. Chem.*, vol. 73, no. 8, pp. 1293–1297, 2001, doi: 10.1351/pac200173081293.

[12] P. Sanguansri and M. A. Augustin, “Nanoscale materials development - a food industry perspective,” *Trends Food Sci. Technol.*, vol. 17, no. 10, pp. 547–556, 2006, doi: 10.1016/j.tifs.2006.04.010.

[13] J. Weiss, P. Takhistov, and D. J. McClements, “Functional materials in food nanotechnology,” *J. Food Sci.*, vol. 71, no. 9, pp. 107–116, 2006, doi: 10.1111/j.1750-3841.2006.00195.x.

[14] Knez, E. Markočič, M. Leitgeb, M. Primožič, M. Knez Hrnčič, and M. Škerget, “Industrial applications of supercritical fluids: A review,” *Energy*, vol. 77, pp. 235–243, 2014, doi: 10.1016/j.energy.2014.07.044.

[15] P. Münüklü and P. J. Jansens, “Particle formation of an edible fat (rapeseed 70) using the supercritical melt micronization (ScMM) process,” *J. Supercrit. Fluids*, vol. 40, no. 3, pp. 433–442, 2007, doi: 10.1016/j.supflu.2006.07.015.

[16] E. Weidner, Z. Znez, and Z. Novak, “Process for preparing particles or powders,” WO 952021688, 1995.

[17] T. Fornari and R. P. Stateva, “High Pressure Fluid Technology for Green Food Processing,” *Food Eng. Ser.*, vol. 1, p. 517, 2015, doi: 10.1007/978-3-319-10611-3.

[18] A. M. Grumezescu, “ENCAPUSLATIONS - Nanotechnology in the Agri-Food Industry, Volume 2,” vol. 2, p. 902, 2017, doi: https://doi.org/10.1556/066.2017.46.1.16.

[19] M. J. Lakkis, “Encapsulation and Controlled Release Technologies in Food Systems,” vol. 1, p. 383, 2016, doi: 10.1002/9781118946893.

[20] Z. Knez and E. Weidner, “Particles formation and particle design using supercritical fluids,” *Curr. Opin. Solid State Mater. Sci.*, vol. 7, no. 4–5, pp. 353–361, 2003, doi: 10.1016/j.cossms.2003.11.002.

[21] Y. Hakuta, H. Hayashi, and K. Arai, “Fine particle formation using supercritical fluids,” *Curr. Opin. Solid State Mater. Sci.*, vol. 7, no. 4–5, pp. 341–351, 2003, doi: 10.1016/j.cossms.2003.12.005.

[22] N. Elvassore, M. Flaibani, A. Bertucco, and P. Caliceti, “Thermodynamic Analysis of Micronization Processes from Gas-Saturated Solution,” *Ind. Eng. Chem. Res.*, vol. 42, no. 23, pp. 5924–5930, 2003, doi: 10.1021/ie030278a.

[23] Z. Akbari, M. Amanlou, J. Karimi-Sabet, A. Golestani, and M. S. Niassar, “Application of supercritical fluid technology for preparation of drug loaded solid lipid nanoparticles,” *Int. J. Nanosci. Nanotechnol.*, vol. 16, no. 1, pp. 13–33, 2020.

[24] C. D. Pascual and P. Subra-Paternault, “Supercritical Fluid Nanotechnology: Advances and Applications in Composites and Hybrid Nanomaterials,” *Pascale Subra-Paternault*, vol. 1, p. 566, 2015, doi: https://doi.org/10.1201/b19242.

[25] A. Tandya, R. Mammucari, F. Dehghani, and N. R. Foster, “Dense gas processing of polymeric controlled release formulations,” *Int. J. Pharm.*, vol. 328, no. 1 SPEC. ISS., pp. 1–11, 2007, doi: 10.1016/j.ijpharm.2006.08.016.

[26] S. Do Yeo and E. Kiran, “Formation of polymer particles with supercritical fluids: A review,” *J. Supercrit. Fluids*, vol. 34, no. 3, pp. 287–308, 2005, doi: 10.1016/j.supflu.2004.10.006.

[27] S. K. Ghosh, “Functional Coatings and Microencapsulation: A General Perspective,” *Funct. Coatings By Polym. Microencapsul.*, vol. 1, pp. 1–28, 2006, doi: 10.1002/3527608478.ch1.

[28] P. T. da Silva *et al.*, “Microencapsulation: concepts, mechanisms, methods and some applications in food technology,” *Ciência Rural*, vol. 44, no. 7, pp. 1304–1311, 2014, doi: 10.1590/0103-8478cr20130971.

[29] R. G. Bodade and A. G. Bodade, “Microencapsulation of bioactive compounds and enzymes for therapeutic applications,” *Biopolym. Formul.*, vol. 17, pp. 381–404, 2020, doi: 10.1016/b978-0-12-816897-4.00017-5.

[30] N. V. N. Jyothi, P. M. Prasanna, S. N. Sakarkar, K. S. Prabha, P. S. Ramaiah, and G. Y. Srawan, “Microencapsulation techniques, factors influencing encapsulation efficiency,” *J. Microencapsul.*, vol. 27, no. 3, pp. 187–197, 2010, doi: 10.3109/02652040903131301.

[31] R. P. Singh, N. sarju, A. Sharma, S. G. Singh, and K. Sanket, “Microchip for drug delivery system: A review,” *J. Appl. Pharm. Sci.*, vol. 1, no. 4, pp. 07–11, 2011.

[32] R. Urbas, R. Milošević, N. Kašiković, Ž. Pavlović, and U. S. Elesini, “Microcapsules application in graphic arts industry: a review on the state-of-the-art,” *Iran. Polym. J. (English Ed.*, vol. 26, no. 7, pp. 541–561, 2017, doi: 10.1007/s13726-017-0541-1.

[33] F. Temelli, “Perspectives on supercritical fluid processing of fats and oils,” vol. 47, pp. 583–590, 2009, doi: 10.1016/j.supflu.2008.10.014.

[34] M. Goslinska and S. Heinrich, “Characterization of waxes as possible coating material for organic aerogels,” *Powder Technol.*, 2019, doi: 10.1016/j.powtec.2019.08.096.

[35] L. Koen, “The Micronisation of Synthetic Waxes,” no. April, p. 176, 2003, doi: 10.1.1.947.7060.

[36] C. TRECORA, “Waxes in coatings.” [Online]. Available: https://d1io3yog0oux5.cloudfront.net/trecchem/files/pages/products-services/polymer-products/Coatings+20160225.pdf. [Accessed: 10-Nov-2020].

[37] F. R. of G. Kuehnle, Adolf (Hoechster, “PROCESS FOR THE PRODUCTION OF MICRONIZED WAXES,” 1989.

[38] L. S. Tu, F. Dehghani, and N. . Foster, “Micronisation and microencapsulation of pharmaceuticals using a carbon dioxide antisolvent,” *Powder Technol.*, vol. 126, no. 2, pp. 134–149, Jul. 2002, doi: 10.1016/S0032-5910(02)00045-1.

[39] A. K. Anal, “Recent advances in microencapsulation of probiotics for industrial applications and targeted delivery,” vol. 18, pp. 240–251, 2007, doi: 10.1016/j.tifs.2007.01.004.

[40] A. Semenzato, G. Amabile, K. Vezzù, P. Caliceti, and A. Bertucco, “Compressed fluid based process for development of cosmetic products,” *AIChE Annu. Meet. Conf. Proc.*, 2006, doi: h.

[41] L. Granjou, “Micronized polymer powder and cosmetic composition thereof,” US 2012/0029076 A1, 2012.

[42] I. Bureau, “Micronized Polymer Powder and Cosmetic Composition thereof Field,” WO 2010/12032 A2, 2010.

[43] C. Erkey, “Supercritical Fluid Science and Technology Series Editor – Erdogan Kiran Vol . 1 Supercritical Fluids and Organometallic Compounds : From Recovery of Trace Metals to Synthesis of Nanostructured Materials .,” *Supercrit. Fluid Sci. Technol. Ser. Ed. - Erdogan Kiran*, vol. 1, p. 248, 2014, doi: http://dx.doi.org/10.1016/B978-0-444-59413-6.00001-7.

[44] Y. Pérez De Diego, “Production of controlled drug delivery microparticles using supercritical CO2,” Delft, 2002.

[45] R. Parhi and P. Suresh, “Supercritical Fluid Technology: a Review,” *J. Adv. Pharm. Sci. Technol.*, vol. 1, no. 1, pp. 13–36, 2013, doi: 10.14302/issn.2328-0182.japst-12-145.

[46] J. Xu, H. Zhang, B. Zhu, and J. Xie, “Critical supercritical-boiling-number to determine the onset of heat transfer deterioration for supercritical fluids,” *Sol. Energy*, vol. 195, no. August 2019, pp. 27–36, 2020, doi: 10.1016/j.solener.2019.11.036.

[47] N. R. Abedin, “Micronization of Polyethylene Wax in an Extrusion Process using Supercritical Carbon Dioxide,” Waterloo, Ontario, Canada, 2011.

[48] I. Pasquali, R. Bettini, and F. Giordano, “Solid-state chemistry and particle engineering with supercritical fluids in pharmaceutics,” *Eur. J. Pharm. Sci.*, vol. 27, no. 4, pp. 299–310, 2006, doi: 10.1016/j.ejps.2005.11.007.

[49] A. Kordikowski, T. Shekunov, and P. York, “Polymorph Control of Sulfathiazole in Supercritical CO 2,” *Pharm. Res.*, vol. 18, no. 5, pp. 682–688, 2001, doi: 10.1023/a:1011045729706.

[50] J. Fages *et al.*, “Particle generation for pharmaceutical applications using supercritical fluid technology,” *Powder Technol. Elservier*, pp. 219–226, 2004, doi: 10.1016/j.powtec.2004.02.007.

[51] I. Pasquali and R. Bettini, “Are pharmaceutics really going supercritical?,” *Int. J. Pharm.*, vol. 364, no. 2, pp. 176–187, 2008, doi: 10.1016/j.ijpharm.2008.05.014.

[52] G. Brunner, “Supercritical fluids : technology and application to food processing,” vol. 67, pp. 21–33, 2005, doi: 10.1016/j.jfoodeng.2004.05.060.

[53] M. Türk, “Particle Formation with Supercritical Fluids Challenges and Limitations,” *Supercrit. Fluid Sci. Technol.*, vol. Volume 6, pp. 1–139, 2014, doi: https://doi.org/10.1016/B978-0-444-59486-0.00009-7.

[54] A. Dibenedetto and I. Tommasi, “Biological Utilization of Carbon Dioxide: The Marine Biomass Option,” *Carbon Dioxide Recover. Util. Springer Netherlands, (2003), 315-324*, pp. 315–324, 2003, doi: 10.1007/978-94-017-0245-4_13.

[55] P. M. V. R. & A. R. Barron, “3.4: Supercritical Fluid Chromatography,” *LibreTexts*, 2020. [Online]. Available: https://chem.libretexts.org/. [Accessed: 10-Aug-2020].

[56] A. Aguiar-Ricardo, “Building dry powder formulations using supercritical CO2 spray drying,” *Curr. Opin. Green Sustain. Chem.*, vol. 5, pp. 12–16, 2017, doi: 10.1016/j.cogsc.2017.03.005.

[57] J. Eastoe, C. Yan, and A. Mohamed, “Microemulsions with CO 2 as a solvent,” in *Current Opinion in Colloid and Interface Science*, vol. 17, no. 5, 2012, pp. 266–273.

[58] J. J and P. M., “Particle design using supercritical fluids: Literature and patent survey,” *J. Supercrit. Fluids*, vol. 20, no. 3, p. 244, 2005, doi: 10.1016/S0896-8446(01)00064-X.

[59] C. Vemavarapu, M. J. Mollan, M. Lodaya, and T. E. Needham, “Design and process aspects of laboratory scale SCF particle formation systems,” *Int. J. Pharm.*, vol. 292, no. 1–2, pp. 1–16, 2005, doi: 10.1016/j.ijpharm.2004.07.021.

[60] A. V. M. Nunes and C. M. M. Duarte, “Dense CO2 as a Solute, Co-Solute or Co-Solvent in Particle Formation Processes: A Review,” pp. 2017–2041, 2017, doi: 10.3390/ma4112017.

[61] E. Lack, E. Weidner, Z. Knez, and S. Gruner, “Particle generation with supercritical CO2,” *Proc. 1st*, 2000.

[62] Z. Knez, M. Škerget, M. Knez Hrnčič, and D. Čuček, “Particle Formation Using Sub- and Supercritical Fluids,” in *Supercritical Fluid Technology for Energy and Environmental Applications*, 2014, pp. 31–67.

[63] E. Reverchon, “Supercritical-assisted atomization to produce micro- and/or nanoparticles of controlled size and distribution,” *Ind. Eng. Chem. Res.*, vol. 41, no. 10, pp. 2405–2411, 2002, doi: 10.1021/ie010943k.

[64] E. Reverchon and A. Antonacci, “Polymer microparticles production by supercritical assisted atomization,” *J. Supercrit. Fluids*, vol. 39, no. 3, pp. 444–452, 2007, doi: 10.1016/j.supflu.2006.03.005.

[65] A. Martín and M. J. Cocero, “Micronization processes with supercritical fluids: Fundamentals and mechanisms,” *Adv. Drug Deliv. Rev.*, vol. 60, no. 3, pp. 339–350, 2008, doi: 10.1016/j.addr.2007.06.019.

[66] A. Tabernero, E. M. Martín del Valle, and M. A. Galán, “Supercritical fluids for pharmaceutical particle engineering: Methods, basic fundamentals and modelling,” *Chem. Eng. Process. Process Intensif.*, vol. 60, pp. 9–25, 2012, doi: 10.1016/j.cep.2012.06.004.

[67] R. Adami, “Micronization of Phamaceuticals and food Ingredients using supercritical fluid techniques,” University of Salermo, 2007.

[68] L. Gradón and J. Marijnsissen, “Optimizatio of Aerol Drug Delivery,” *Springer-Science + Bus. Media, B.V*, vol. 1, no. IX, p. 315, 2003, doi: 10.1007/978-94-017-0267-6.

[69] F. Graser and G. Wickenhaeuser, “Conditioning of finely divided crude organic pigments,” US4451654A, 1982.

[70] K. Y, “Matsushita Electric Ind. Co. Ltd,” JP 5132656, 1991.

[71] B. E. W. Kenneth Andrew Nielsen, John Nicholas Argyropoulos, “Methods for producing coating powders, catalysts and drier water-borne coatings by spraying compositions with compressed fluids,” EP0711586A2, 1996.

[72] A. C.-H. K. Kenneth A. Nielsen, Jeffrey J. Lear, John N. Argyropoulos, “Methods for admixing compressed fluids with solvent-borne compositions comprising solid polymers,” US5312862, 1994.

[73] C. W. G. Kenneth A. Nielsen, David C. Busby, Marc D. Donohue, “Method for spraying polymeric compositions with reduced solvent emission and enhanced atomization Abstract,” US5290603, 1994.

[74] K. Andrew *et al.*, “Methods for the spray application of water-borne coatings with compressed fluids,” EP 0 609 540 B1, 1998.

[75] R. E. Sievers and U. Karst, “Procédé et appareil de production de particules fines,” EP000677332B1, 2002.

[76] Y. Karasawa, “Process and apparatus for pulverizing solid particles,” DE1940027B4, 1995.

[77] E. Weidner, M. Petermann, and Z. Knez, “Multifunctional composites by high-pressure spray processes,” *Curr. Opin. Solid State Mater. Sci.*, vol. 7, no. 4–5, pp. 385–390, 2003, doi: 10.1016/j.cossms.2003.09.002.

[78] Ž. Knez, “High pressure process technology - Quo vadis?,” *Chem. Eng. Res. Des.*, vol. 82, no. 12, pp. 1541–1548, 2004, doi: 10.1205/cerd.82.12.1541.58045.

[79] K. Z. Weinder. E, Steiner. R, “Powder Generation from Polythyleneglycols with Compressible Fluids,” *Elsiever Sci. B.V*, pp. 223–228, 2000.

[80] P. Kappler, W. Leiner, M. Petermann, and E. Weidner, “Size and Morphology of Particles Generated By Spraying Polymer-Melts With Carbon Dioxide,” *ISSF 8th*, no. January, 2003.

[81] J. Kerč, S. Srčič, Ž. Knez, and P. Senčar-Božič, “Micronization of drugs using supercritical carbon dioxide,” *Int. J. Pharm.*, vol. 182, no. 1, pp. 33–39, 1999, doi: 10.1016/S0378-5173(99)00063-0.

[82] P. Senčar-Božič, S. Srčič, Ž. Knez, and J. Kerč, “Improvement of nifedipine dissolution characteristics using supercritical CO2,” *Int. J. Pharm.*, vol. 148, no. 2, pp. 123–130, 1997, doi: 10.1016/S0378-5173(96)04838-7.

[83] M. Rodrigues, N. Peiriço, H. Matos, E. Gomes De Azevedo, M. R. Lobato, and A. J. Almeida, “Microcomposites theophylline/hydrogenated palm oil from a PGSS process for controlled drug delivery systems,” *J. Supercrit. Fluids*, vol. 29, no. 1–2, pp. 175–184, 2004, doi: 10.1016/S0896-8446(03)00034-2.

[84] J. Li, H. A. Matos, and E. G. De Azevedo, “Two-phase homogeneous model for particle formation from gas-saturated solution processes,” *J. Supercrit. Fluids*, vol. 32, no. 1–3, pp. 275–286, 2004, doi: 10.1016/j.supflu.2004.01.004.

[85] J. Li, M. Rodrigues, A. Paiva, H. A. Matos, and E. G. De Azevedo, “Modeling of the PGSS process by crystallization and atomization,” *AIChE J.*, vol. 51, no. 8, pp. 2343–2357, 2005, doi: 10.1002/aic.10478.

[86] M. Strumendo, A. Bertucco, and N. Elvassore, “Modeling of particle formation processes using gas saturated solution atomization,” *J. Supercrit. Fluids*, vol. 41, no. 1, pp. 115–125, 2007, doi: 10.1016/j.supflu.2006.09.003.

[87] J. Fages *et al.*, “Particle generation for pharmaceutical applications using supercritical fluid technology,” *Powder Technol. Elservier*, 2004, doi: 10.1016/j.powtec.2004.02.007.

[88] E. Weidner, “High pressure micronization for food applications,” *J. Supercrit. Fluids*, vol. 47, no. 3, pp. 556–565, 2009, doi: 10.1016/j.supflu.2008.11.009.

[89] Jimbin MaiGang SuPablo Oliver Velarde Pena, “Powderous formulation,” EP2925153A1, 2013.

[90] F. E. W. I. J. A. S. M. Akkermans, “Edible oil composition,” WO2011134627A1, 2011.

[91] E. 2181604 A1, “Dispersion structuring agent,” EP 2181604 A1, 2007.

[92] E. De Paz, Á. Martín, C. M. M. Duarte, and M. José, “Formulation of β -carotene with poly- (ε -caprolactones) by PGSS process,” *Powder Technol.*, vol. 217, pp. 77–83, 2012, doi: 10.1016/j.powtec.2011.10.011.

[93] J. Yun, S. Lee, J. Park, and B. Chun, “Particle Formation of Lecithin Process with Particles from Gas- Saturated Solutions using Supercritical Carbon Dioxide,” vol. 2, no. 0, pp. 22–26, 2012, doi: 10.1016/j.apcbee.2012.06.005.

[94] P. MÜNÜKLÜ, “Particle Formation of Ductile Materials using the PGSS Technology with Supercritical Carbon Dioxide,” Delft, 2005.

[95] L. G. Hanu, P. Alessi, A. Kilzer, and S. Kareth, “Manufacturing and characterization of water filled micro-composites,” *J. Supercrit. Fluids*, vol. 66, pp. 274–281, 2012, doi: 10.1016/j.supflu.2011.12.017.

[96] M. Pemsel, S. Schwab, A. Scheurer, D. Freitag, R. Schatz, and E. Schlücker, “Advanced PGSS process for the encapsulation of the biopesticide Cydia pomonella granulovirus,” vol. 53, pp. 174–178, 2010, doi: 10.1016/j.supflu.2009.12.006.

[97] M. Knez, D. Cör, M. T. Verboten, and Ž. Knez, “Application of supercritical and subcritical fluids in food processing,” no. April, pp. 59–67, 2018, doi: 10.1093/fqsafe/fyy008.

[98] J. Letourneau *et al.*, “Micronized cocoa butter particles produced by a supercritical process,” *Chem. Eng. Process. Process Inten- sification, Elsevier, 2005, 4th Int. Conf. Conveying Handl. Part. Solids*, pp. 201–207, 2003, doi: 10.1016/j.cep.2004.03.013.

[99] M. Lubary, T. W. De Loos, H. Joop, and G. W. Hofland, “Production of microparticles from milk fat products using the Supercritical Melt Micronization (ScMM) process,” *J. Supercrit. Fluids*, vol. 55, no. 3, pp. 1079–1088, 2011, doi: 10.1016/j.supflu.2010.10.010.

[100] L. Zhu, H. Lan, B. He, W. Hong, and J. Li, “Encapsulation of Menthol in Beeswax by a Supercritical Fluid Technique,” vol. 2010, p. 7, 2010, doi: 10.1155/2010/608680.

[101] P. J. Ginty, M. J. Whitaker, K. M. Shakesheff, and S. M. Howdle, “Drug delivery goes supercritical,” *Mater. Today*, vol. 8, no. 8 SUPPL., pp. 42–48, 2005, doi: 10.1016/S1369-7021(05)71036-1.

[102] S. P. Nalawade, F. Picchioni, and L. P. B. M. Janssen, “Batch production of micron size particles from poly(ethylene glycol) using supercritical CO2 as a processing solvent,” *Chem. Eng. Sci.*, vol. 62, no. 6, pp. 1712–1720, 2007, doi: 10.1016/j.ces.2006.04.034.

[103] P. De Tarso, “pombalina.uc.pt digitalis.uc.pt,” Universidade de Coimbra, 2020.

[104] Ž. Knez, M. Knez Hrnčič, and M. Škerget, “Particle Formation and Product Formulation Using Supercritical Fluids,” *Annual Review of Chemical and Biomolecular Engineering*, vol. 6, no. 1, pp. 379–407, 2015.

[105] Z. Mandžuka and Ž. Knez, “Influence of temperature and pressure during PGSS™ micronization and storage time on degree of crystallinity and crystal forms of monostearate and tristearate,” *J. Supercrit. Fluids*, vol. 45, no. 1, pp. 102–111, 2008, doi: 10.1016/j.supflu.2007.11.006.

[106] T. Wendt, G. Brandin, and E. Weidner, “PGSS - The innovative production of fluid-filled microcapsules for the food industry,” *Proc. Eur. Congr. Chem. Eng.*, no. September, pp. 16–20, 2007.

[107] L. G. Hanu, P. Alessi, A. Kilzer, and S. Kareth, “Manufacturing and characterization of water filled micro-composites,” *J. Supercrit. Fluids*, vol. 66, pp. 274–281, 2012, doi: 10.1016/j.supflu.2011.12.017.

[108] S. S. Co., “Catalog of Industrial Hydraulic Spray Products.” [Online]. Available: https://www.spray.com/. [Accessed: 10-Oct-2020].

[109] C. Spraying Systems, “SK Series SprayDry Nozzles,” 2001. [Online]. Available: https://www.spray.com/. [Accessed: 10-Nov-2020].

[110] T. De Vries, “Scale up of fat powder production using supercritical melt micronisation,” Weesp, 2010.

[111] M. Â. P. R. Cerqueira, R. N. C. Pereira, Ó. L. da S. Ramos, J. A. C. Teixeira, and A. A. Vicente, “Edible food packaging: Materials and processing technologies,” *Edible Food Packag. Mater. Process. Technol.*, pp. 1–445, 2017, doi: 10.1201/b19468.

[112] W. Carrillo, C. Carpio, D. Morales, E. Vilcacundo, and M. Álvarez, “Fatty acids composition in macadamia sedes oil (Macadamia integrifolia) from Ecuador,” *Asian J. Pharm. Clin. Res.*, vol. 10, no. 2, pp. 303–306, 2017, doi: 10.22159/ajpcr.2017.v10i2.15618.

[113] C. Scaman, “Food Additives Data Book,” *Food Res. Int.*, vol. 36, no. 8, p. 871, 2003, doi: 10.1016/s0963-9969(03)00081-4.

[114] P. Schuck and A. Ouest, “Milk Powder : Physical and Functional Properties of Milk Powders,” *Elsiever Sci. B.V*, vol. 1, pp. 117–124, 2011.

[115] Y. Qiu, Y. Chen, G. G. . Zhang, Y. Lawrence, and R. V. Mantri, “Developing Solid Oral Dosage Forms,” *Pharm. Theory Prat.*, vol. 2, p. 1176, 2016.

[116] A. G. Kravanja, P. Kotnik, and B. Ljubec, “Formulation of nimodipine, fenobibrate, and o-vanillin with Brij S100 and PEG 4000 using the PGSS process,” *J. Supercrit. Fluids*, pp. 245–253, 2018, doi: 10.1016/j.supflu.2018.01.021.

[117] A. Pestieau, F. Krier, P. Lebrun, A. Brouwers, B. Streel, and B. Evrard, “Optimization of a PGSS (particles from gas saturated solutions) process for a fenofibrate lipid-based solid dispersion formulation,” *Int. J. Pharm.*, vol. 485, no. 1–2, pp. 295–305, 2015, doi: 10.1016/j.ijpharm.2015.03.027.

[118] D. B. Hibbert, “Experimental design in chromatography: A tutorial review,” *J. Chromatogr. B Anal. Technol. Biomed. Life Sci.*, vol. 910, pp. 2–13, 2012, doi: 10.1016/j.jchromb.2012.01.020.

[119] D. C. Montgomery, “Design and Analysis of Experiments Eighth Edition,” *Jonh Wiley Sons*, vol. 8, p. 730, 2012.

[120] M. Brion, S. Jaspart, L. Perrone, G. Piel, and B. Evrard, “The Journal of Supercritical Fluids The supercritical micronization of solid dispersions by Particles from Gas Saturated Solutions using experimental design,” vol. 51, pp. 50–56, 2009, doi: 10.1016/j.supflu.2009.06.021.

[121] C. A. Garc, “Modeling of the Production of Lipid Microparticles Using PGSS ® Technique,” *Molecules*, p. 14, 2020, doi: 10.3390/molecules25214927.

[122] J. Antony, “Design of Experiments for Engineers and Scientists,” *Elsiever Sci. B.V*, vol. 7, pp. 87–112, 2014, doi: 10.1016/B978-0-08-099417-8.00007-9.

[123] N. N. I. of S. and Technology, “Nist Chemistry Weebok, SRD 69,” *Welcome to the NIST Chemistry WebBook*. [Online]. Available: https://webbook.nist.gov/. [Accessed: 29-Oct-2020].

[124] E. González-González, V., Valero-Coss, R. O., & Campos-López, “Thermal properties of jojoba wax,” *Jounal Therm. Anal.*, vol. 15, pp. 315–323, 1980, doi: 10.1007/BF02156609.

[125] C. Spraying Systems, “Spraydry Nozzles.” [Online]. Available: https://www.spray.com/. [Accessed: 10-Oct-2020].

[126] A. R. Sampaio de Sousa, A. L. Simplício, H. C. de Sousa, and C. M. M. Duarte, “Preparation of glyceryl monostearate-based particles by PGSS®-Application to caffeine,” *J. Supercrit. Fluids*, vol. 43, no. 1, pp. 120–125, 2007, doi: 10.1016/j.supflu.2007.03.015.

[127] C. A. García-González, A. Argemí, A. R. S. De Sousa, C. M. M. Duarte, J. Saurina, and C. Domingo, “Encapsulation efficiency of solid lipid hybrid particles prepared using the PGSS® technique and loaded with different polarity active agents,” *J. Supercrit. Fluids*, vol. 54, no. 3, pp. 342–347, 2010, doi: 10.1016/j.supflu.2010.05.011.

[128] H. Every, D. Feyecon, and I. Cosmetic, “FeyeCon,” 2014.

[129] D. Geldart, E. C. Abdullah, A. Hassanpour, L. C. Nwoke, and I. Wouters, “Characterization of powder flowability using measurement of angle of repose,” *China Particuology*, vol. 4, no. 3–4, pp. 104–107, 2006, doi: 10.1016/s1672-2515(07)60247-4.

[130] I. D. Nogueira and C. M. M. Duarte, “Encapsulation of perfluorocarbon gases into lipid-based carrier by PGSS,” *J. Supercrit. Fluids*, vol. 82, pp. 206–212, 2013, doi: 10.1016/j.supflu.2013.05.015.

[131] C. M. M. Varona, S., Martin, A., Jose Cocero, M., & Duarte, “Encapsulation of Lavandin Essential Oil in Poly- (e -caprolactones) by PGSS Process,” no. 7, pp. 1187–1192, 2013, doi: 10.1002/ceat.201200592.

[132] S. Varona, S. Kareth, Á. Martín, and M. José, “Formulation of lavandin essential oil with biopolymers by PGSS for application as biocide in ecological agriculture,” *J. Supercrit. Fluids*, vol. 54, no. 3, pp. 369–377, 2010, doi: 10.1016/j.supflu.2010.05.019.

[133] L. Casettari, E. Castagnino, S. Stolnik, A. Lewis, S. M. Howdle, and L. Illum, “Surface Characterisation of Bioadhesive PLGA / Chitosan Microparticles Produced by Supercritical Fluid Technology,” pp. 1668–1682, 2011, doi: 10.1007/s11095-011-0403-z.

[134] X. Hu, Y. Guo, L. Wang, D. Hua, Y. Hong, and J. Li, “Coenzyme Q 10 nanoparticles prepared by a supercritical fluid-based method,” *J. Supercrit. Fluids*, vol. 57, no. 1, pp. 66–72, 2011, doi: 10.1016/j.supflu.2011.01.007.

[135] A. V. M. Nunes, A. P. C. Almeida, S. R. Marques, A. R. S. De Sousa, T. Casimiro, and C. M. M. Duarte, “Processing triacetyl-b-cyclodextrin in the liquid phase using supercritical CO 2,” *J. Supercrit. Fluids*, vol. 54, no. 3, pp. 357–361, 2010, doi: 10.1016/j.supflu.2010.05.020.

[136] A. V Nunes *et al.*, “Supercritical fluids strategies to produce hybrid structures for drug delivery,” *J. Control. Release*, vol. 148, no. 1, pp. e11–e12, doi: 10.1016/j.jconrel.2010.07.005.

[137] K. Vezzù, D. Borin, A. Bertucco, S. Bersani, S. Salmaso, and P. Caliceti, “Production of lipid microparticles containing bioactive molecules functionalized with PEG,” vol. 54, pp. 328–334, 2010, doi: 10.1016/j.supflu.2010.05.013.

[138] V. R. Sinha, K. Bansal, R. Kaushik, R. Kumria, and A. Trehan, “Poly- e -caprolactone microspheres and nanospheres : an overview,” vol. 278, pp. 1–23, 2004, doi: 10.1016/j.ijpharm.2004.01.044.

[139] S. Pollak, M. Petermann, S. Kareth, and A. Kilzer, “Manufacturing of pulverised nanocomposites-Dosing and dispersion of additives by the use of supercritical carbon dioxide,” *J. Supercrit. Fluids*, vol. 53, no. 1–3, pp. 137–141, 2010, doi: 10.1016/j.supflu.2009.11.015.

[140] G. Lévai *et al.*, “Production of encapsulated quercetin particles using supercritical fluid technologies,” *Powder Technol.*, vol. 317, pp. 142–153, 2017, doi: 10.1016/j.powtec.2017.04.041.

[141] C. Rodriguez-rojo, Soraya & Rego, Duarte & Nunes, Ana & Nogueira, Isabel & Cocero, Maria & Duarte, “Supercritical Fluids (SCF) strategies to produce double-walled particles for drug delivery applications,” *12th European Meeting on Supercritical Fluids*, no. April 2015, p. 10, 2010.

[142] F. Jordan, A. Naylor, C. A. Kelly, S. M. Howdle, A. Lewis, and L. Illum, “Sustained release hGH microsphere formulation produced by a novel supercritical fluid technology: In vivo studies,” *J. Control. Release*, vol. 141, no. 2, pp. 153–160, 2010, doi: 10.1016/j.jconrel.2009.09.013.

[143] S. Salmaso, S. Bersani, N. Elvassore, A. Bertucco, and P. Caliceti, “Biopharmaceutical characterisation of insulin and recombinant human growth hormone loaded lipid submicron particles produced by supercritical gas micro-atomisation,” *Int. J. Pharm.*, vol. 379, no. 1–2, pp. 51–58, 2009, doi: 10.1016/j.ijpharm.2009.06.014.

[144] A. M. Master, M. E. Rodriguez, M. E. Kenney, N. L. Oleinick, and A. Sen Gupta, “Delivery of the photosensitizer Pc 4 in PEG–PCL micelles for in vitro PDT studies,” *J. Pharm. Sci.*, vol. 99, no. 5, pp. 2386–2398, 2010, doi: 10.1002/jps.

[145] A. R. Sampaio de Sousa, R. Silva, F. H. Tay, A. L. Simplício, S. G. Kazarian, and C. M. M. Duarte, “Solubility enhancement of trans-chalcone using lipid carriers and supercritical CO2 processing,” *J. Supercrit. Fluids*, vol. 48, no. 2, pp. 120–125, 2009, doi: 10.1016/j.supflu.2008.09.025.

[146] M. Calderone, E. Rodier, J. J. Letourneau, and J. Fages, “Solidification of Precirol® by the expansion of a supercritical fluid saturated melt: From the thermodynamic balance towards the crystallization aspect,” *J. Supercrit. Fluids*, vol. 42, no. 2, pp. 189–199, 2007, doi: 10.1016/j.supflu.2007.02.004.

[147] A. Tandya, F. Dehghani, and N. R. Foster, “Micronization of cyclosporine using dense gas techniques,” *J. Supercrit. Fluids*, vol. 37, no. 3, pp. 272–278, 2006, doi: 10.1016/j.supflu.2005.10.004.

[148] M. J. Whitaker *et al.*, “The production of protein-loaded microparticles by supercritical fluid enhanced mixing and spraying,” *J. Control. Release*, vol. 101, no. 1-3 SPEC. ISS., pp. 85–92, 2005, doi: 10.1016/j.jconrel.2004.07.017.

[149] J. Hao, M. J. Whitaker, B. Wong, G. Serhatkulu, K. M. Shakesheff, and S. M. Howdle, “Plasticization and Spraying of Poly (DL-lactic acid) Using Supercritical Carbon Dioxide: Control of Particle Size,” *J. Pharm. Sci.*, vol. 93, no. 4, pp. 1083–1090, 2004, doi: 10.1002/jps.20002.

[150] W. Chen, X. Hu, Y. Hong, Y. Su, H. Wang, and J. Li, “Ibuprofen nanoparticles prepared by a PGSS™-based method,” *Powder Technol.*, vol. 245, pp. 241–250, 2013, doi: 10.1016/j.powtec.2013.04.042.

[151] C. Saldanha Do Carmo *et al.*, “Formulation of pea protein for increased satiety and improved foaming properties,” *RSC Adv.*, vol. 6, no. 8, pp. 6048–6057, 2016, doi: 10.1039/c5ra22452g.

A Overview of the past of the PGSS process

Table A.1 Literature review of the PGSS process

Core Material	Coating Material	T (°C)	P (bar)	Morphology and size	Ref
C3F8	Gelucire ® 50/13	80	85	Particles with holes	[130]
Lavandin Essential Oil	Poly-(epsilon-caprolactones)	50–70	50–110	Spherical Particles 100–700 µm	[131]
	PEG	70–90	50–90	30–100 µm	[132]
Chitosan	PLGA mPeg	40	138	90–100 µm	[133]
CoQ10	PEG 6000	80	100–250	0,2 µm	[134]
Flufenamic acid	triacetyl-β-cyclodextrin	35	250	-	[135], [136]
Ribonuclease A	PEGgylated, Tristearin, Phosphatidylcholine	50–65	130–140	4–15 µm	[137]
	PEG 5000, Triestearin (TS), Phosphatidycholine (PC)	45–65	100–170	4–15 µm	[138]

Table A.2 Continuation of table A.1 on a literature review of the PGSS process

Core Material	Coating Material	T (°C)	P (bar)	Morphology and size	Ref
-	Polybutylenterephthalate/ zinc oxide and Bentonite as additive	230	50–410	100–300 µm spherical particles	[139]
Caffeine	Glyceryl monostearate (Lumulse)	72	130	-	[127]
Glutathione	waxy triglyceride (Cutina ® HR)				
Ketoprofen	Silanized TiO2				
Quercetin	Gelucire ® 43/01	70	130	-	[140]
	GMS				
	HP-β-CD				
Flufenamic acid	PEG 4000/20000 Gelucire ® 43/01 and 50/13	50–70	120–150	500 nm–10 µm	[141]
YNS3107	PEG 4000, PEG 400, poloxamer 407	80	177	30 µm	[120]
Human Growth hormone (hgH)	PLGA/PLA	32	76	60–100 µm	[142]
Insulin Human Growth hormone (rh-GH)	Tristearin /phosphatidycholine/PEG mixtures Tween-80	40	150	200 nm	[143],[144]
Trans - chalcone	Precito ® atos , Gelucire ® 50/13	42–52	120	2–7 µm	[145]
-	Monostearate	70–80	60–210	10–40 µm	[105]
	Tristearate	60–70			
Caffeine	GMS	62	130	5,5 µm Neddle aggregates	[126]

Table A.3 Continuation of table A.1 on a literature review of the PGSS process

Core Material	Coating Material	T (°C)	P (bar)	Morphology and size	Ref
-	Precirol ®	50	110	-	[146]
Cyclosporine	-	25–45	160 – 200	150 nm	[147]
Lysozyme	P(DLLA)	35	320	150 µm Irregular/porous	[148]
Ribonuclease					
Insulin					
-	P(DLLA)	35	306	10–20 µm fibres	[149]
Nifedipine	PEG 400	50–70	100–200	10–30 µm	[81]
Felodipine		70	200	42 µm Irregular/Porous	
Fenobiate		65–80	190	32 µm	
-	PEG (1500/4000/8000/35000)	45–70	100–250	150–400 µm spheres	[79]
Ibuprofen	PEG 600	60	100–250	20–500 nm spheres	[150]
-	Pea protein	51–75	73–207	-	[151]

B

B Overview of the experimental work

B.1. PGSS apparatus and equipment

Table B.1 Instruments and valves of the PGSS process

	TT	Temperature transmitter
	TC	Temperature controller
	PC	Pressure indicate and controller
	-	Flexible hole
	-	Ball valve
	-	Needle valve
	-	Check valve
	-	Safety valve
	-	Flowmeter
	-	Filter

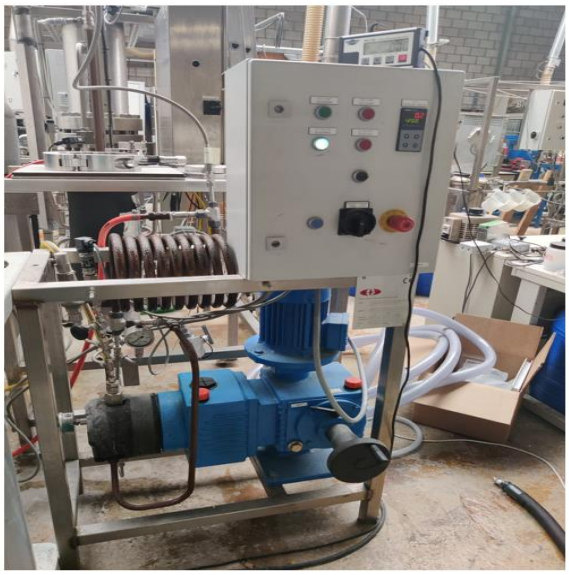

Pump (P-01) with sensor

Bottle of CO_2

Heater (E-03)

Cooler (E-01)

Heater (E-04)

Heater (E-02)

Vessel with mechanical stirrer

Drum

Figure B.1 Types of equipment used in the PGSS process

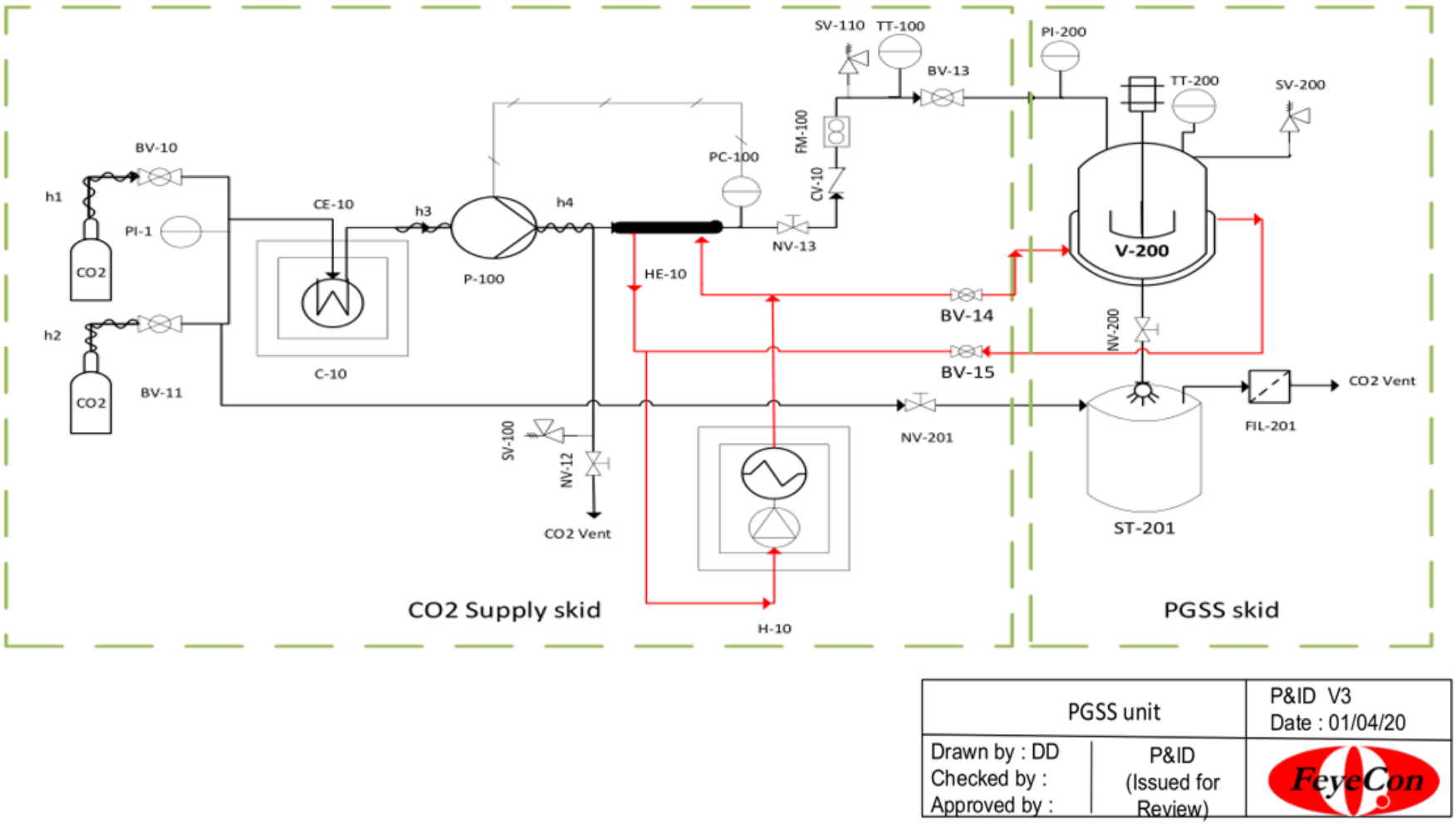

Figure B.2 PFD do PGSS provided by Feyecon Development & Implementation B.V

B.2. Calculations performed for the flows of mixture and CO_2

Table B.2 Vessel dimensions and time of the process

L_{vessel} (Length of a vessel)	13 cm
D_{vessel} (Diameter of a vessel)	10 cm
t (time of the process) with/without stirring	50/30 seconds

For the calculations of the flow of Jojoba wax, we first calculated volume of mixture in a vessel by the level measured before by the following equation:

$$V_{mixture} = level\ of\ mixture\ \times {r_{vessel}}^2 \times \pi \quad \textbf{(Eq. B.1)}$$

After the calculation of the mixture volume, the mass flow can be calculated by the following equation:

$$Q_m = \frac{V_{mixture}}{t} \times \rho_{jojoba\ wax} \quad \textbf{(Eq. B.2)}$$

The flow of CO_2, is calculated by the following formula:

$$Q_{CO_2} = \frac{m_{CO_2}}{t} \quad \textbf{(Eq. B.3)}$$

B.3. Calibrations curves obtained in order to calculated encapsulation efficiency of the pigment

Table B.3 Absorbances measures for the pigment

$C_{pigment}$ (mg/ml)	Heating				Without heating			
	ABS 1	ABS 2	ABS 3	AVG(ABS)	ABS 1	ABS 2	ABS 3	AVG(ABS)
0	0.000	0.000	0.000	0.000	0.000	0.000	0.000	0.000
0.1	0.220	0.219	0.219	0.219	0.328	0.328	0.327	0.328
0.2	0.436	0.435	0.433	0.435	0.682	0.680	0.673	0.678
0.3	0.705	0.704	0.703	0.704	1.072	1.077	1.077	1.075
0.4	0.976	0.976	0.976	0.976	1.443	1.442	1.435	1.440
0.5	1.296	1.297	1.299	1.297	1.821	1.821	1.821	1.821

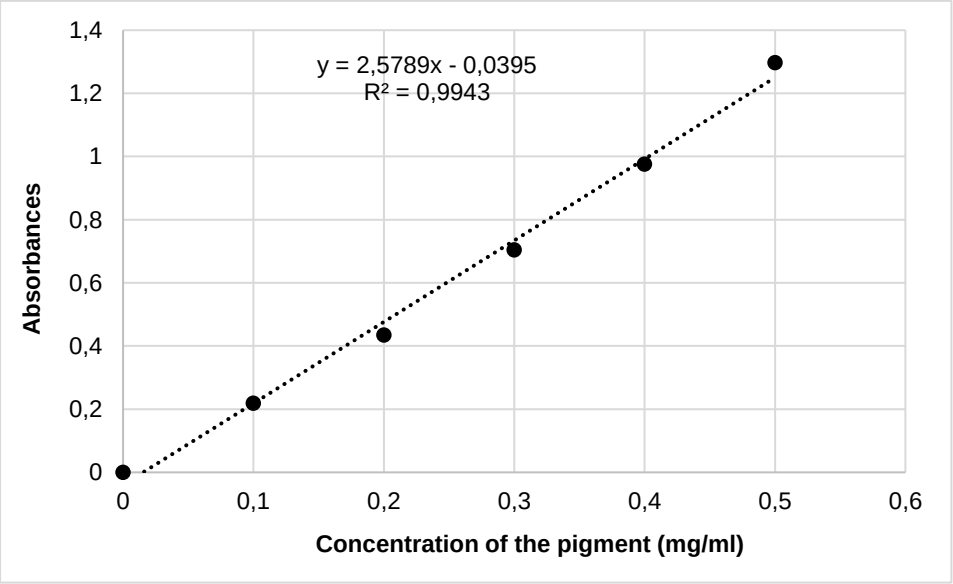

Figure B.3 Calibration curve of the absorbance heating

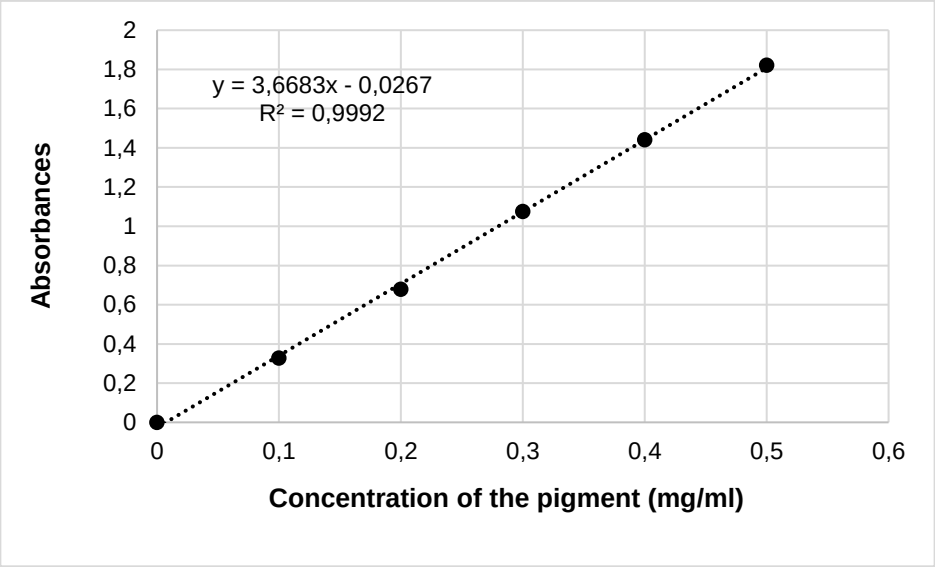

Figure B.4 Calibration curve of the absorbance without heating

C

C Experiments and results of the tests produced in section 4.1

Table C.1 shows all the PGSS experiments performed and the respective operating conditions. **Table C.2** and **C3** shows the particle size observed in all the experiments tests. **Table C.4** shows all absorbances observed in order to calculate the encapsulation efficiency.

Table C.1 Conditions and remain results of tests for section 4.1

Test	Pressure (bar)	Temperature (ºC)	Quantity (g)	Quantity of Jojoba wax + Pigment (g)	Quantity of oil (g)	Pigment loading (%)	Level (cm)	Nozzle (mm)	Time of stirring (s)	CO_2 (kg)	Flow of Jojoba wax (kg/s)	Flow of CO_2 (kg/s)	Powder produced (g)
2	**75**	83	100	99.0+1.0	5.0	1%	3.5	76M/0.500	50	0.2	0.005	0.004	92.6
3	**100**	83	100	99.0+1.0	5.0	1%	3.5	76M/0.500	50	0.3	0.005	0.006	95.1
1	**120**	83	100	99.0+1.0	5.0	1%	3.5	76M/0.500	50	0.4	0.005	0.008	83.8
4	**150**	83	100	99.0+1.0	5.0	1%	3.5	76M/0.500	50	0.8	0.005	0.016	89.5
5	120	**76**	100	99.0+1.0	5.0	1%	3.5	76M/0.500	50	0.4	0.005	0.008	87.3
6	120	**93**	100	99.0+1.0	5.0	1%	3.5	76M/0.500	50	0.3	0.005	0.006	80.3
7	120	83	**50**	49.5+0.5	2.5	1%	1.5	76M/0.500	50	0.7	0.002	0.014	37.0
8	120	83	**200**	198.0+2.0	10.0	1%	6	76M/0.500	50	0.3	0.008	0.006	189.0
9	120	83	**300**	297.0+3.0	15.0	1%	7.5	76M/0.500	50	0.2	0.010	0.004	283.3
10	120	83	100	95.0+5.0	20.0	**5%**	3.5	76M/0.500	50	0.4	0.005	0.008	77.8
11	120	83	100	90.0+10.0	30.0	**10%**	3.5	76M/0.500	50	0.3	0.005	0.006	88.8
12	120	83	100	80.0+20.0	50.0	**20%**	3.5	76M/0.500	50	0.5	0.005	0.010	118
13	120	83	100	99.0+1.0	5.0	1%	3.5	**63M/0.093**	50	0.4	0.005	0.008	101.4
14	120	83	100	99.0+1.0	5.0	1%	3.5	**80M/0.340**	50	0.3	0.005	0.006	101
15	120	83	100	99.0+1.0	5.0	1%	3.5	**70M/0.710**	50	0.3	0.005	0.006	94.2
16	120	83	100	99.0+1.0	5.0	1%	3.5	76M/0.500	**0**	0.2	0.008	0.007	92.9

Table C.2 Size of the particles (μm) in the different tests

Test	2	3	1	4	5	6	7	8	9
	75 bar	**100 bar**	**120 bar**	**150 bar**	**76ºC**	**93ºC**	**50g**	**200g**	**300g**
	55.47	56.19	40.71	28.82	15.37	56.62	53.12	88.71	106.03
	54.99	67.75	32.18	26.88	31.73	58.91	31.57	86.69	74.24
	60.41	38.75	32.29	21.38	34.73	57.4	31.07	62.74	76.02
	72.08	73.02	34.02	21.88	14.99	74.96	38.33	60.32	70.71
	74.04	32.47	46.63	28.29	31.67	87.73	60.44	65.99	84.99
	69.22	90.86	42.74	26.37	29.4	61.33	42.76	83.64	79.11
	60.41	58.77	48.22	28.26	13.88	81.26	32.83	84.39	92.31
	83.36	43.13	42.41	24.22	17.62	77.8	26.41	59.26	88.62
	72.08	53.71	50.44	21.52	32.17	77.82	24.51	51.44	94.33
	71.11	49.03	45.39	22.65	15.19	58.01	27.85	79.1	109.42

Table C.3 Continuation of table C.2

Test	10	11	12	13	14	15	16
	5 % Pigment	**10 % Pigment**	**20% Pigment**	**Nozzle 63M**	**Nozzle 80M**	**Nozzle 70M**	**Without stirring**
	47.11	53.31	30.03	15.79	36.64	61.27	17.55
	53.75	42.07	25.63	7.22	31.81	59.59	40.22
	85.23	44.05	62.92	13.68	48.46	56.73	36.51
	43.13	57.45	26.11	12.07	36.35	61.49	41.49
	74.41	47.81	44.19	21.11	40.28	66.33	43.51
	55.2	41.31	46.88	20.53	39.14	60.62	16.94
	46.33	36.77	26.52	19.13	40.31	69.79	8.42
	40.95	51.25	36.43	18.13	44.58	77.35	16.97
	35.27	26.24	49.36	33.66	33.77	52.82	36.25
	44.53	23.03	49.79	28.04	37.33	67.29	32.01

Table C.4 Absorbance measured and pigment concentration calculated for encapsulation efficiency (%)

		Heating					Without Heating				
Test	**Condition**	**ABS**	**ABS**	**ABS**	**AVG (ABS)**	**$C_{pigment}$ (mg/ml)**	**ABS**	**ABS**	**ABS**	**AVG (ABS)**	**$C_{pigment}$ (mg/ml)**
2	**75 bar**	0.179	0.178	0.179	0.179	0.08	0.179	0.178	0.179	0.179	0.06
3	**100 bar**	0.190	0.191	0.191	0.191	0.09	0.191	0.192	0.191	0.191	0.06
1	**120 bar**	0.180	0.179	0.18	0.180	0.09	0.180	0.181	0.181	0.181	0.06
4	**150 bar**	0.180	0.18	0.18	0.180	0.09	0.181	0.179	0.182	0.181	0.06
5	**76ºC**	0.179	0.178	0.18	0.179	0.08	0.18	0.18	0.18	0.180	0.06
6	**93ºC**	0.192	0.193	0.191	0.192	0.09	0.185	0.184	0.185	0.185	0.06
7	**50g**	0.597	0.596	0.597	0.597	0.25	0.342	0.342	0.342	0.342	0.10
8	**200g**	0.220	0.219	0.22	0.220	0.10	0.189	0.189	0.189	0.189	0.06
9	**300g**	0.225	0.225	0.224	0.225	0.10	0.188	0.188	0.188	0.188	0.06
10	**5%**	0.698	0.689	0.698	0.698	0.29	0.347	0.346	0.347	0.347	0.10
11	**10%**	1.181	0.180	1.181	1.181	0.47	0.421	0.421	0.42	0.421	0.12
12	**20%**	1.997	1.996	1.997	1.997	0.79	0.504	0.502	0.505	0.504	0.14
13	**63M**	0.188	0.187	0.188	0.188	0.09	0.182	0.182	0.182	0.182	0.06
14	**80M**	0.190	0.189	0.191	0.190	0.09	0.186	0.186	0.186	0.186	0.06
15	**80M**	0.181	0.181	0.181	0.181	0.09	0.180	0.18	0.18	0.180	0.06
16	**Without stirring**	0.183	0.184	0.182	0.183	0.09	0.182	0.181	0.181	0.182	0.06

D Overview of the experimental work for DoE

In all the experiments performed in section 4.2, we used the 76M nozzle (0. 500mm), 1% of Pigment loading, and the solution was stirred for 50 seconds. D.1 shows all the PGSS experiments performed, and the respective operating conditions in section 4.2. Sections D.2, D.3, D.4, D.5 show the remain results performed with the program STATISTICA for DoE. (In these sections A represents quantity, B represents Temperature and C represents Pressure)

D.1. Experiments and results of the tests produced in section 4.2

Table D.1 shows all the PGSS experiments performed and the respective operating conditions. Table D.2 shows the particle size observed in all the experiments tests. Table D.3 shows all absorbances observed in order to calculate the encapsulation efficiency.

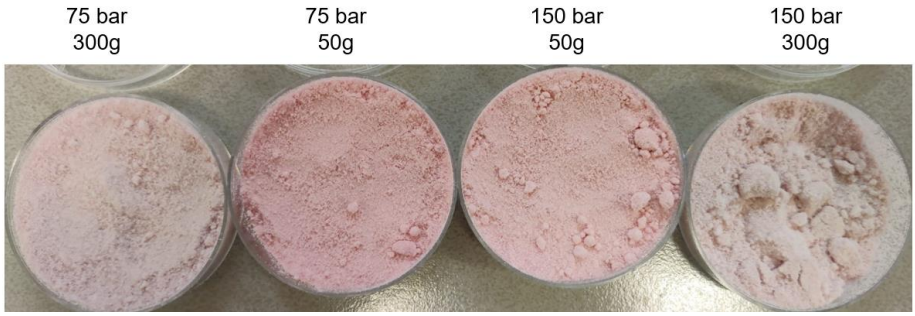

Figure D.1 Powders obtained at 76ºC

Figure D.2 Powders obtained at 93ºC

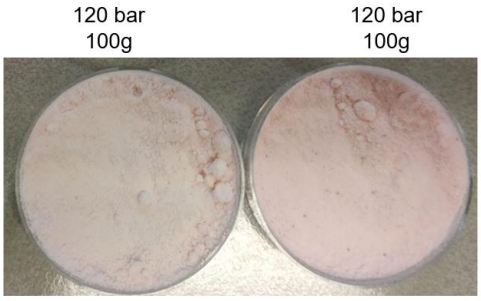

Figure D.3 Powders obtained at 83ºC

Table D.1 Conditions and remain results of the tests in section 4.2

Test	Pressure (bar)	Temperature (ºC)	Quantity (g)	Quantity of Jojoba wax + Pigment (g)	Quantity of oil (g)	Level (cm)	CO_2 (kg)	Flow of Jojoba wax (kg/s)	Flow of CO_2 (kg/s)	GPR	% wt CO_2	Powder produced (g)
1	75	76	50	49.5+0.5	1.5	1.5	0.2	0.002	0.004	1.97	80%	39
3	75	93	50	49.5+0.5	1.5	1.5	0.2	0.002	0.004	1.97	80%	34
3	75	76	300	297.0+3.0	7.5	7.5	0.1	0.010	0.002	0.20	25%	293
4	120	83	100	99.0+1.0	5.0	3.5	0.4	0.005	0.008	1.69	80%	88
5	150	76	50	49.5+0.5	1.5	1.5	0.6	0.002	0.012	5.90	92%	42
6	75	93	300	297.0+3.0	7.5	7.5	0.1	0.010	0.002	0.20	25%	261
7	150	93	300	297.0+3.0	7.5	7.5	0.4	0.010	0.008	0.79	57%	288
8	150	93	50	49.5+0.5	1.5	1.5	0.6	0.002	0.012	5.90	92%	38
9	150	76	300	297.0+3.0	7.5	7.5	0.4	0.010	0.008	0.79	57%	302
10	120	83	100	99.0+1.0	5.0	3.5	0.4	0.005	0.008	1.69	80%	87

Table D.2 Particle size observed in the different tests of section 4.2

Test	Pressure (bar)	Temperature (°C)	Quantity (g)	Particle size (µm)									
1	75	76	50	41.86	40.57	60.06	60.26	39.09	56.61	54.58	51.44	41.58	51.41
3	75	93	50	43.27	43.75	54.35	67.58	48.17	69.05	62.69	50.93	49.15	49.94
3	75	76	300	44.7	42.1	44.66	68.39	107.59	105.79	45.39	48.27	52.72	99.98
4	120	83	100	45.11	52.45	45.99	42.17	39.79	53.35	45.02	52.05	48.45	48.31
5	150	76	50	24.26	26.64	34	11.94	22.19	22.99	21.33	32.83	23.26	26.46
6	75	93	300	94.99	174.77	78.75	51.35	52.62	110.22	70.4	77.76	81.74	104.03
7	150	93	300	77.83	91.24	104.82	60.72	59.94	38.02	87.87	52.14	65.1	74.66
8	150	93	50	38.78	41.38	36.15	39.34	51.57	51.51	43.79	32.31	53.22	47.97
9	150	76	300	37.39	51.75	70.82	44.65	42.79	35.56	36.5	54.86	35.94	77.69
10	120	83	100	44.47	44.98	35.61	52.14	57.16	40.54	52.72	55.2	35.64	45.11

Table D.3 Absorbance measured and pigment concentration calculated for encapsulation efficiency (%) (section 4.2)

		Heating					Without Heating				
Test	**Condition**	**ABS**	**ABS**	**ABS**	**AVG (ABS)**	**$C_{pigment}$ (mg/ml)**	**ABS**	**ABS**	**ABS**	**AVG (ABS)**	**$C_{pigment}$ (mg/ml)**
1	**75 bar/ 76ºC/50g**	0.254	0.253	0.254	0.254	0.11	0.188	0.187	0.188	0.188	0.06
2	**75 bar/ 93ºC/50g**	0.160	0.16	0.160	0.160	0.08	0.183	0.183	0.183	0.183	0.06
3	**75 bar/ 76ºC/300g**	0.191	0.191	0.19	0.191	0.09	0.184	0.182	0.185	0.184	0.06
4	**120 bar/ 83ºC/100g**	0.183	0.182	0.183	0.183	0.09	0.181	0.181	0.181	0.181	0.06
5	**150 bar/ 76ºC/50g**	0.234	0.234	0.234	0.234	0.11	0.187	0.187	0.186	0.187	0.06
6	**75 bar/ 93ºC/300g**	0.183	0.183	0.183	0.183	0.09	0.184	0.183	0.184	0.184	0.06
7	**150 bar/ 93ºC/300g**	0.161	0.161	0.16	0.161	0.08	0.184	0.184	0.184	0.184	0.06
8	**150 bar/ 93ºC/50g**	0.201	0.201	0.201	0.201	0.09	0.181	0.181	0.181	0.181	0.06
9	**150 bar/ 76ºC/300g**	0.182	0.182	0.182	0.182	0.09	0.183	0.182	0.183	0.183	0.06
10	**120 bar/ 83ºC/100g**	0.182	0.181	0.182	0.182	0.09	0.179	0.180	0.179	0.179	0.06

D.2. DoE Analysis for the size of the particles

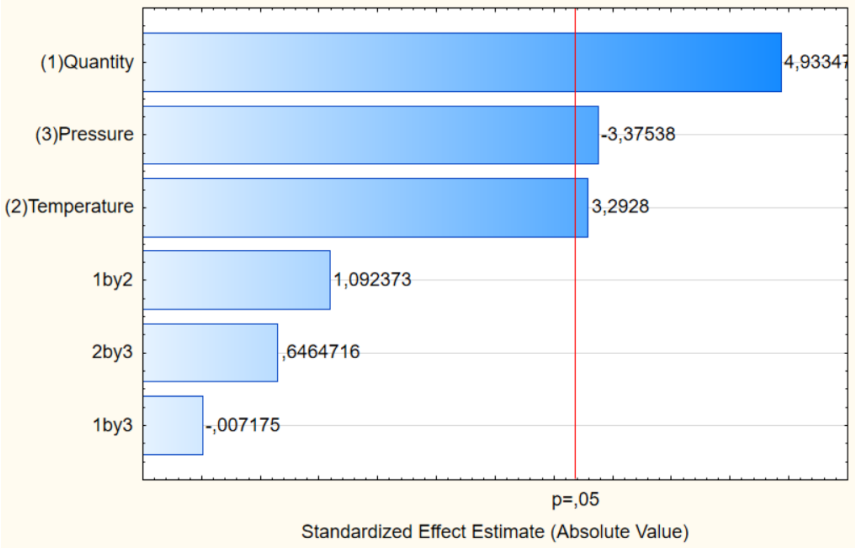

Figure D.4 Pareto Chart of Standardized Effects of particle size (µm)

Table D.4 Anova Condensed results for the particle size (µm)

	SS	df	MS	$F_{observed}$	p-value
A	1347.454	1	1347.454	31.66925	**0.001346**
B	600.259	1	600.259	14.10791	**0.009442**
C	630.746	1	630.746	14.82445	**0.008457**
Error	255.286	6	42.548		
Total SS	2833.746	9			

Note: SS = Sum of squares, df= degrees of freedom, MS = mean squared value

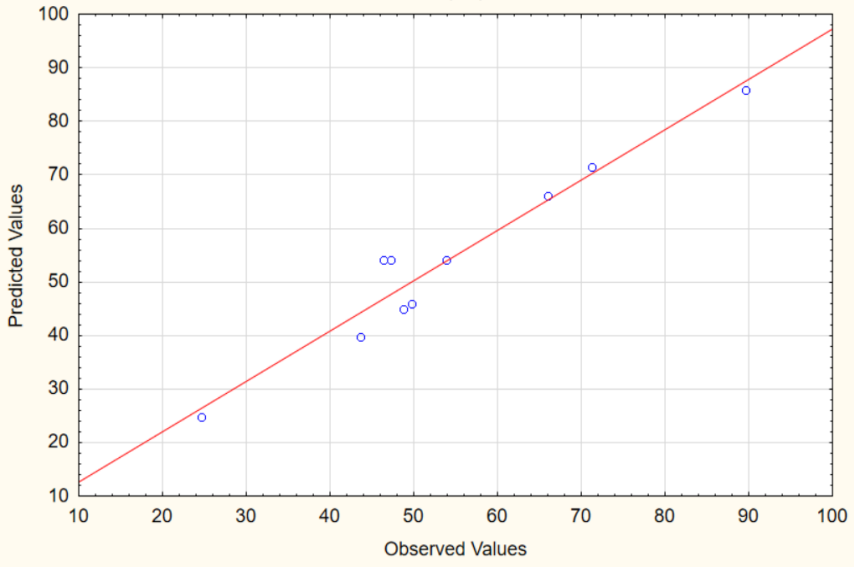

Figure D.5 Observed vs Predicted values of particle size (μm)

Table D.5 Effects Estimate of particle size (μm)

	EFFECT	Std. Error
Mean/int	**54.11**	**2.35**
A	**25.96**	**5.26**
B	**17.32**	**5.26**
C	**-17.76**	**5.26**
AB	5.75	5.26
AC	-0.04	5.26
BC	3.40	5.26

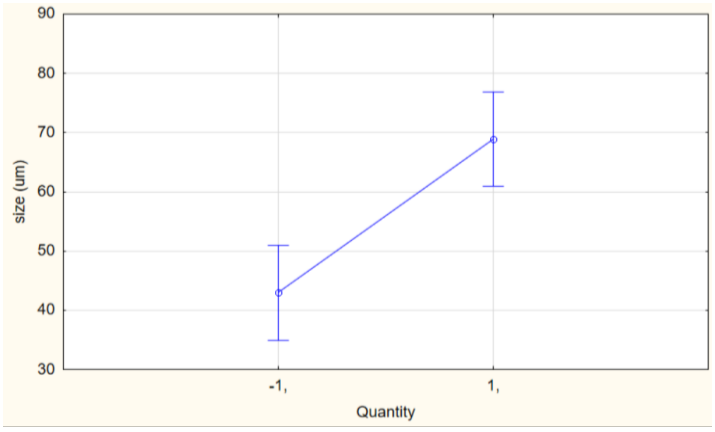

Figure D.6 Plot of Marginal Means and Conf. Limits (95%) of size for the quantity

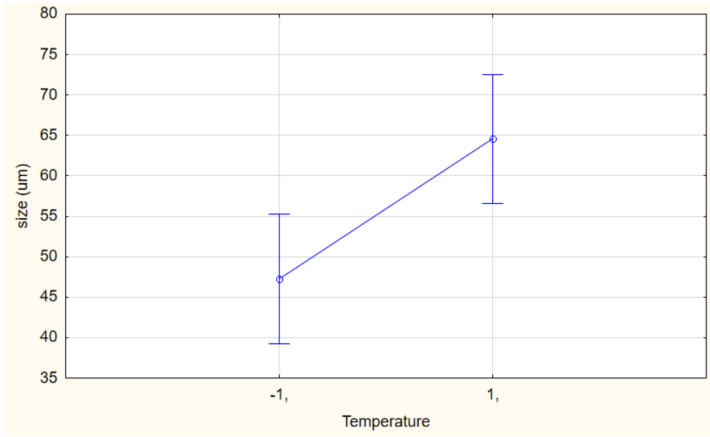

Figure D.7 Plot of Marginal Means and Conf. Limits (95%) of size for the temperature

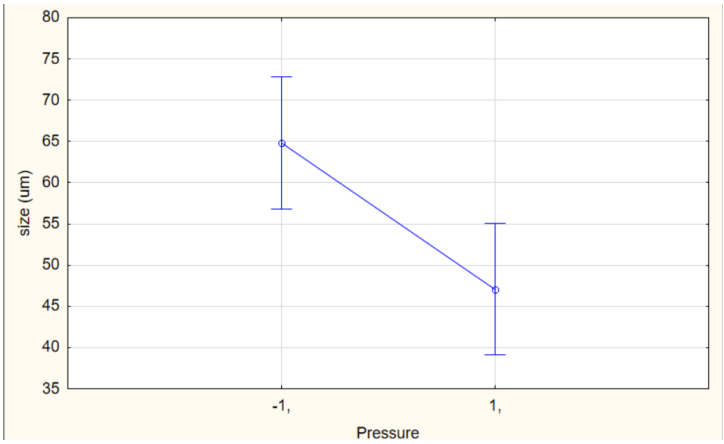

Figure D.8 Plot of Marginal Means and Conf. Limits (95%) of size for the pressure

D.3. DoE Analysis for the bulk density

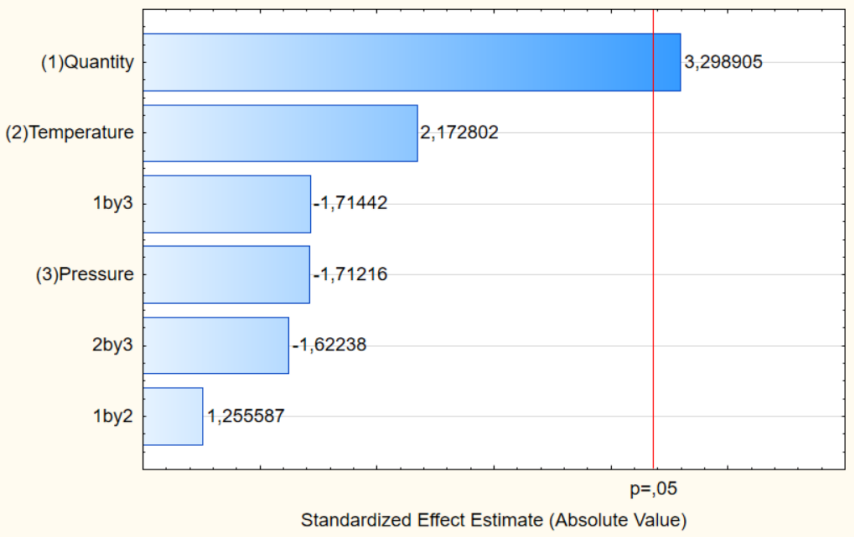

Figure D.9 Pareto Chart of Standardized Effects of Bulk density (kg/m^3)

Table D.6 Anova Condensed results for the bulk density (kg/m^3)

	SS	df	MS	$F_{observed}$	p-value
A	13201.32	1	13201.32	4.891015	0.057940
Error	21592.77	8	2699.10		
Total SS	34794.09	9			

Note: SS = Sum of squares, df= degrees of freedom, MS = mean squared value

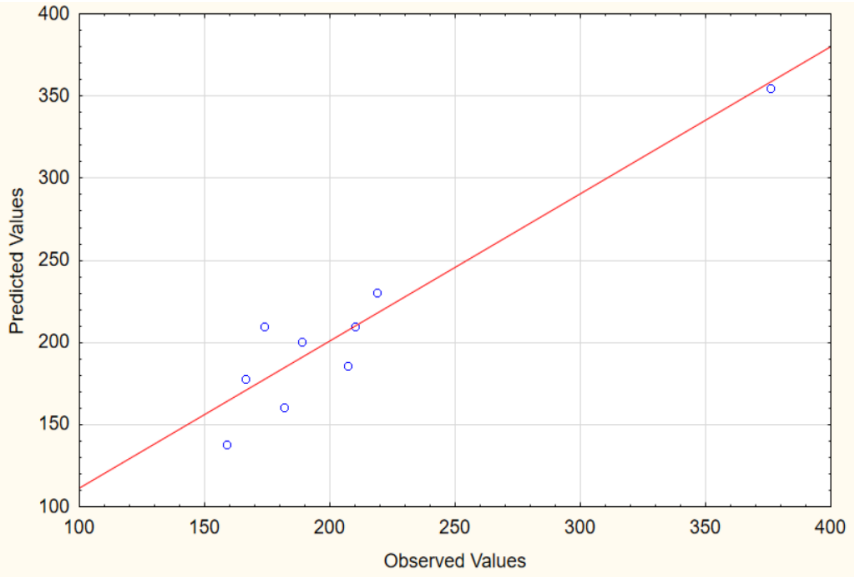

Figure D.10 Observed vs Predicted values of bulk density (kg/m^3)

Table D.7 Effects Estimate of bulk density (kg/m^3)

	EFFECT	Stand. Error
Mean/int	**209.90**	**11.01**
A	**81.24**	**24.63**
B	53.51	24.63
C	-42.17	24.63
AB	30.92	24.63
AC	-42.22	24.63
BC	-39.96	24.63

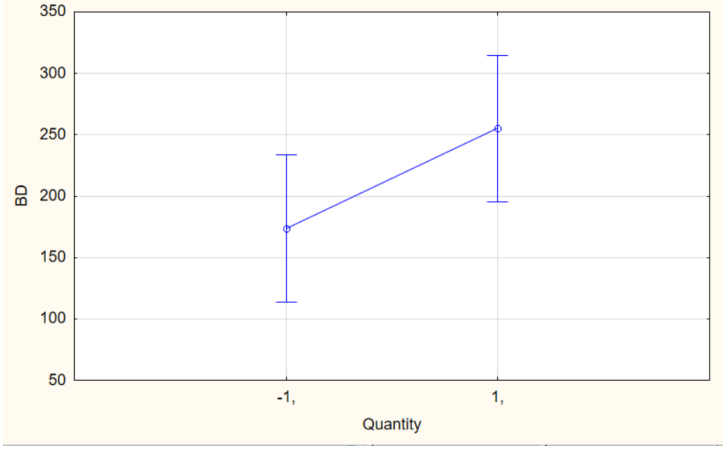

Figure D.11 Plot of Marginal Means and Conf. Limits (95%) of bulk density for the quantity

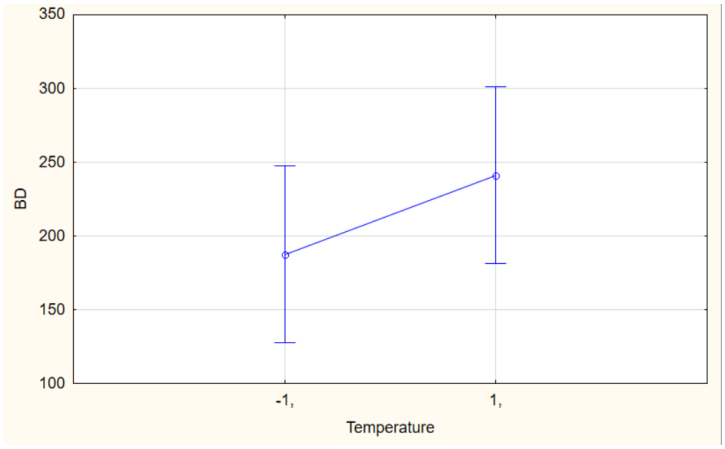

Figure D.12 Plot of Marginal Means and Conf. Limits (95%) of bulk density for the temperature

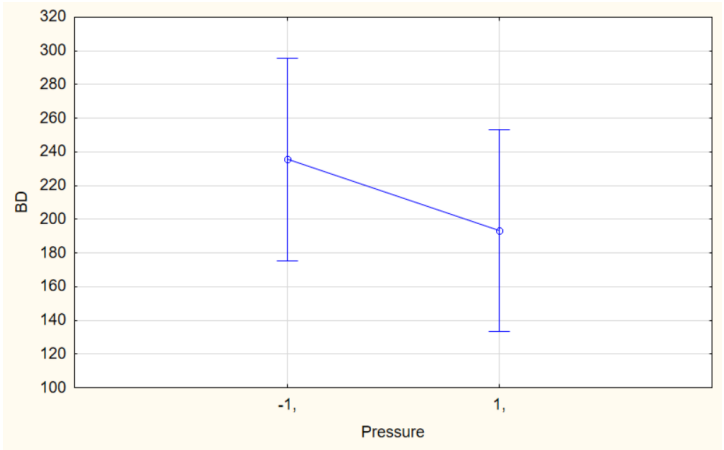

Figure D.13 Plot of Marginal Means and Conf. Limits (95%) of bulk density for the pressure

D.4. DoE Analysis of the yield collected particles

Table D.8 ANOVA results for the yield collected particles (%)

	SS	df	MS	$F_{observed}$	p-value
A	0.013235	1	0.013235	1.577791	0.297997
B	0.017571	1	0.017571	2.094603	0.243628
C	0.003797	1	0.003797	0.452633	0.549273
AB	0.002495	1	0.002495	0.297387	0.623456
AC	0.022654	1	0.022654	2.700595	0.198855
BC	0.000604	1	0.000604	0.072026	0.805806
Error	0.025166	3	0.008389		
Total SS	0.085522	9			

Note: SS = Sum of squares, df= degrees of freedom, MS = mean squared value

From the data presented in the ANOVA **table D.8**, it can be concluded that there is a significant effect of A (Quantity), B (Temperature) and C (Pressure) on a yield of the collected particles (%) at 95% confidence level. However, the effect interactions don't prove to be significant for the studied model. The goal is to get bigger values of yield (%), and after analysing the isolated effects, we can conclude at 95% confidence level: The higher the quantity, the higher temperature and lower the pressure the higher is the value of yield collected particles (%).

Thus the final Equation in Terms of Factors for yield collected particles (yield %) is:

$$Yield\ (\%) = 0{,}82 + 0{,}08 \times Quantity + 0{,}09 \times Temperature - 0{,}04 \times Pressure - 0{,}04 \times Quantity \times Temperature + 0{,}11 \times Quantity \times Pressure - 0{,}02 \times Temperature \times Pressure$$

(Eq D.1)

The R-square is 0,70574, and adjusted R-square is 0,11722.

Table D.9 Effects Estimate of yield collected particles (%)

	EFFECT	Stand. Error
Mean/int	**0.82**	**0.03**
A	0.08	0.06
B	0.09	0.06
C	-0.04	0.06
AB	-0.04	0.06
AC	0.11	0.06
BC	-0.02	0.06

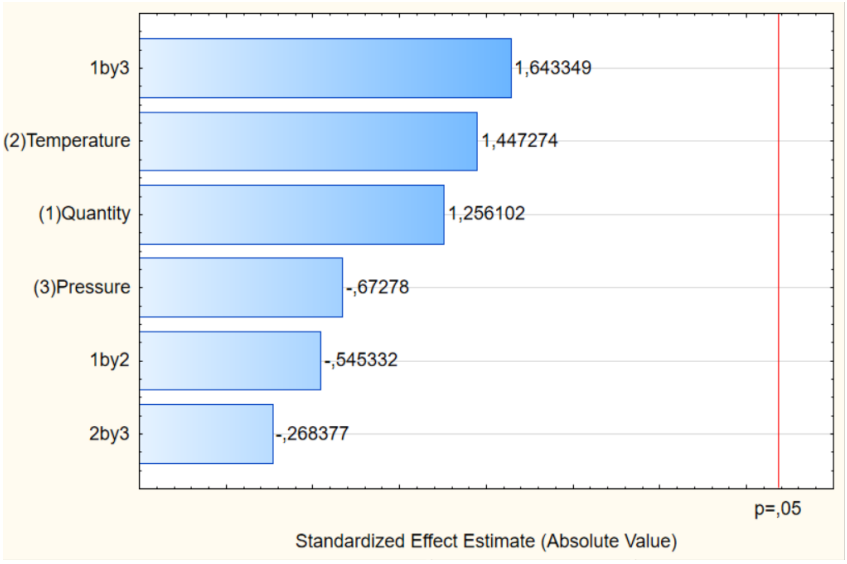

Figure D.14 Pareto Chart of Standardized Effects of yield collected particles (%)

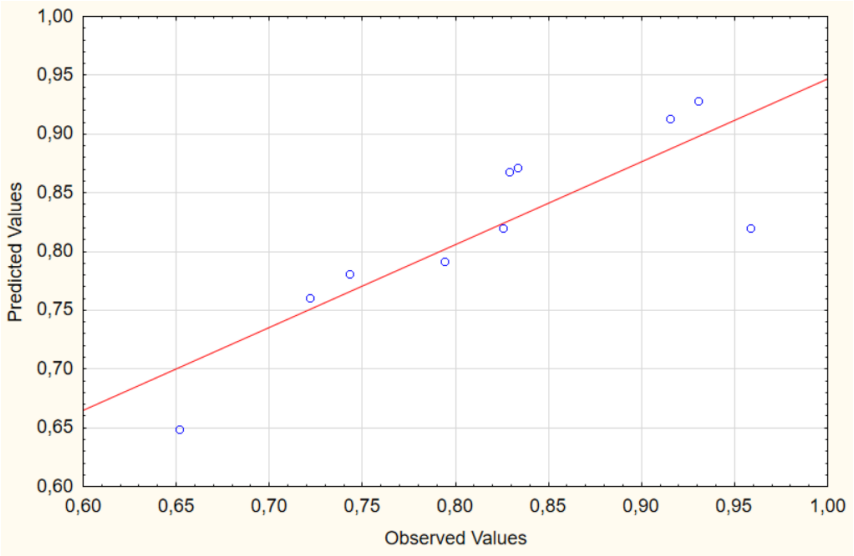

Figure D.15 Observed vs Predicted values of yield collected particles (%)

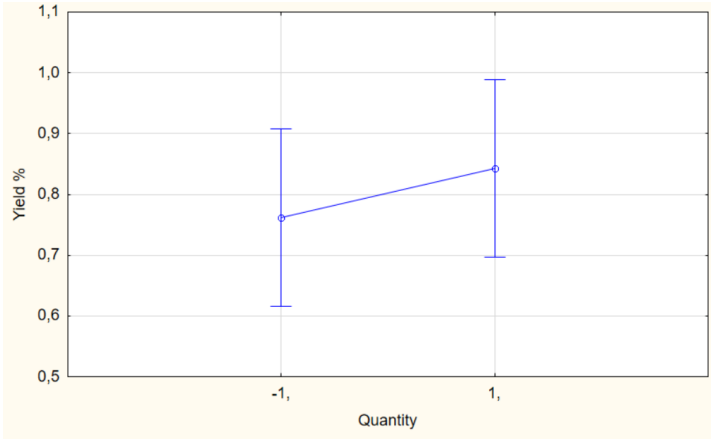

Figure D.16 Plot of Marginal Means and Conf. Limits (95%) of yield collected particles for the quantity

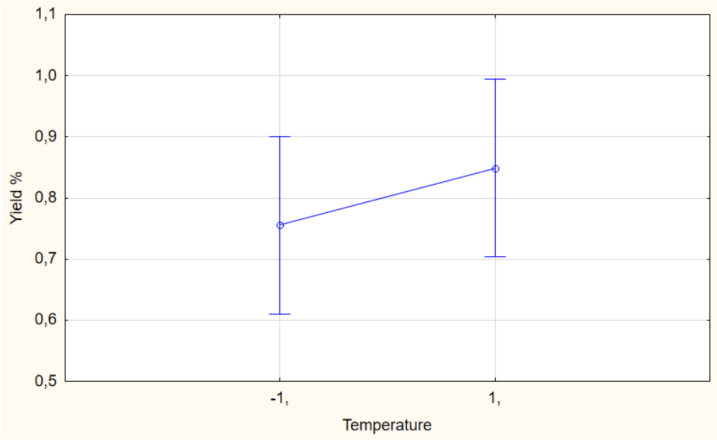

Figure D.17 Plot of Marginal Means and Conf. Limits (95%) of yield collected particles for the temperature

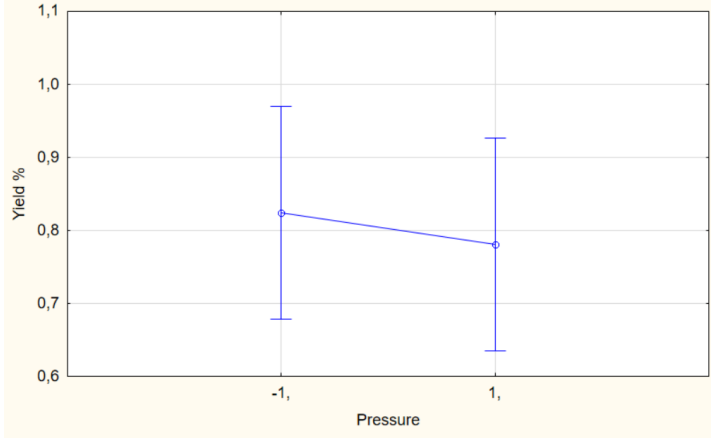

Figure D.18 Plot of Marginal Means and Conf. Limits (95%) of yield collected particles for the pressure

D.5. DoE Analysis of the encapsulation efficiency (%)

Table D.10 ANOVA results for encapsulation efficiency (%)

	SS	df	MS	$F_{observed}$	p-value
A	0.011479	1	0.011479	5.540204	0.099964
B	0.017941	1	0.017941	8.658960	0.060383
C	0.000000	1	0.000000	0.000039	0.995424
AB	0.004334	1	0.004334	2.091764	0.243878
AC	0.004645	1	0.004645	2.241948	0.231230
BC	0.001704	1	0.001704	0.822313	0.431355
Error	0.006216	3	0.002072		
Total SS	0.046319	9			

Note: SS = Sum of squares, df= degrees of freedom, MS = mean squared value

From the data presented in the ANOVA **table, D.10**, seems that no effect or interaction influence on encapsulation efficiency (%), in the PGSS process at 95% confidence level. This means the quantity, pressure and temperature don't influence encapsulation efficiency. However, it was possible to analyse the isolated effects. Therefore we can conclude at 95% confidence level: the pressure doesn't have any influence on EE% but increases on quantity and temperature it will increase the value of EE%.

Thus the final Equation in Terms of Factors for encapsulation efficiency (EE %) is :

$$EE\ (\%) = 0{,}64 + 0{,}08 \times Quantity + 0{,}09 \times Temperature - 0{,}0002 \times Pressure - 0{,}05 \times Quantity \times Temperature + 0{,}05 \times Quantity \times Pressure - 0{,}03 \times Temperature \times Pressure$$

(Eq.D.2)

The R-square is 0.8658, and adjusted R-square is 0.59741.

Table D.11 Effects Estimate of encapsulation efficiency (%)

	EFFECT	Stand. Error
Mean/int	**0.64**	**0.01**
A	0.08	0.03
B	0.09	0.03
C	0.0002	0.03
AB	-0.05	0.03
AC	0.05	0.03
BC	-0.03	0.03

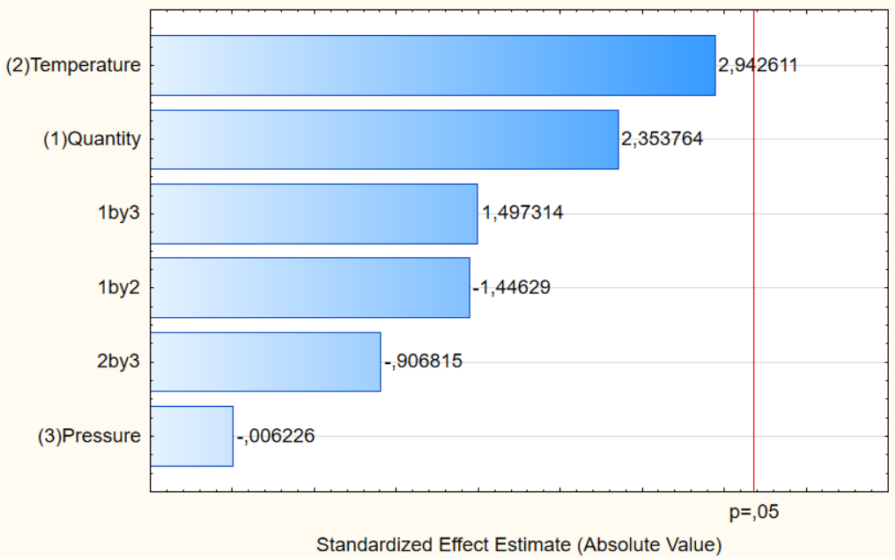

Figure D.19 Pareto Chart of Standardized Effects of encapsulation efficiency (%)

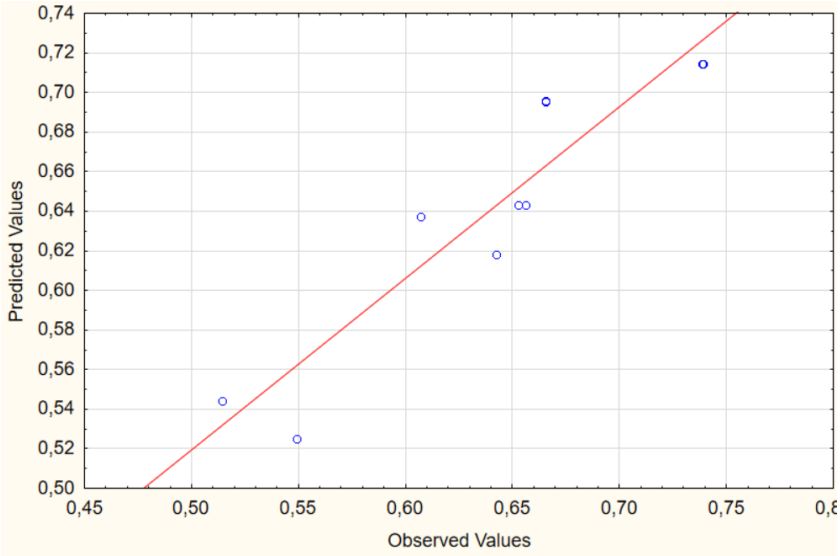

Figure D.20 Observed vs Predicted values of encapsulation efficiency (%)

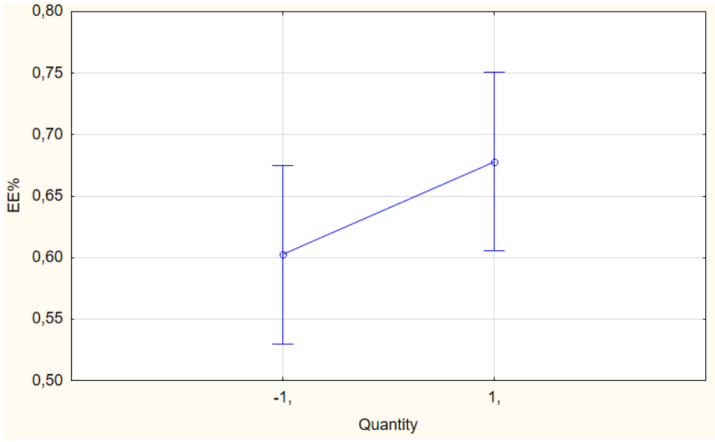

Figure D.21 Plot of Marginal Means and Conf. Limits (95%) of encapsulation efficiency for the quantity

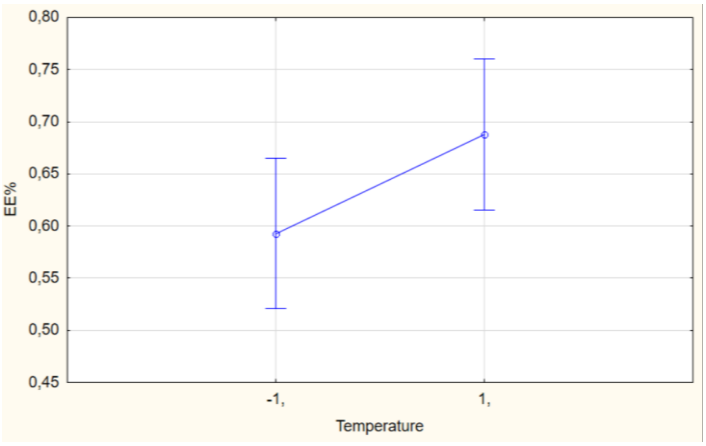

Figure D.22 Plot of Marginal Means and Conf. Limits (95%) of encapsulation efficiency for the temperature

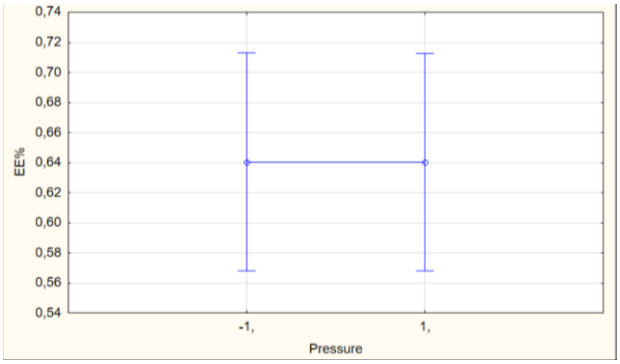

Figure D.23 Plot of Marginal Means and Conf. Limits (95%) of encapsulation efficiency for the pressure

E Conditions and powders produced for a cosmetic project

Note: All powders produced for the cosmetic project we used nozzle 76M (0,500mm) and we stirred solution for 50 seconds.

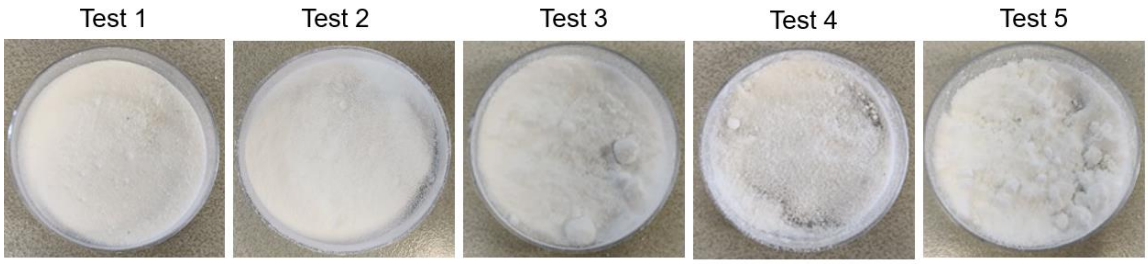

Figure E.1 Best powders produced

Figure E.2 Intermediate powders produced

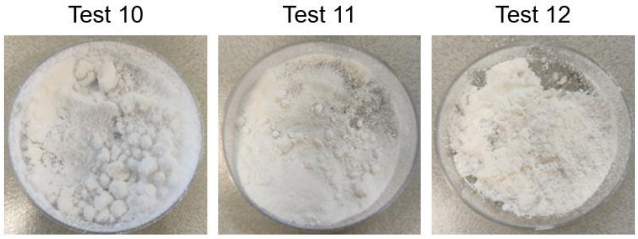

Figure E.3 Intermediate/Bad powders produced

Table E.1 Conditions and powders produced for the cosmetic project

Test	Compound 1	Compound 2	Emulsifier	Temperature /Pressure	Quantity (g)	Level (cm)	CO_2 (kg)	Powder produced (g)	Yield of Collected particles (%)
1	87% Fat powder	13% Cocoa Butter	-	60ºC/120 bar	100	3.2	-	64.8	65
2	50% Macadamia wax	50% Fat powder	-	76ºC/130 bar	100	3.2	0.5	88.9	89
3	75% Macadamia wax	25% Sunflower oil	-	76ºC/130 bar	100	3.2	0.5	87.8	88
4	75% Jojoba wax	25% Cocoa Butter	-	76ºC/100 bar	100	3.2	0.3	65.3	65
5	90% Jojoba wax	10% Sunflower oil	-	76ºC/130 bar	100	3.2	0.6	74.8	75
6	50% Jojoba wax	50% Fat powder	-	76ºC/130 bar	80	2.5	0.5	42.8	54
7	50% Macadamia wax	50% Cocoa Butter	-	76ºC/100 bar	60	2.0	0.2	52.5	53
8	75% Macadamia wax	25% Cocoa Butter	-	76ºC/100 bar	60	2.0	0.2	52.5	88
9	50% Jojoba wax	50% Cocoa butter	-	76ºC/100 bar	40	1.4	0.4	24.1	60
10	79% Jojoba wax	21% Sunflower oil	-	83ºC/120 bar	100	3.2	0.7	93.5	94
11	87% Fat powder	13% Cocoa Butter	2.5% Lecithin	76ºC/120 bar	102.5	3.5	0.4	72.5	71
12	75% Jojoba wax	25% Cocoa Butter	2.5% Lecithin	76ºC/120 bar	102.5	3.5	0.5	70.3	69
13	75% Jojoba wax	25% Sunflower oil	-	76ºC/120 bar	100	3.2	0.4	56.2	56
14	50% Beeswax	50% Sunflower oil	-	75ºC/150 bar	100	3.2	0.5	74.4	74
15	75% Fat powder	25% Cocoa Butter	-	60ºC/120 bar	80	2.5	0.6	24.9	31

Table E.2 Continuation of table C.1

Test	Compound 1	Compound 2	Emulsifier	Temperature (ºC)	Quantity (g)	Level (cm)	CO_2 (kg)	Powder produced (g)	Yield of Collected particles (%)
16	50% Beeswax	50% Cocoa Butter	-	75ºC/120 bar	100	3.2	0.4	56.8	57
17	25% Jojoba wax	75% Cocoa Butter	-	76ºC/120 bar	40	1.4	0.5	32.2	81

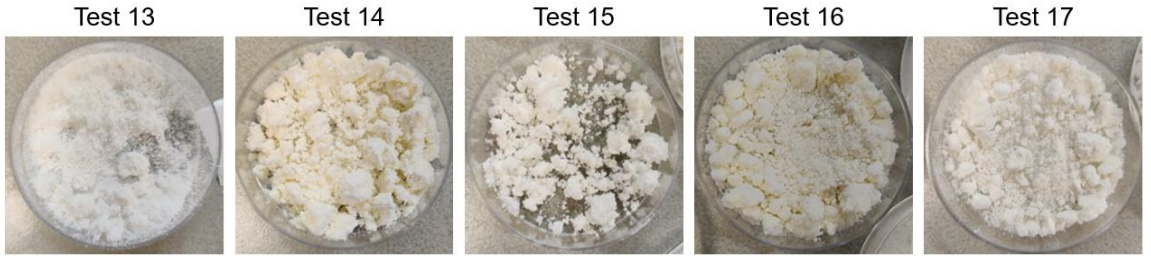

Figure E.4 The worst powders produced

F Overview of the experimental work for the mathematical model

F.1. Calculated values used in the mathematical model

In the mathematical model, we calculated specific heat of Jojoba wax (Cp) by **equation F.1** and calculated enthalpy change of gas under pressure to ambient pressure ($\Delta H_{exp,\ gas}$) by **equation F.2**. The weight fraction gas dissolved in the molten fat (fr_{gas}) was discovered using **figure F.1**. [123] [124]

$$C_p(Jojoba\ wax) = 9{,}51 \times 10^{-4}T + 0{,}129\ cal/g\ .K \qquad \textbf{(Eq. F.1)}$$

Where T is the temperature (356 K)

$$\Delta H_{exp,gas} = E_1 - E_2\ kJ/kg \qquad \textbf{(Eq. F.2)}$$

Where E_1 and E_2 are enthalpies at 120 and 1 bar respectively. (E_1 is 454,44 kJ/kg, and E_2 is 556,78 kJ/kg)

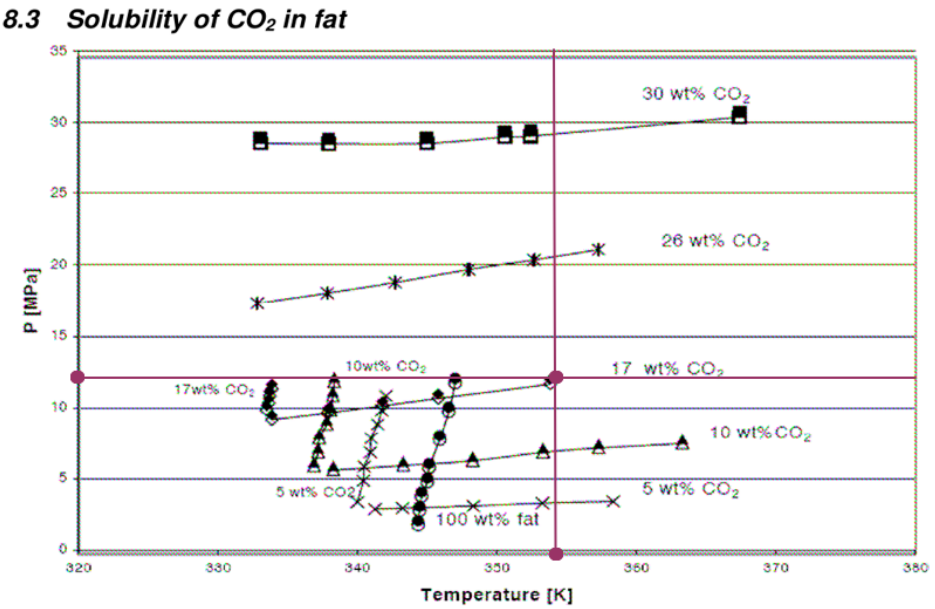

Figure F.1 P-T cross-section showing bubble-point curves (L+V→L), and melting-point curves (S+L→L), for the binary system CO_2+Rp70 [94][110]

F.2. The flow of CO_2 for four different nozzles

The capacity of the liquid being sprayed (L/h) was calculated by the following formula:

$$Capacity\ of\ liquid\ being\ sprayed = Capacity\ of\ water \times \frac{1}{\sqrt{Specific\ gravity}} \quad \textbf{(Eq. F.3)}$$

Where specific gravity is 0.84 kg/m^3.

After that, we calculated the flow of CO_2 (kg/h) by the following formula:

$$Flow\ of\ CO_2 = \frac{Capacity\ of\ liquid\ being\ sprayed}{1000} \times density\ of\ CO_2 \quad \textbf{(Eq. F.4)}$$

Where the density of CO_2 is 286 kg/m^3 at 120 bar and 83ºC. [123]

Table F.1 Calculated flow of CO_2 in the four different nozzles

Nozzle size	Core size	Diameter (mm)	Spray angle (º)	The flow of CO_2 (L/h)	The flow of CO_2 kg/h
63	16	0.093	88	65.95	18.86
80	20	0.340	51	21.44	6.13
76	17	0.500	59	42.44	12.13
70	21	0.710	59	94.45	27.00

The equation and water capacity values used to calculate the flow of CO_2 was provided by Spraying Systems catalogue. Since the catalogue doesn't have values of water capacity at 120 bar, we perform some linearizations [108][125]:

a) Nozzle 63M

Table F.2 Water capacity (L/h) and flow (L/h) of the different pressures for the nozzle 63M

P (bar)	Water Capacity (L/h)	Flow (L/h)
35	34.9	38.08
70	48.8	53.25
100	58	63.28
150	70.6	77.03
200	81.2	88.60
250	90.5	98.74
300	98.9	107.91
350	107	116.75
400	114	124.38
450	120	130.93

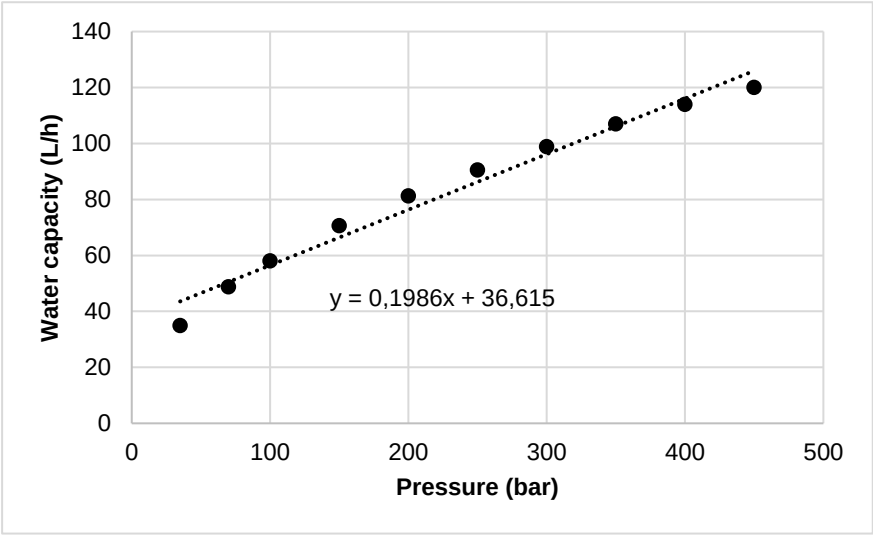

Figure F.2 Lineriazation curve of water capacity under pressure for the nozzle 63M

b) Nozzle 80M

Table F.3 Water capacity (L/h) and flow (L/h) of the different pressures for the nozzle 80M

P (bar)	Water Capacity (L/h)	Flow (L/h)
35	11.6	12.66
70	16	17.46
100	18.9	20.62
150	22.9	24.99
200	26.2	28.59
250	29	31.64
300	31.6	34.48
350	34	37.10
400	36.2	39.50
450	38.2	41.68

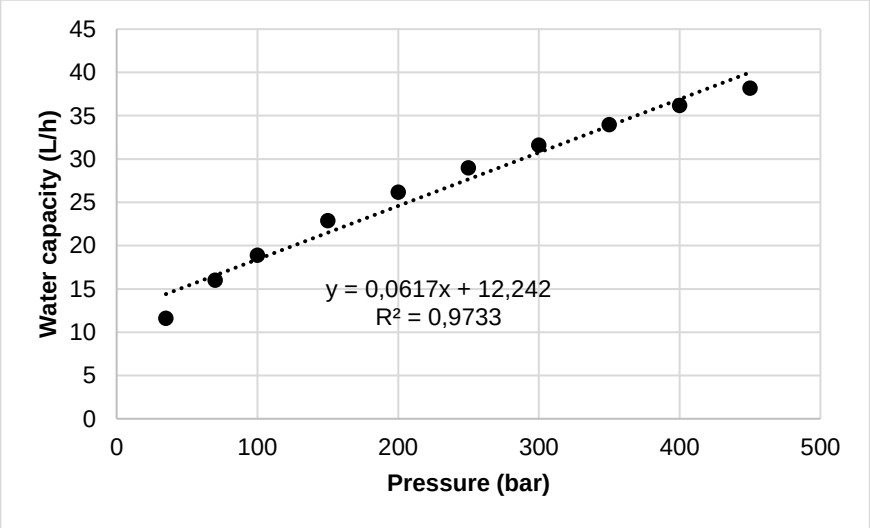

Figure F.3 Lineriazation curve of water capacity under pressure for the nozzle 80M

c) Nozzle 76M

Table F.4 Water capacity (L/h) and flow (L/h) of the different pressures for the nozzle 76M

P (bar)	Water Capacity (L/h)	Flow (L/h)
35	22.8	24.88
70	31.6	34.48
100	37.4	40.81
150	45.4	49.54
200	52	56.74
250	57.7	62.96
300	62.9	68.63
350	67.7	73.87
400	72.1	78.67
450	76.2	83.14

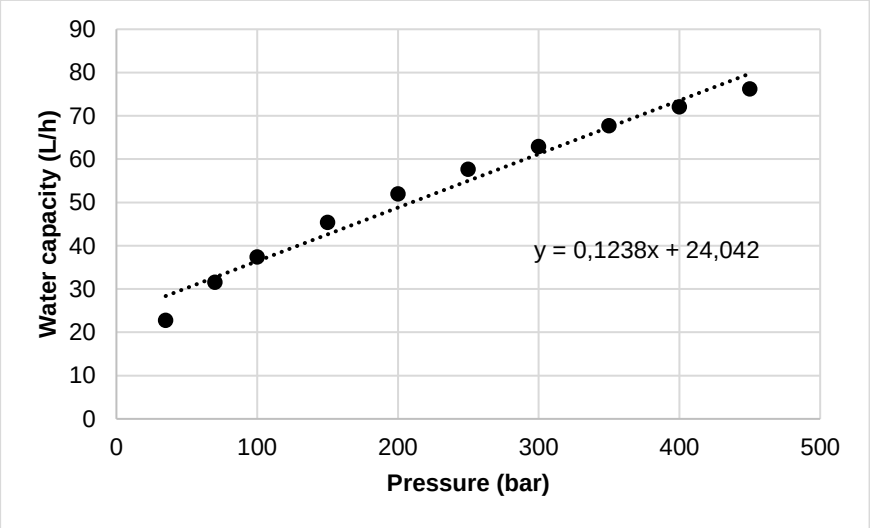

Figure F.4 Lineriazation curve of water capacity under pressure for the nozzle 76M

d) Nozzle 70M

Table F.5 Water capacity (L/h) and flow (L/h) of the different pressures for the nozzle 70M

P (bar)	Water Capacity (L/h)	Flow (L/h)
35	50.4	54.99
70	70.2	76.59
100	83.2	90.78
150	101	110.20
200	116	126.57
250	129	140.75
300	141	153.84
350	151	164.75
400	161	175.67
450	171	186.58

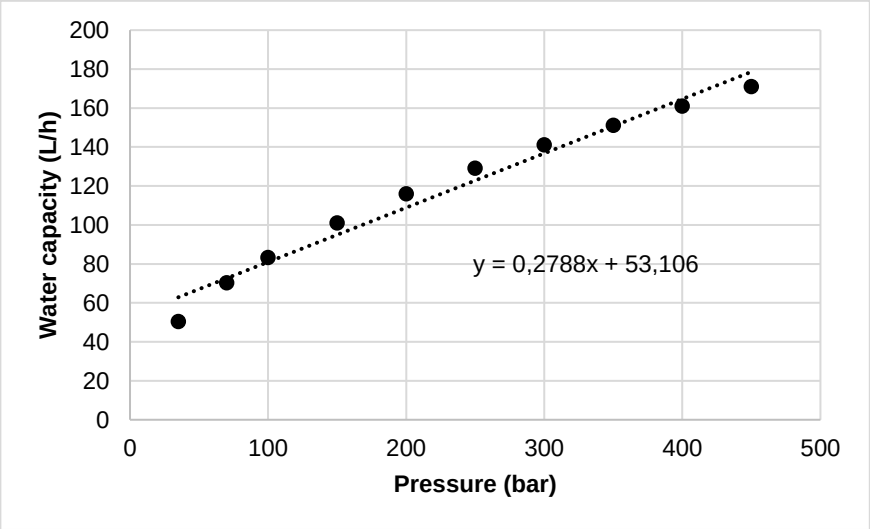

Figure F.5 Lineriazation curve of water capacity under pressure for the nozzle 70M